Supporting Information: Ligand and Solvent Effects on CO_2 Insertion into Group 10 Metal Alkyl Bonds

Anthony P. Deziel,[a] Matthew R. Espinosa,[a] Ljiljana Pavlovic,[b] David J. Charboneau,[a] Nilay Hazari,[a,*] Kathrin H. Hopmann[b,*] & Brandon Q. Mercado[a]

[a]Department of Chemistry, Yale University, P. O. Box 208107, New Haven, Connecticut, 06520, USA. E-mail: nilay.hazari@yale.edu.

[b]Department of Chemistry, UiT The Arctic University of Norway, N-9307 Tromsø, Norway. E-mail: kathrin.hopmann@uit.no.

SI: Experimental Details S2

SII: Synthesis and Characterization of New Compounds S3

SIII: Decomposition of (^{tBu}PSiP)Pd(CH_3) S8

SIV: Salerno Molecular Buried Volume Calculations S13

SV: Determination of Qualitative Rates of CO_2 Insertion S14

SVI: Determination of [CO_2] by Quantitative $^{13}C\{^1H\}$ NMR Spectroscopy S17

SVII: Representative Kinetic Data Workup: Determination of k_1 Using ^1H NMR Spectroscopy S19

SVIII: Representative Kinetic Data Workup: Determination of k_1 Using $^{31}P\{^1H\}$ NMR Spectroscopy S21

SIX: Eyring Analysis for the Insertion of CO_2 into (^{tBu}PBP)Pd(CH_3) in C_6D_6 S23

SX: Solvent Effects: Dielectric Constant and Gutmann Acceptor Number S24

SXI: NMR and IR Spectra of New Compounds S25

SXII: Computational Details S43

SXIII: X-Ray Diffraction Data S57

SXIV: References S60

SI. Experimental Details

All experiments were performed under an N_2 atmosphere using either standard Schlenk techniques or an MBraun glovebox unless noted. Under standard operating procedures for glovebox use: purging was not performed between uses of pentane, benzene, and toluene. Solvents used in synthesis were deoxygenated by sparging with nitrogen and dried through an activated alumina column on an Innovative Technology Inc. system. Commercial chemicals were used as received. Anhydrous CO_2 was obtained from Airgas Inc. C_6D_6 and toluene-d_8 were purchased from Cambridge Isotope Laboratories, Inc., degassed via three freeze-pump-thaw cycles and then dried using a plug of activated alumina. The pressure of CO_2 was measured with a Wallace & Tiernan 61B-1D-0800 Absolute Pressure Gauge. NMR spectra were recorded on Agilent DD2 -400, -500, -600 spectrometers at ambient probe temperatures unless otherwise specified. Chemical shifts for ^{1}H and $^{13}C\{^{1}H\}$ NMR spectra are reported in ppm and referenced to residual internal protio solvent. Chemical shifts for $^{31}P\{^{1}H\}$ NMR spectra are referenced using ^{1}H resonances based on relative gyromagnetic ratios of the nuclei.[1] Elemental analysis was performed by Robertson Microlit Laboratories, Inc. under an inert atmosphere. IR spectra were collected on a Bruker Alpha FTIR spectrometer under 1 atm N_2. Mass spectrometric measurements were performed with a Thermo Fisher QExactive Orbitrap LC-MS system using continuous injection with a syringe. Samples were prepared in a glove box and loaded into a gas tight syringe, Hamilton 1750, for sample injection. The syringe and the PEEK capillaries to the ion source of the MS were cleaned with dry and oxygen-free solvents before sample injection. Samples were held at room temperature and continuously injected using a syringe pump at 50 µL/min. Electrospray was used for desolvatization and ionization, with the electrospray needle held at +3.5kV. Compressed air was used as desolvatization gas, capillary temperature was at 320 °C, probe heater temperature at 40 °C and sheath gas flow was at 5 L/min. Resolution was set to 35,000 M/ΔM. Mass spectra were recorded in the range of 150 to 750 m/z in positive ion mode. Measurements and data post-processing were performed with Thermo Xcalibur 4.1.31.9. Synthetic procedures for (^{tBu}PBP)Pd(CH_3), (^{tBu}PBP)Pd{$OC(O)CH_3$}, (^{Cy}PBP)PdCl, (^{Cy}PBP)Pd(CH_3), (^{Cy}PBP)Pd{$OC(O)CH_3$}, (^{Cy}PBP)NiCl, (^{Cy}PBP)Ni(CH_3), (^{Cy}PBP)Ni{$OC(O)CH_3$}, and (^{tBu}PSiP)PdCl can be found below. $[(\eta^3\text{-allyl})Pd(\mu\text{-Cl})]_2$,[2] $^{Cy}PB^{H}P$,[3] $^{tBu}PB^{H}P$,[4] (^{tBu}PBP)Ni(CH_3),[5] and $^{tBu}PSi^{H}P$ ($^{tBu}PSi^{H}P$ = HSi(Me)(2-P^{t}Bu$_2$-C$_6$H$_4$)$_2$)[6] were synthesized according to literature procedures.

SII. Synthesis and Characterization of New Compounds

The predominant complex used in this work for kinetic studies was (^{tBu}PBP)Pd(CH_3). We were able to characterize this complex via elemental analysis. In contrast, we were unable to characterize (^{Cy}PBP)M(CH_3) (M = Ni or Pd), which we used to make quantitative comparisons of the rates of CO_2 insertion, using elemental analysis. This is likely because we were unable to remove pentane from the samples, despite subjecting the samples to extended periods of vacuum. Consistent with this observation pentane is observed in the crystal structure of (^{Cy}PBP)Ni(CH_3). NMR spectra for all of the new compounds used in this work are provided below and are clean apart from the presence of pentane for complexes using the ^{Cy}PBP ligand.

We also note that a major problem in synthesizing complexes of the type (^{R}PBP)M(CH_3) is the presence of inorganic salts, such as LiCl, in the crude product. However, a routine part of our studies of CO_2 insertion into (^{R}PBP)M(CH_3) was to perform these reactions in the presence of a known quantity of a hexamethylbenzene standard. If there was a significant quantity of magnesium or lithium salts (or any other inorganic compound) present in our samples, the starting complex would not integrate correctly against the standard in the NMR spectrum. Therefore, we can discount the presence of any significant quantity of inorganic salts in our samples but this requires washing as detailed in the experimental procedures.

(^{tBu}PBP)PdCl

[(η^3-allyl)Pd(μ-Cl)]$_2$ (133.5 mg, 0.36 mmol) was dissolved in 5 mL of benzene and added to a 150 mL Schlenk flask equipped with a magnetic stir bar. A 5 mL solution of ^{tBu}PB^{H}P in benzene (332 mg, 0.76 mmol, 2.1 equivalents) was then added to the flask. The solution was allowed to stir at room temperature for three hours under N_2. A gradual color change from yellow to dark orange was observed. The solution was filtered through a plug of Celite and the volatiles were removed under vacuum. The precipitate was triturated with *n*-pentane to remove any excess benzene and then washed with 3 x 3 mL *n*-pentane to yield crude (^{tBu}PBP)PdCl. The solid was recrystallized in benzene layered with *n*-pentane at room temperature to yield colorless crystals of (^{tBu}PBP)PdCl (265 mg, 63%). ^{1}H and ^{31}P NMR spectra matched those previously reported in the literature.[7]

(^{tBu}PBP)Pd(CH_3)

(^{tBu}PBP)PdCl (146 mg, 0.25 mmol) was dissolved in 5 mL of benzene and added to a 4-dram scintillation vial. 0.18 mL of a 1.6 M MeLi solution in diethyl ether (0.28 mmol, 1 equivalent) was added dropwise to the benzene solution. An immediate color change to black was observed. The solution was allowed to stir for 30 minutes and then was filtered through Celite to separate the salt precipitate from the desired product. The volatiles were removed from the filtrate under vacuum to give crude (^{tBu}PBP)Pd(CH_3) as a brown solid. The solid was then recrystallized twice in *n*-pentane at -35 °C to yield (^{tBu}PBP)Pd(CH_3)

as colorless crystals (85 mg, 60%). Crystals suitable for X-ray diffraction were grown from *n*-pentane at -35 °C.

^{1}H NMR (400 MHz, C_6D_6): δ 7.18 (dd, $^{3}J_{HH}$ = 5.7, 3.3 Hz, 2H, C*H*), 7.02 (dd, $^{3}J_{HH}$ = 5.6, 3.3 Hz, 2H, CH_{Ar}), 3.76 (t, *J* = 2.1 Hz, 4H, CH_2), 1.23 (t, *J* = 6.7 Hz, 36H, C(CH_3)$_3$), 0.37 (t, *J* = 3.8 Hz, 3H, CH_3). ^{13}C{^{1}H} NMR (151 MHz, C_6D_6): δ 139.54 (t, *J* = 9.0 Hz, 4°), 118.55 (s, *C*H), 109.51 (s, *C*H), 42.53 (t, *J* = 14.4 Hz, CH_2), 35.79 (t, *J* = 6.1 Hz, *C*(CH$_3$)$_3$), 29.74 (t, *J* = 4.0 Hz, C(*C*H$_3$)$_3$), -9.47 (t, *J* = 9.8 Hz, *C*H$_3$). ^{31}P{^{1}H} NMR (202 MHz, C_6D_6): δ 97.06 (s, ^{tBu}*P*B*P*). Anal. Found (Calcd. For $C_{25}H_{47}BN_2P_2Pd$) C 54.04 (54.12), H 8.31 (8.54), N 4.71 (5.05). HRMS (ESI$^+$): 539.2072 [M-CH$_3$]$^+$. Calc for [$C_{24}H_{44}BN_2P_2Pd$]: 539.2103.

<u>(^{tBu}PBP)Pd{OC(O)CH$_3$}</u>

(^{tBu}PBP)Pd(CH$_3$) (8.7 mg, 0.0157 mmol) was dissolved in 500 μL of C_6D_6 and added to a J-Young NMR tube. The solution was degassed via three freeze-pump-thaw cycles and 1 atm CO_2 was added via a Schlenk line. The solution was allowed to stand for 6 hours at room temperature. The volatiles were removed under vacuum and the complex was washed with 1 x 2 mL cold *n*-pentane to yield the product, (^{tBu}PBP)Pd{OC(O)CH$_3$} as a beige solid (8.8 mg, 93%). Crystals suitable for X-ray diffraction were grown from *n*-pentane at -35 °C.

^{1}H NMR (500 MHz, C_6D_6) δ 7.13 (dd, *J* = 5.8, 3.2 Hz, 2H, C*H*), 6.93 (dd, *J* = 5.7, 3.3 Hz, 2H, C*H*), 3.55 (s, 4H, CH_2), 2.41 (s, 3H, CH_3), 1.28 (t, *J* = 7.0 Hz, 36H, C(CH_3)$_3$). ^{13}C{^{1}H} NMR (151 MHz, C_6D_6): δ 175.29 (s, (O*C*(O))), 138.84 (t, *J* = 9.0 Hz, 4°), 119.07 (s, *C*H), 109.26 (s, *C*H), 39.60 (t, *J* = 14.4 Hz, *C*H$_2$), 35.33 (t, *J* = 6.1 Hz, *C*(CH$_3$)$_3$), 29.39 (t, *J* = 3.8 Hz, C(*C*H$_3$)$_3$), 25.98 (s, *C*H$_3$). ^{31}P{^{1}H} NMR (202 MHz, C_6D_6): δ 86.95 (s, ^{tBu}*P*B*P*). IR (Diamond ATR cell, cm^{-1}): 1598 (CO_2), 1290 (CO_2). Anal. Found (Calcd. For $C_{26}H_{47}BN_2O_2P_2Pd$) C 52.29 (52.15), H 7.91 (7.91), N 4.54 (4.68). HRMS (ESI$^+$): 539.2070 [M-OAc]$^+$. Calc for [$C_{24}H_{44}BN_2P_2Pd$]: 539.2115.

<u>(^{Cy}PBP)PdCl</u>

[(η^3-allyl)Pd(μ-Cl)]$_2$ (10.9 mg, 0.030 mmol) was dissolved in 5 mL of benzene and added to a 150 mL Schlenk flask equipped with a magnetic stir bar. A 5 mL solution of ^{Cy}PB^{H}P in benzene (34 mg, 0.063 mmol, 2.1 equivalents) was then added to the flask. The solution was allowed to stir for three hours under N_2. A gradual color change from yellow to colorless was observed. The solution was filtered through a plug of Celite and the volatiles were removed under vacuum. The beige precipitate was washed with 3 x 3 mL *n*-pentane to yield the product, (^{Cy}PBP)PdCl, as a white solid (29.8 mg, 69%).

^{1}H NMR (C_6D_6, 400 MHz): δ 7.20 (dd, *J* = 5.7, 3.2 Hz, 2H, C*H*), 7.05 (dd, *J* = 5.7, 3.2 Hz, 2H, C*H*), 3.45 (s, 4H, CH_2), 2.19-2.05 (m, 8H, P(C$_6H_{11}$)$_2$), 1.85-1.47 (m, 20H, P(C$_6H_{11}$)$_2$), 1.38-0.97 (m, 16H, P(C$_6H_{11}$)$_2$). ^{13}C{^{1}H} NMR (151 MHz, C_6D_6): δ 139.07 (t, *J* = 9.5 Hz, 4°), 119.19 (s, *C*H), 109.69 (s, *C*H), 40.01 (t, *J* = 15.6 Hz, *C*H$_2$), 33.78 (t, *J* = 10.1 Hz, P(*C*$_6$H$_{11}$)$_2$), 29.13 (s, P(*C*$_6$H$_{11}$)$_2$, 28.82 (s, P(*C*$_6$H$_{11}$)$_2$), 27.00 (m, P(*C*$_6$H$_{11}$)$_2$, 26.91 (m, P(*C*$_6$H$_{11}$)$_2$, 26.28 (s, P(*C*$_6$H$_{11}$)$_2$). ^{31}P{^{1}H} NMR (162 MHz,

C_6D_6): δ 63.16 (s, ^{Cy}*P*B*P*). Anal. Found (Calcd. for $C_{32}H_{52}N_2BP_2PdCl$) C 56.81 (56.57), H 7.72 (7.71), N 3.88 (4.12). HRMS (ESI$^+$): 643.2690 [M-Cl]$^+$. Calc for [$C_{32}H_{52}BN_2P_2Pd$]: 643.2745.

(^{Cy}PBP)Pd(CH_3)

(^{Cy}PBP)PdCl (35 mg, 0.052 mmol) was dissolved in 3 mL of toluene, added to a 4-dram scintillation vial and cooled in a cold well with a dry ice/acetone mixture. 30 μL of a 1.6 M MeLi solution in diethyl ether was added dropwise to the cold solution. An immediate color change to dark orange was observed. After 2 minutes, the solution was filtered through a plug of Celite and the volatiles were removed under vacuum. The solution was redissolved in 20 mL of *n*-pentane and filtered through a plug of Celite. After concentration under reduced pressure, the (^{Cy}PBP)Pd(CH_3) product was recrystallized twice from pentane at -35 °C (8.4 mg, 25%).

^{1}H NMR (400 MHz, C_6D_6) δ 7.21 (dd, *J* = 5.7, 3.2 Hz, 2H, C*H*), 7.11 (dd, *J* = 5.6, 3.2 Hz, 2H, C*H*), 3.64 (s, 4H, CH_2), 2.11-1.97 (m, 8H, P(C_6H_{11})$_2$), 1.74-1.45 (m, 20H, P(C_6H_{11})$_2$), 1.31-0.98 (m, 16H, P(C_6H_{11})$_2$), 0.30 (t, *J* = 4.4 Hz, 3H, CH_3). ^{13}C{^{1}H} NMR (151 MHz, C_6D_6): δ 139.97 (t, *J* = 9.5 Hz, 4°), 118.57 (s, *C*H), 109.73 (s, *C*H), 43.11 (t, *J* = 15.6 Hz, *C*H_2), 34.81 (t, *J* = 9.8 Hz, P(*C*$_6$H$_{11}$)$_2$), 29.25 (s, P(*C*$_6$H$_{11}$)$_2$), 29.11 (vt, *J* = 3.2 Hz, P(*C*$_6$H$_{11}$)$_2$), 27.19 (m, P(*C*$_6$H$_{11}$)$_2$), 27.12 (m, P(*C*$_6$H$_{11}$)$_2$), 26.53 (s, P(*C*$_6$H$_{11}$)$_2$), -15.16 (t, *J* = 10.7 Hz, *C*H$_3$). ^{31}P{^{1}H} NMR (162 MHz, C_6D_6): δ 70.88 (s, ^{Cy}*P*B*P*). HRMS (ESI$^+$): 643.2682 [M-CH_3]$^+$. Calc for [$C_{32}H_{52}BN_2P_2Pd$]: 643.2745.

(^{Cy}PBP)Pd{OC(O)CH_3}

(^{Cy}PBP)Pd(CH_3) (17.1 mg, 0.028 mmol) was dissolved in 500 μL of C_6D_6 and added to a J-Young NMR tube. The solution was degassed via three freeze-pump-thaw cycles and 1 atm CO_2 was added via a Schlenk line. The solution was allowed to stand for 1 hour at room temperature. The volatiles were then removed under vacuum and the complex was washed with cold *n*-pentane to yield the product, (^{tBu}PBP)Pd{OC(O)CH_3} (11.8 mg, 64%).

^{1}H NMR (400 MHz, C_6D_6): δ 7.19 (dd, *J* = 5.8, 3.1 Hz, 2H, C*H*), 7.02 (dd, *J* = 5.8, 3.2 Hz, 2H, C*H*), 3.44 (s, 4H, CH_2), 2.46 (s, 3H, CH_3), 2.27-2.08 (m, 8H, P(C_6H_{11})$_2$), 1.75-1.49 (m, 20H, P(C_6H_{11})$_2$), 1.44-0.97 (m, 16H, P(C_6H_{11})$_2$). ^{13}C{^{1}H} NMR (151 MHz, C_6D_6): δ 175.28 (s, (O*C*(O))), 139.23 (t, *J* = 9.2 Hz, 4°), 119.05 (s, *C*H), 109.42 (s, *C*H), 39.43 (t, *J* = 15.9 Hz, *C*H_2), 33.99 (t, *J* = 9.8 Hz, P(*C*$_6$H$_{11}$)$_2$), 28.93 (s, P(*C*$_6$H$_{11}$)$_2$), 28.68 (vt, *J* = 2.9 Hz, P(*C*$_6$H$_{11}$)$_2$), 27.10 (m, P(*C*$_6$H$_{11}$)$_2$), 27.03 (m, P(*C*$_6$H$_{11}$)$_2$), 26.29 (s, P(*C*$_6$H$_{11}$)$_2$), 25.24 (s, *C*H$_3$). ^{31}P{^{1}H} NMR (202 MHz, C_6D_6): δ 62.42 (s, ^{Cy}*P*B*P*). IR (Diamond ATR cell, cm^{-1}): 1598 (CO_2), 1290 (CO_2). HRMS (ESI$^+$): 643.2685 [M-OAc]$^+$. Calc for [$C_{32}H_{52}BN_2P_2Pd$]: 643.2745.

(^{Cy}PBP)NiCl

^{Cy}PB^{H}P (100 mg, 0.187 mmol) and $NiCl_2$•DME (41 mg, 0.187 mmol, 1 equivalent) were dissolved in

40 mL of diethyl ether and added to a 250 mL Schlenk flask equipped with a magnetic stir bar. It is necessary for this reaction to be performed under dilute conditions, as an unknown blue decomposition product is formed under more concentrated conditions. The solution was allowed to stir for 18 hours at room temperature under N_2. The volatiles were removed under reduced pressure and a yellow solid was isolated. The solid was washed with *n*-pentane and recrystallized from toluene layered with *n*-pentane to yield (^{Cy}PBP)NiCl (30.1 mg, 26%) as yellow crystals, which were suitable for X-ray diffraction.
^{1}H NMR (500 MHz, C_6D_6): δ 7.17 (m, 2H, C*H*), 7.00 (m, 2H, C*H*), 3.39 (s, 4H, CH_2), 2.31-2.23 (m, 4H, P(C$_6H_{11}$)$_2$), 2.17-2.09 (m, 4H, P(C$_6H_{11}$)$_2$), 1.85-1.73 (m, 4H, P(C$_6H_{11}$)$_2$), 1.73-1.66 (m, 4H, P(C$_6H_{11}$)$_2$), 1.66-1.48 (m, 12H, P(C$_6H_{11}$)$_2$), 1.29-1.01 (m, 16H, P(C$_6H_{11}$)$_2$). ^{13}C{^{1}H} NMR (151 MHz, C_6D_6): δ 139.76 (t, *J* = 7.8 Hz, *C*H), 118.91 (s, *C*H), 109.09 (s, *C*H), 40.12 (t, *J* = 18.2 Hz, *C*H$_2$), 33.53 (app. t, *J* = 9.2 Hz, P(*C*$_6$H$_{11}$)$_2$), 29.15 (s, P(*C*$_6$H$_{11}$)$_2$), 28.75 (t, *J* = 2.3 Hz, P(*C*$_6$H$_{11}$)$_2$), 27.20-27.14 (m, P(*C*$_6$H$_{11}$)$_2$), 27.12-27.06 (m, P(*C*$_6$H$_{11}$)$_2$), 26.51 (s, P(*C*$_6$H$_{11}$)$_2$). ^{31}P{^{1}H} NMR (202 MHz, C_6D_6): δ 65.6 (s, ^{Cy}*PBP*).

(^{Cy}PBP)Ni(CH$_3$)

(^{Cy}PBP)NiCl (100 mg, 0.16 mmol) and 50 mL of pentane were added to a 100 mL Kontes valve flask equipped with a magnetic stir bar and the flask was cooled to -35 °C. Once the flask was cooled, 0.23 mL of a 0.70 M MeMgCl solution in THF was added dropwise to the Kontes valve flask (0.16 mmol, 1 equivalent). The resulting heterogeneous mixture was stirred for 1 hour or until all the (^{Cy}PBP)NiCl had reacted. It was straight forward to determine when the (^{Cy}PBP)NiCl had reacted because (^{Cy}PBP)NiCl is insoluble in *n*-pentane. Thus, when there was no yellow precipitate, the reaction was complete. After the reaction reached completion, the Kontes valve flask containing a yellow solution was moved into a glovebox and its contents were filtered using a Celite plug to remove insoluble $MgCl_2$. This was done to prevent reversion to the chloride complex through a salt metathesis reaction. The solvent was removed in *vacuo* and the resulting yellow oil was triturated three times in *n*-pentane. The sample was then redissolved in *n*-pentane and filtered through a plug of Celite. The *n*-pentane was concentrated to give crystals and the complex was subsequently recrystallized twice to yield yellow crystals (25 mg, 26%), which were suitable for X-ray diffraction.
^{1}H NMR (600 MHz, C_6D_6): δ 7.21 (dd, *J* = 5.7, 3.2 Hz, 2H, C*H*), 7.07 (dd, *J* = 5.7, 3.2 Hz, 2H, C*H*), 3.59 (s, 4H, CH_2), 2.16-2.03 (m, 8H, P(C$_6H_{11}$)$_2$), 1.74-1.65 (m, 8H, P(C$_6H_{11}$)$_2$), 1.64-1.45 (m, 12H, P(C$_6H_{11}$)$_2$), 1.35-1.03 (m, 16H, P(C$_6H_{11}$)$_2$), 0.04 (t, *J* = 6.14, 3H, CH_3). ^{13}C{^{1}H} NMR (151 MHz, C_6D_6): δ 140.43 (t, *J* = 8.1 Hz, 4°), 118.37 (s, *C*H), 109.17 (s, *C*H), 42.83 (t, *J* = 18.5 Hz, *C*H$_2$), 34.42 (t, *J* = 8.7 Hz, P(*C*$_6$H$_{11}$)$_2$), 29.32 (s, P(*C*$_6$H$_{11}$)$_2$), 29.08 (s, P(*C*$_6$H$_{11}$)$_2$), 27.38 (t, *J* = 6.1 Hz, P(*C*$_6$H$_{11}$)$_2$), 27.28 (t, *J* = 4.6 Hz, P(*C*$_6$H$_{11}$)$_2$), 26.72 (s, P(*C*$_6$H$_{11}$)$_2$), -11.41 (t, *J* = 11.3 Hz, CH_3). ^{31}P{^{1}H} NMR (202 MHz, C_6D_6): δ 75.20 (s, ^{Cy}*PBP*). HRMS (ESI$^+$): 595.3027 [M-CH$_3$]$^+$. Calc for [$C_{32}H_{52}BN_2P_2Pd$]: 595.3052.

(^{tBu}PSiP)PdCl

[(η^3-allyl)Pd(μ-Cl)]$_2$ (25 mg, 0.068 mmol) was dissolved in 3 mL of benzene and added to a 150 mL

Schlenk flask equipped with a magnetic stir bar. A 3 mL solution of $^{tBu}PSi^{H}P$ in benzene (83 mg, 0.17 mmol, 2.5 equivalents) was then added to the flask. The solution was allowed to stir for three hours at room temperature under N_2. The yellow solution was filtered through a plug of Celite and the volatiles were removed under reduced pressure. The precipitate was triturated with *n*-pentane to remove any excess benzene and then washed with 3 x 3 mL of cold *n*-pentane to yield crude (^{tBu}PSiP)PdCl. The solid was then washed with 1 x 2 mL of benzene to yield spectroscopically pure (^{tBu}PSiP)PdCl (18 mg, 21%). ^{1}H NMR (400 MHz, C_6D_6): δ 8.00 (d, *J* = 7.5 Hz, 2H, C*H*), 7.72 (d, *J* = 7.9 Hz, 2H, C*H*), 7.26 (t, *J* = 7.3 Hz, 2H, C*H*), 7.10 (t, *J* = 7.6 Hz, 2H, C*H*), 1.58 (t, *J* = 7.4 Hz, 18H, C(CH_3)$_3$), 1.39 (t, *J* = 6.8 Hz, 18H, C(CH_3)$_3$), 0.62 (t, *J* = 1.3 Hz, 3H, Si(CH_3)). ^{13}C{^{1}H} NMR (151 MHz, C_6D_6): δ 156.40 (t, *J* = 26.3 Hz, *C*H), 140.77 (t, *J* = 16.2 Hz, *C*H), 134.15 (s, *C*H), 133.04 (t, *J* = 11.6 Hz, *C*H), 130.20 (s, *C*H), 38.24 (t, *J* = 6.6 Hz, *C*(CH$_3$)$_3$), 37.56 (t, *J* = 6.4 Hz, *C*(CH$_3$)$_3$), 31.58 (t, *J* = 3.2 Hz, C(*C*H$_3$)$_3$), 31.18 (t, *J* = 3.8 Hz, C(*C*H$_3$)$_3$), 10.30 (s, Si(*C*H$_3$). ^{31}P{^{1}H} NMR (162 MHz, C_6D_6): δ 83.3 (s, *P*Si*P*).

SIII. Decomposition of (^{tBu}PSiP)Pd(CH$_3$)

(^{tBu}PSiP)PdCl (^{tBu}PSiP = Si(Me)(2-P^{t}Bu$_2$-C$_6$H$_4$)$_2$) was slurried in C_6D_6 or toluene-d_8 and added to a J-Young NMR tube. The solution was cooled to -77 °C in a cold well and 12.8 μL of a 1.6 M MeLi solution in diethyl ether (21 μmol, 1 equivalent) was added dropwise. The remaining (^{tBu}PSiP)PdCl dissolved upon addition of the MeLi solution, and an immediate color change to dark orange was observed. The solution was allowed to warm up to ambient temperature. Initial formation of (^{tBu}PSiP)Pd(CH$_3$) was observed by ^{1}H and ^{31}P{^{1}H} NMR spectroscopy (Figures S1-S2). However, decomposition occurs rapidly at room temperature, and 17% of the (^{tBu}PSiP)Pd(CH$_3$) species is converted to a new complex after 5 minutes and complete decomposition to essentially that same product is observed after 24 hours (Figures S3-S4). Performing the reaction at -35 °C slowed, but did not prevent decomposition. The major decomposition product is the rearranged species, [(κ^2-^{t}Bu$_2$PC$_6$H$_4$SiMe$_2$)Pd(κ^2-^{t}Bu$_2$PC$_6$H$_4$)]. Crystals of this complex suitable for X-ray diffraction were grown from *n*-pentane at -35 °C (Figure S5).

For (^{tBu}PSiP)Pd(CH$_3$): ^{1}H NMR (500 MHz, toluene-d_8): δ 8.86 (d, *J* = 7.5 Hz, 2H, C*H*), 7.83 (d, *J* = 8.3 Hz, 2H, C*H*), 7.30 (t, *J* = 7.4 Hz, 2H, C*H*), 7.16 (t, *J* = 7.6 Hz, 2H, C*H*), 1.38 (t, *J* = 6.8 Hz, 18H, P(C(C*H*$_3$)$_3$)), 1.24 (t, J = 6.8 Hz, 18H, P(C(C*H*$_3$)$_3$)), 0.74 (s, 3H, Si(C*H*$_3$)), 0.50 (s, 3H, C*H*$_3$). ^{31}P{^{1}H} NMR (202 MHz, toluene-d_8): δ 89.64 (s, ^{tBu}P Si P).

For [(κ^2-^{t}Bu$_2$PC$_6$H$_4$SiMe$_2$)Pd(κ^2-^{t}Bu$_2$PC$_6$H$_4$)]: ^{1}H NMR (400 MHz, C_6D_6): δ 8.33-8.28 (m, 1H, C*H*), 7.73-7.67 (m, 2H, C*H*), 7.43-7.37 (m, 2H, C*H*), 7.26 (td, *J* = 7.7, 3.4 Hz, 1H, C*H*), 7.15-7.09 (m, 2H, CH), 1.35 (d, *J* = 5.0 Hz, 18H, C(C*H*$_3$)$_3$), 1.32 (d, *J* = 3.9 Hz, 18H, C(C*H*$_3$)$_3$), 0.99 (d, *J* = 2.7 Hz, 6H, Si(C*H*$_3$)$_2$). ^{31}P{^{1}H} NMR (162 MHz, C_6D_6): δ 93.94 (d, *J* = 14.2 Hz, *P*^{t}Bu$_2$), -9.97 (td, *J* = 70.8, 13.5 Hz, *P*^{t}Bu$_2$).

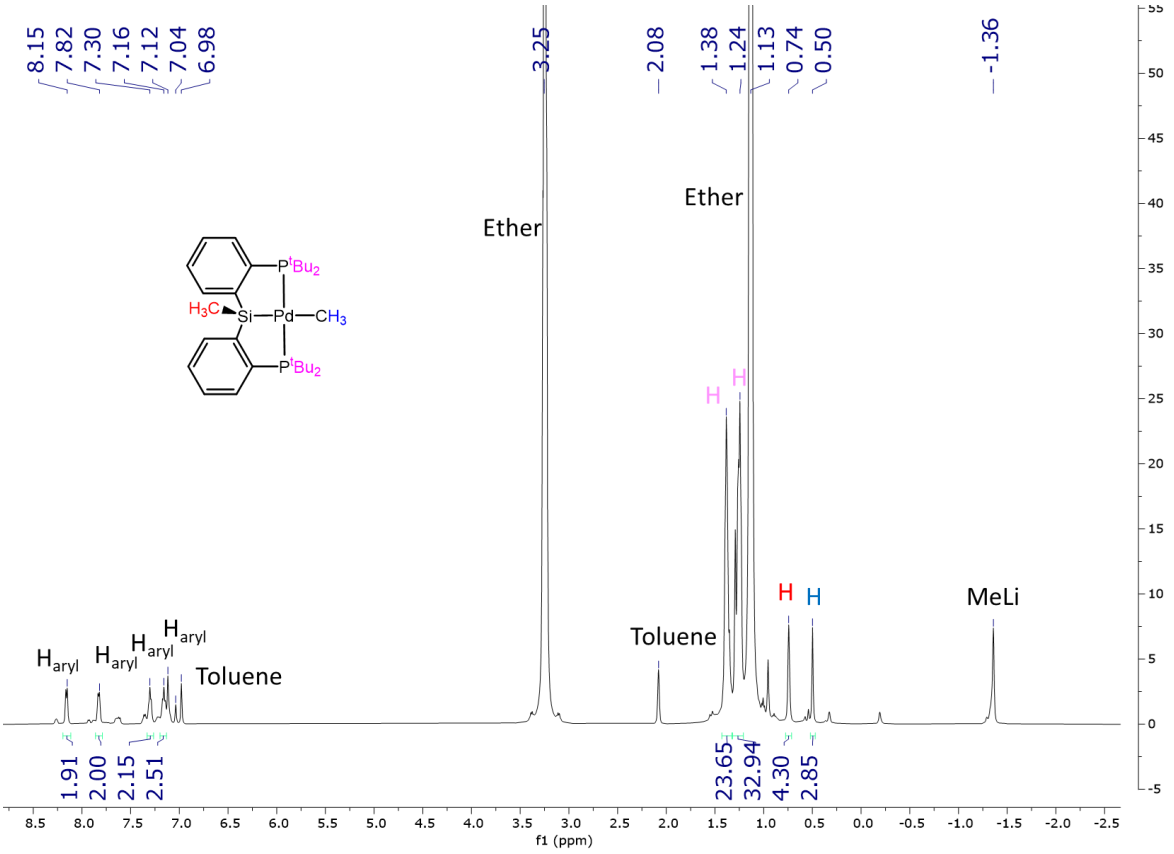

Figure S1. Initial ^{1}H NMR spectrum of (^{tBu}PSiP)Pd(CH$_3$), taken 5 minutes after addition of MeLi. The major signals are the (^{tBu}PSiP)Pd(CH$_3$) product, which are labeled on the spectrum. Solvent signals and residual MeLi are also labeled, whereas the smaller unlabeled peaks are for the rearranged decomposition product, [(κ^2-^{t}Bu$_2$PC$_6$H$_4$SiMe$_2$)Pd(κ^2-^{t}Bu$_2$PC$_6$H$_4$)].

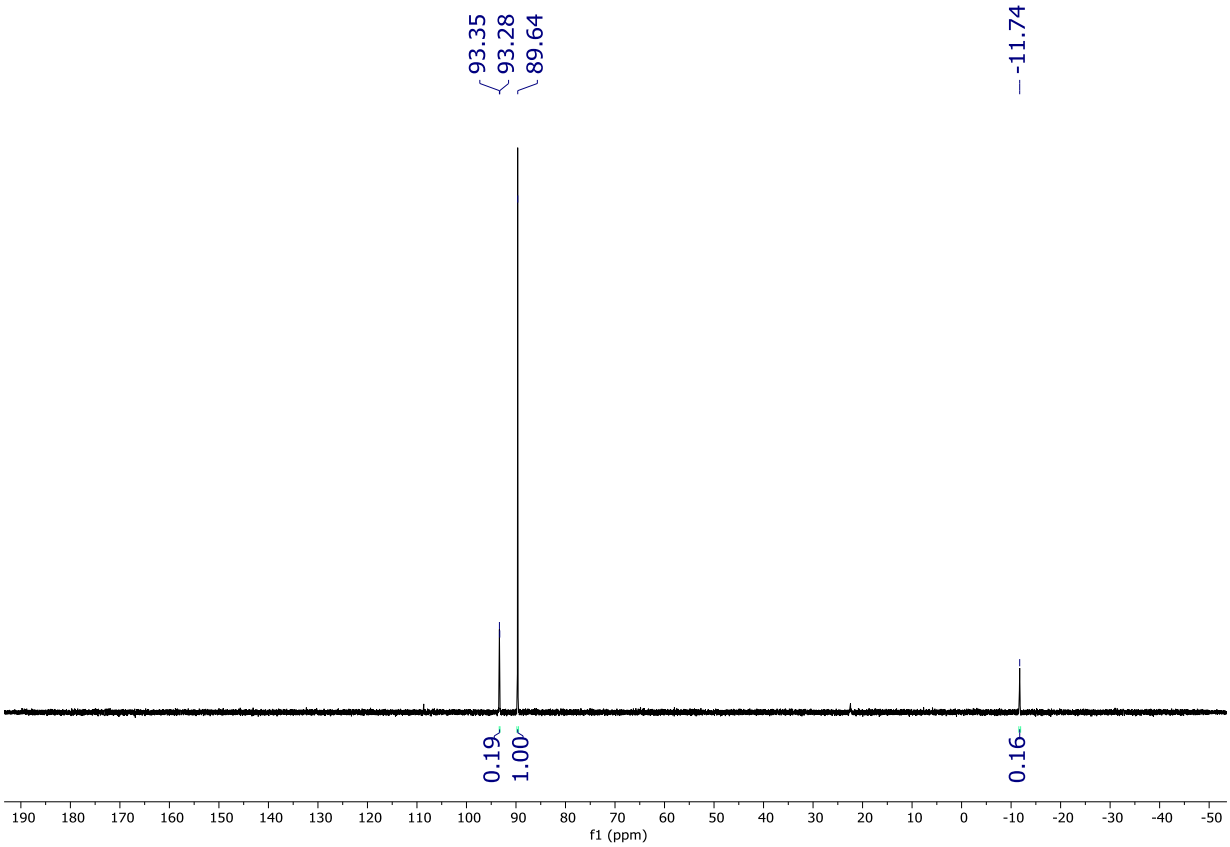

Figure S2. Initial $^{31}P\{^{1}H\}$ NMR spectrum of (^{tBu}PSiP)Pd(CH_3), taken 5 minutes after addition of MeLi. The major signal at 89.64 ppm is the (^{tBu}PSiP)Pd(CH_3) product, and the signals at 93.32 and -11.74 ppm correspond to the rearranged decomposition product, [(κ^2-$^{t}Bu_2PC_6H_4SiMe_2$)Pd(κ^2-$^{t}Bu_2PC_6H_4$)].

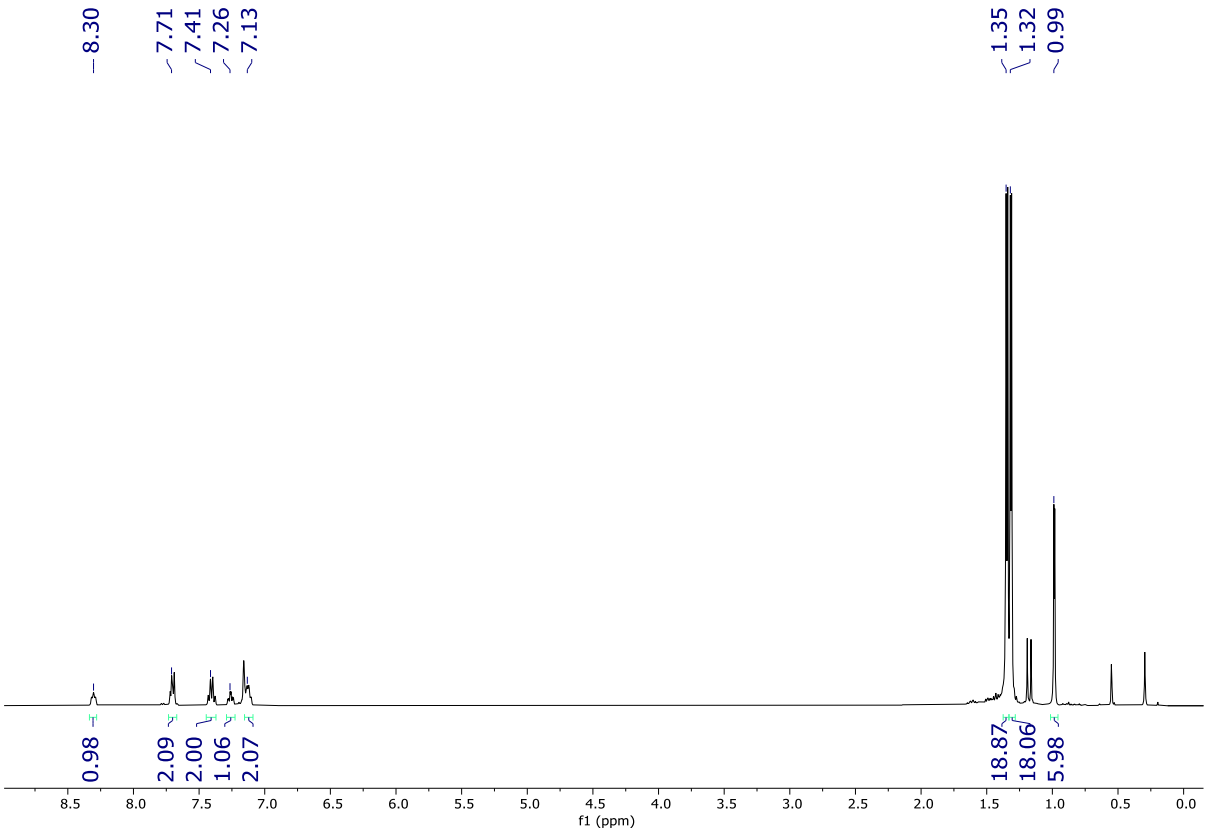

Figure S3. ^{1}H NMR spectrum showing the complete decomposition of (^{tBu}PSiP)Pd(CH_3). The peaks are picked for the major decomposition product, which is the rearranged product [(κ^2-$^{t}Bu_2PC_6H_4SiMe_2$)Pd(κ^2-$^{t}Bu_2PC_6H_4$)].

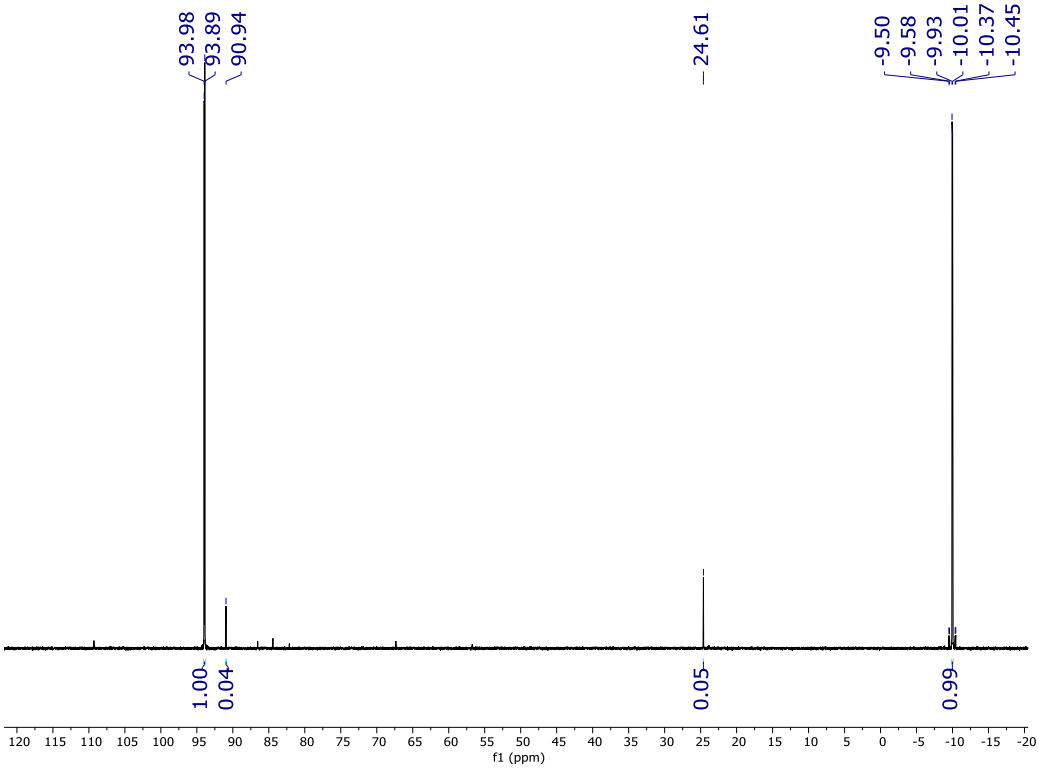

Figure S4. $^{31}P\{^{1}H\}$ NMR spectrum showing the complete decomposition of (^{tBu}PSiP)Pd(CH_3). The major product is the rearranged product, [(κ^2-$^{t}Bu_2PC_6H_4SiMe_2$)Pd(κ^2-$^{t}Bu_2PC_6H_4$)] at 93.94 and -9.97 ppm.

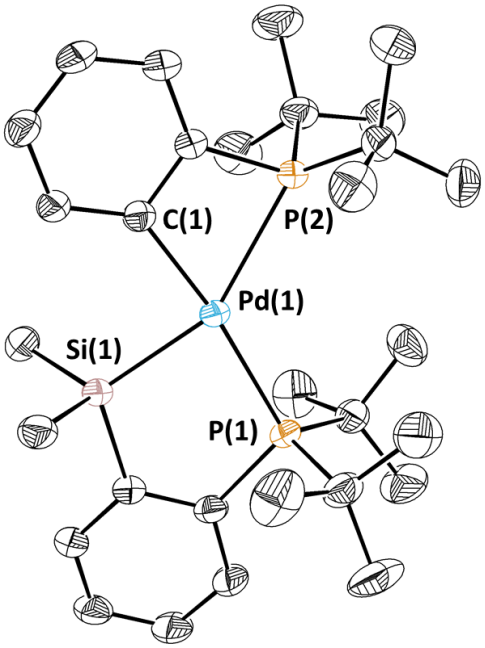

Figure S5. Solid-state structure of [(κ^2-$^{t}Bu_2PC_6H_4SiMe_2$)Pd(κ^2-$^{t}Bu_2PC_6H_4$)], the decomposition product of (^{tBu}PSiP)Pd(CH_3) with 30% thermal ellipsoid probability levels. The hydrogen atoms are omitted for clarity.

SIV. Salerno Molecular Buried Volume Calculations

The percent buried volume (%V_{bur}) of (^{Cy}PBP)Ni(CH_3) and (^{tBu}PBP)Ni(CH_3) were calculated using the Salerno molecular buried volume calculation (SambVca 2.1) software.[8] Starting geometries are based on their solid state structures.[5] For the calculations, the sphere radius was set to 3.5 Å and the sphere was centered on the metal center. The bond radii were scaled by 1.17 and hydrogen atoms were included in the calculations. The resulting topographic maps qualitatively demonstrate the steric bulk (Figure S6), where the figures are viewed down the z-axis with the metal methyl bond coming out of the plane defined by P-Ni-P. The calculated %V_{bur} are below and indicate that (^{Cy}PBP)Ni(CH_3) is less sterically bulky than (^{tBu}PBP)Ni(CH_3).

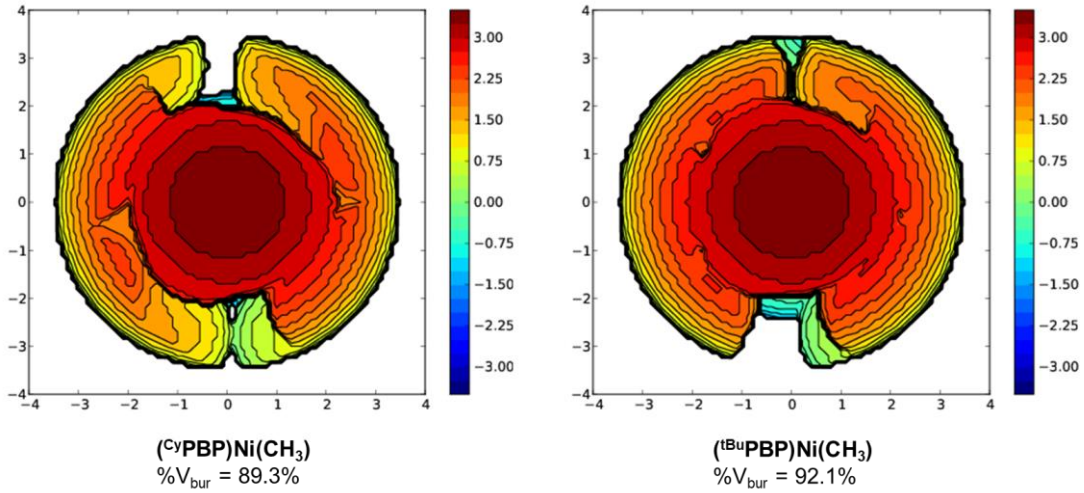

Figure S6. Topographic maps demonstrating the steric bulk of (^{Cy}PBP)Ni(CH_3) (left) and (^{tBu}PBP)Ni(CH_3) (right), calculated using the Salerno molecular buried volume calculation (SambVca 2.1).

SV: Determination of Qualitative Rates of CO_2 Insertion

The qualitative rates for the insertion of CO_2 into (^{R}PBP)M(CH_3) (R = Cy, ^{t}Bu; M = Ni, Pd) were determined through time course experiments using $^{31}P\{^{1}H\}$ NMR spectroscopy. 3.0 mg of (^{Cy}PBP)Ni(CH_3), (^{Cy}PBP)Pd(CH_3), and (^{tBu}PBP)Pd(CH_3) were each dissolved in 500 μL of C_6D_6 and added to separate J-Young NMR tubes containing PPh_3 as a standard for $^{31}P\{^{1}H\}$ NMR spectroscopy. The solutions were degassed via three freeze-pump-thaw cycles and 1 atm CO_2 was added via a Schlenk line. The tubes were allowed to stand at room temperature and were periodically checked by $^{31}P\{^{1}H\}$ NMR to monitor the disappearance of (^{R}PBP)M(CH_3) and appearance of (^{R}PBP)M{OC(O)CH_3}, using the standard to confirm mass balance. Quantitative conversion was observed for (^{Cy}PBP)Pd(CH_3) and (^{tBu}PBP)Pd(CH_3), whereas the appearance of decomposition products including (^{Cy}PBP)H is seen for (^{Cy}PBP)Ni(CH_3) (Figures S7-S8). Reaction times were 1 hour, 6 hours, and 4 days for (^{Cy}PBP)Pd(CH_3), (^{tBu}PBP)Pd(CH_3), and (^{Cy}PBP)Ni(CH_3), respectively.

An analogous experiment monitoring the insertion of CO_2 into (^{tBu}PBP)Ni(CH_3) was conducted. 1.8 mg of (^{tBu}PBP)Ni(CH_3) was dissolved in 500 μL of C_6D_6 and added to a J-Young NMR tube containing PPh_3 as a standard for $^{31}P\{^{1}H\}$ NMR spectroscopy. After the solution was degassed via three freeze-pump-thaw cycles, 1 atm of CO_2 was added. The solution was allowed to stand at room temperature and was periodically checked by $^{31}P\{^{1}H\}$ NMR spectroscopy to monitor the disappearance of (^{tBu}PBP)Ni(CH_3) and appearance of (^{tBu}PBP)Ni{OC(O)CH_3}, using the standard to confirm mass balance. After 10 days at room temperature, 29% of the (^{tBu}PBP)Ni(CH_3) starting material remained, with 51% converted to the CO_2 insertion product, (^{tBu}PBP)Ni{OC(O)CH_3}. The insertion product was assigned based off of the shift at 84.9 ppm in the $^{31}P\{^{1}H\}$ NMR spectrum, which is near the reported literature shift of 85.2 ppm for the electronically similar (^{tBu}PBP)Ni{OC(O)H} complex.[9] The remaining 20% of the mass balance was not identified but several unidentified products are present in the spectra (Figure S9).

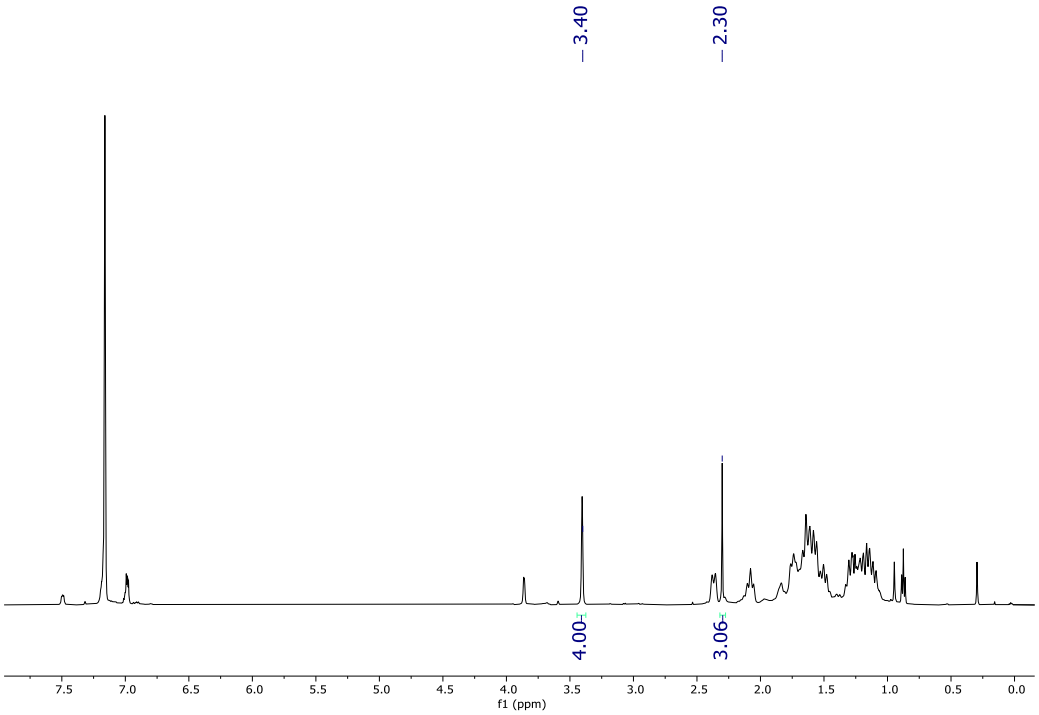

Figure S7. ^{1}H NMR spectrum 4 days after the room temperature insertion of 1 atm CO_2 into (^{Cy}PBP)Ni(CH_3). Diagnostic peaks for the major insertion product, (^{Cy}PBP)Ni{OC(O)CH_3}, appear at 3.40 and 2.30 ppm.

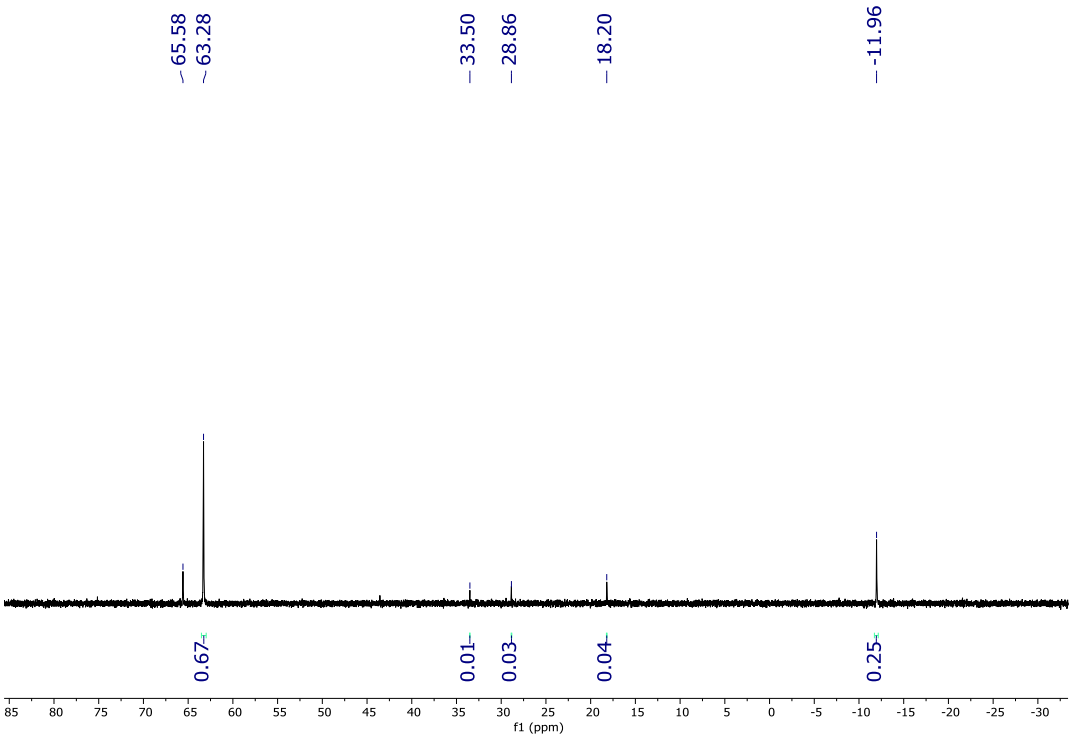

Figure S8. $^{31}P\{^{1}H\}$ NMR spectrum 4 days after the room temperature insertion of 1 atm CO_2 into (^{Cy}PBP)Ni(CH_3). The insertion product, (^{Cy}PBP)Ni{OC(O)CH_3} corresponds to the major peak at 63.28 ppm. Free (^{Cy}PBP)H (-11.96 ppm) and other unidentified decomposition products (33.50, 28.86, and 18.20 ppm) are formed during the insertion.

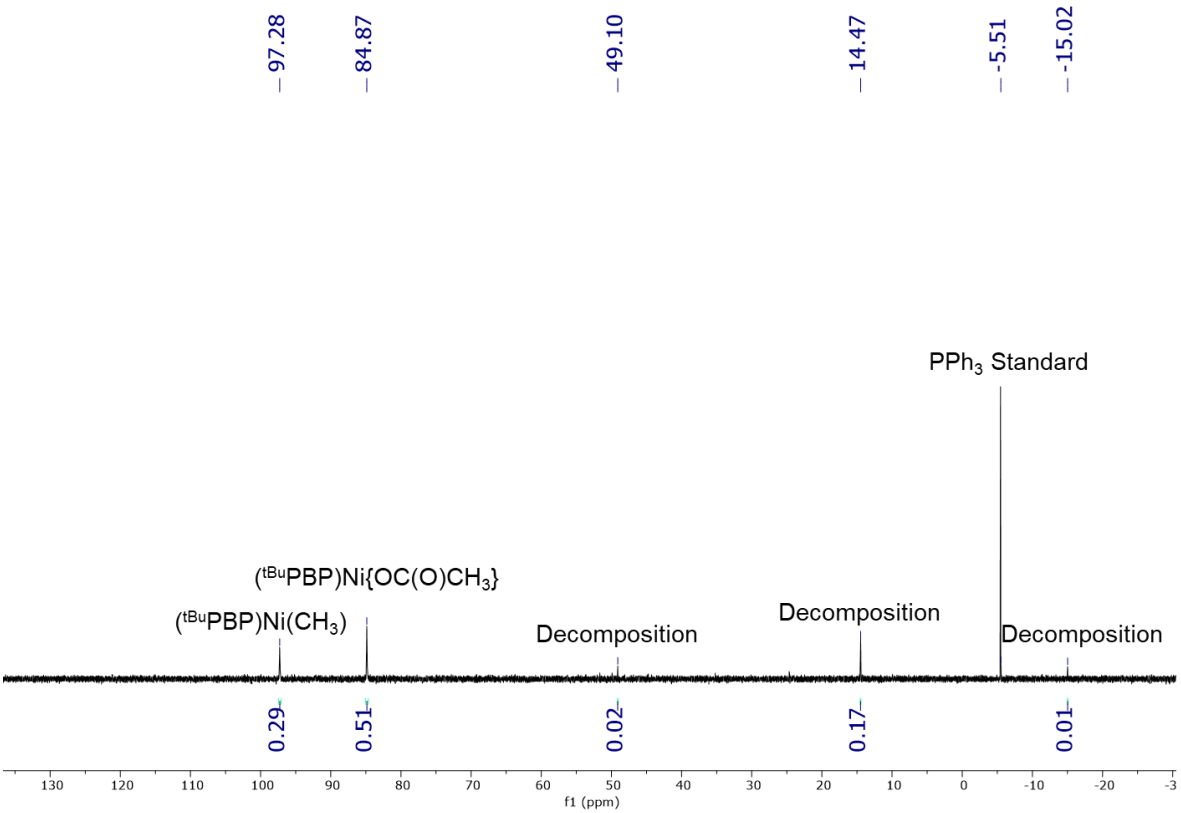

Figure S9. $^{31}P\{^{1}H\}$ NMR spectrum 10 days after the room temperature insertion of 1 atm CO_2 into (^{tBu}PBP)Ni(CH_3). The desired insertion product, (^{tBu}PBP)Ni{OC(O)CH_3}, was formed in 51% yield (84.87 ppm) with 29% of the starting complex, (^{tBu}PBP)Ni(CH_3), (97.28 ppm) remaining. Decomposition products (49.10, 14.47, and -15.02 ppm) account for the remaining 20% of mass balance.

SVI. Determination of [CO_2] by Quantitative $^{13}C\{^1H\}$ NMR Spectroscopy

In order to obtain k_1 values from experimentally measured k_{obs} values, the concentration of CO_2 dissolved in solution must be known. A modified literature procedure was used to measure [CO_2] using quantitative $^{13}C\{^1H\}$ NMR spectroscopy.[10] Specifically, a J-Young NMR tube was charged with 500 μL of solvent and 10 μL of toluene as an internal standard. The solution was degassed via three freeze-pump-thaw cycles and 1 atm CO_2 was added via a Schlenk line. The J-Young NMR tube was then inserted into a 500 MHz NMR spectrometer set to the desired temperature, and an inverse-gated $^{13}C\{^1H\}$ NMR spectrum was acquired using a relaxation delay of 60 seconds (the relaxation time of CO_2 is approximately 10 seconds under our conditions). The concentration of CO_2 was determined through comparison of the integration of the toluene quaternary carbon peak at 137.90 ppm with the integration of the CO_2 peak at 124.77 ppm. A representative $^{13}C\{^1H\}$ NMR is shown in Figure S10. Although the quaternary carbon peak is used for the determination of the concentration of CO_2, the other toluene peaks also integrate as expected (Figure S11). Each experiment was replicated and the results are summarized in Table S1.

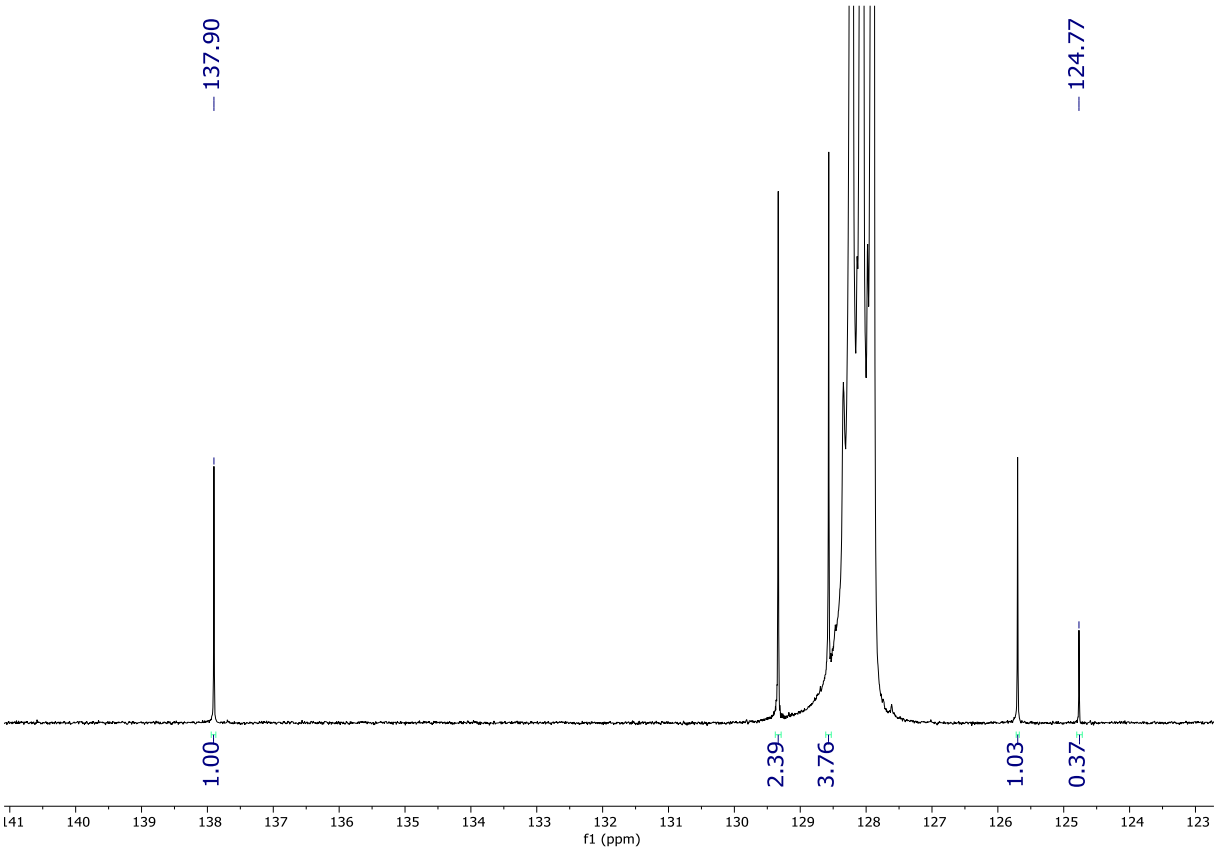

Figure S10. Determination of [CO_2] in C_6D_6 at 40 °C using $^{13}C\{^1H\}$ NMR spectroscopy. The integration of the quaternary toluene standard peak (137.91 ppm) with known concentration is compared to the integration of the CO_2 peak (124.84 ppm) to determine [CO_2].

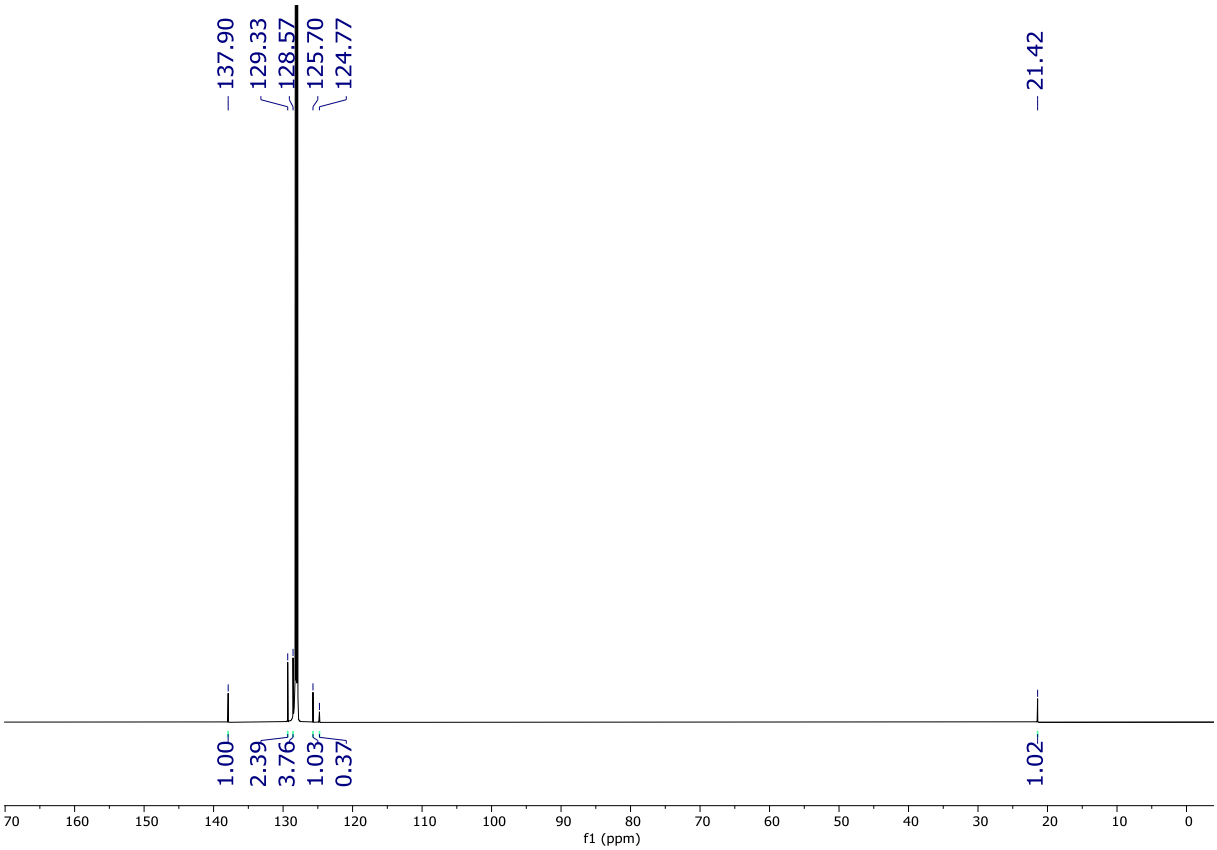

Figure S11. Full spectrum for the determination of [CO_2] in C_6D_6 at 40 °C using $^{13}C\{^1H\}$ NMR spectroscopy. The toluene peaks at 137.90, 125.70, and 21.42 ppm integrate in a 1:1:1 ratio. The toluene peaks at 129.33 and 128.57 ppm have higher integrations (2.39 and 3.76) than expected due to overlap with the solvent C_6D_6 peak.

Solvent	Temperature (°C)	[CO_2]
Benzene-d_6	40	0.060
Benzene-d_6	45	0.053
Benzene-d_6	50	0.049
Benzene-d_6	55	0.045
Benzene-d_6	60	0.040
Toluene-d_8	40	0.063
1,4-Dioxane	40	0.098
Glyme	40	0.095
THF	40	0.090

Table S1. Summary of the measured [CO_2] in different solvents and at different temperatures. The concentration of CO_2 is the average of two trials.

SVII. Representative Kinetic Data Workup: Determination of k_1 Using ^{1}H NMR Spectroscopy

Experimental

In a nitrogen-filled glovebox, (^{tBu}PBP)Pd(CH_3) (2.0 mg, 0.0036 mmol) was added to a J-Young NMR tube with 400 μL of C_6D_6 and 100 μL of a 0.054 M hexamethylbenzene stock solution. The J-Young NMR tube was attached to a Schlenk line with a J-Young to 24/40 adaptor, and vacuum was pulled on the closed system to remove air. The tube was degassed via three freeze-pump-thaw cycles. The pressure of CO_2 in the Schlenk line was measured with a Wallace & Tiernan 61B-1D-0800 Absolute Pressure Gauge prior to addition of CO_2 to the tube. A low-pressure regulator on the CO_2 cylinder allowed for the pressure of CO_2 to be varied to pressures below 1 atm, so that the order of [CO_2] in the rate law could be determined. CO_2 was then introduced into the J-Young NMR tube. The tube was inserted into a 500 MHz NMR spectrometer, with the temperature preset to 40 °C. After the temperature regulated back to 40 °C, the sample was taken out and shaken, and placed back into the NMR probe. A ^{1}H NMR array experiment was conducted, where a new ^{1}H spectrum (8 scans) was acquired every 32 seconds (Figure S12). When required, the temperature in the NMR spectrometer was determined using an ethylene glycol standard.

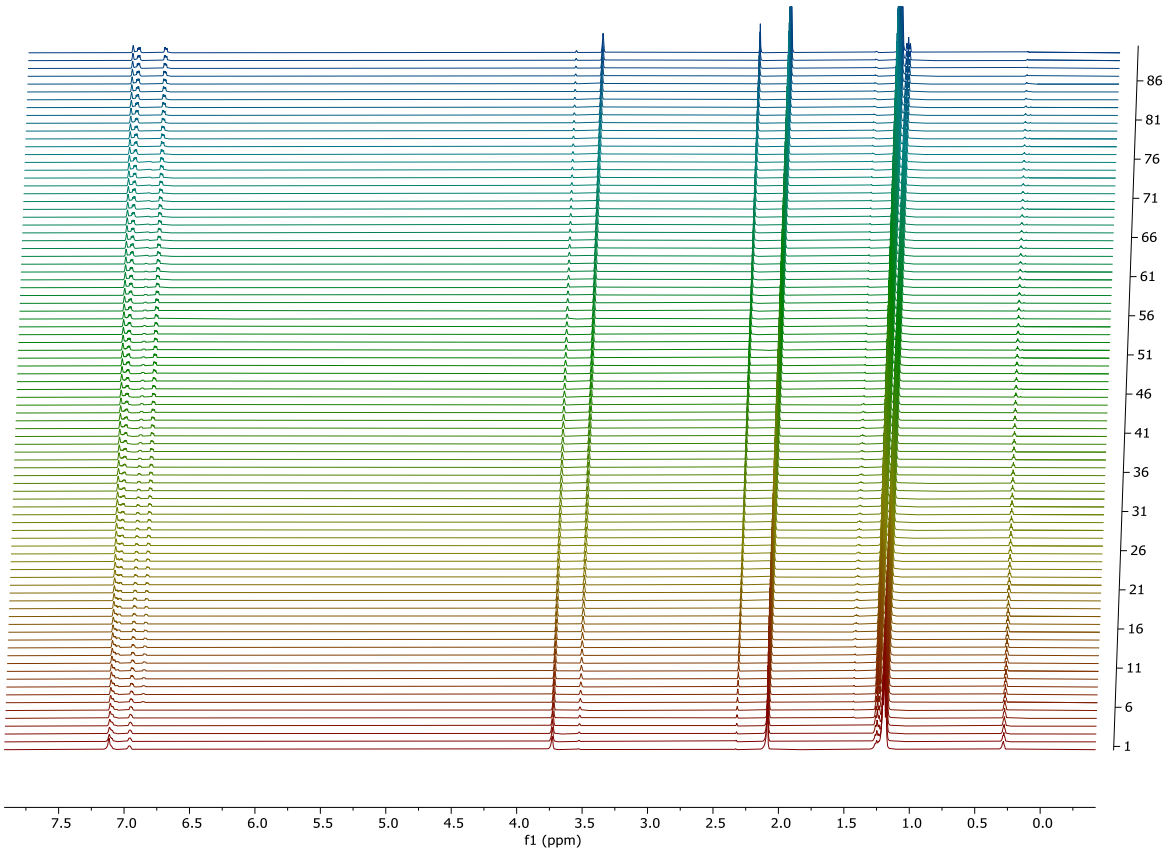

Figure S12. Representative ^{1}H NMR array for the insertion of CO_2 into (^{tBu}PBP)Pd(CH_3) at 40 °C in C_6D_6.

Data Workup

The ^{1}H NMR array was baseline and phase corrected before integration of the (^{tBu}PBP)Pd(CH_3) (3.73 and 0.30 ppm), (^{tBu}PBP)Pd{OC(O)CH_3} (3.53 and 2.33 ppm), and hexamethylbenzene standard (2.09 ppm) peaks. The disappearance of the -C*H*$_2$ and -C*H*$_3$ peaks of the (^{tBu}PBP)Pd(CH_3) complex and the appearance of the -C*H*$_2$ and -C*H*$_3$ peaks of the (^{tBu}PBP)Pd{OC(O)CH_3} complex could be used to monitor reaction progress. Ultimately, the disappearance of the (^{tBu}PBP)Pd(CH_3) -C*H*$_2$ peak at 3.73 ppm was used to determine kinetic rates. Using the Data Analysis feature of Mestrenova, a table of the absolute integrals for each spectrum was generated. The following data analysis was performed using Microsoft Excel. The concentration of (^{tBu}PBP)Pd(CH_3) was obtained by dividing the absolute integration of the -C*H*$_2$ peak by the absolute integration of the hexamethylbenzene standard for each spectrum, then multiplying by 18/4 to correct for number of protons, as well as multiplying by the known concentration of hexamethylbenzene. Once the concentration of (^{tBu}PBP)Pd(CH_3) was calculated for each spectrum, a graph of ln([(^{tBu}PBP)Pd(CH_3)]) vs. time was plotted, where the slope of the line yields k_{obs}. The first data point was omitted in all cases due to a broad spectrum as a result of the sample heating up to the NMR probe temperature. A value of k_1 can be extracted from k_{obs} by dividing by the [CO_2], which was determined by quantitative ^{13}C{^{1}H} NMR experiments (see SVI).

SVIII. Representative Kinetic Data Workup: Determination of k_1 Using $^{31}P\{^1H\}$ NMR Spectroscopy

Experimental

In a nitrogen-filled glovebox, (^{tBu}PBP)Pd(CH_3) (2.0 mg, 0.0036 mmol) was added to a J-Young NMR tube with 500 μL of 1,4-dioxane and a C_6D_6 capillary with a PPh_3 as a standard. The J-Young NMR tube was attached to a Schlenk line with a J-Young to 24/40 adaptor, and vacuum was pulled on the adaptor and closed J-Young to remove air. The tube was degassed via three freeze-pump-thaw cycles. An initial $^{31}P\{^1H\}$ NMR spectrum was taken with the degassed sample at 40° C to shim the instrument, in order to collect kinetics as soon as possible after the insertion. The J-Young NMR tube was then reattached to the Schlenk line and vacuum was pulled on the adaptor and closed J-Young to remove air. The pressure of CO_2 in the Schlenk line was measured with a Wallace & Tiernan 61B-1D-0800 Absolute Pressure Gauge prior to addition of CO_2 to the tube. CO_2 at 1 atm was introduced into the J-Young NMR tube. The tube was inserted into a 500 MHz NMR spectrometer, with the temperature preset to 40 °C. After the temperature regulated back to 40 °C, the sample was taken out and shaken, and placed back into the NMR probe. A $^{31}P\{^1H\}$ NMR array experiment was conducted, where a new $^{31}P\{^1H\}$ spectrum (32 scans) was acquired every 54 seconds (Figure S13).

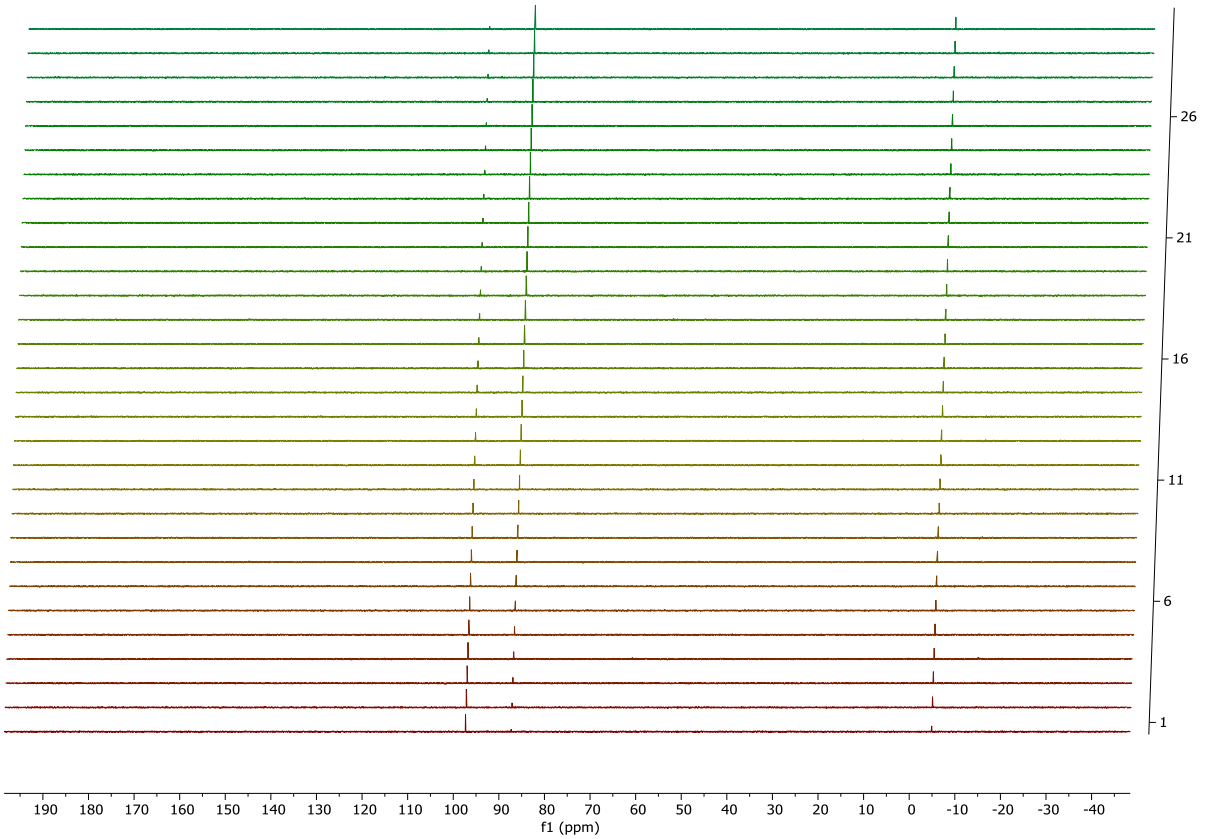

Figure S13. Representative $^{31}P\{^1H\}$ NMR array for the insertion of CO_2 into (^{tBu}PBP)Pd(CH_3) at 40 °C in 1,4-dioxane.

Data Workup

The $^{31}P\{^{1}H\}$ NMR array was baseline and phase corrected before integration of the (^{tBu}PBP)Pd(CH_3) (97.3 ppm), (^{tBu}PBP)Pd{OC(O)CH_3} (87.5 ppm), and PPh_3 standard (-5.0 ppm) peaks. The disappearance of the phosphine peak of the (^{tBu}PBP)Pd(CH_3) complex and the appearance of the phosphine peak of the (^{tBu}PBP)Pd{OC(O)CH_3} complex could be used to monitor reaction progress (Figure S14a). Ultimately, the disappearance of the (^{tBu}PBP)Pd(CH_3) phosphine peak at 97.3 ppm was used to determine kinetic rates. Using the Data Analysis feature of Mestrenova, a table of the absolute integrals for each spectrum could be generated. The following data analysis was done using Microsoft Excel. The concentration of (^{tBu}PBP)Pd(CH_3) was obtained by dividing the absolute integration of the phosphine peak by the absolute integration of the PPh_3 standard for each spectrum. This number was then multiplied by the ratio of the known concentration of (^{tBu}PBP)Pd(CH_3) at time t = 0 to the PPh_3 standard, in order to obtain a concentration at each point. Once the concentration of (^{tBu}PBP)Pd(CH_3) was calculated for each spectrum, a graph of ln([(^{tBu}PBP)Pd(CH_3)]) vs. time was plotted, where the slope of the line yields k_{obs} (Figure S14b). The first data point was omitted in all cases due to a broad spectrum as a result of the sample heating up to the NMR probe temperature. A value of k_1 can be extracted from k_{obs} by dividing by the [CO_2], which was determined by quantitative $^{13}C\{^{1}H\}$ NMR experiments (see SVI).

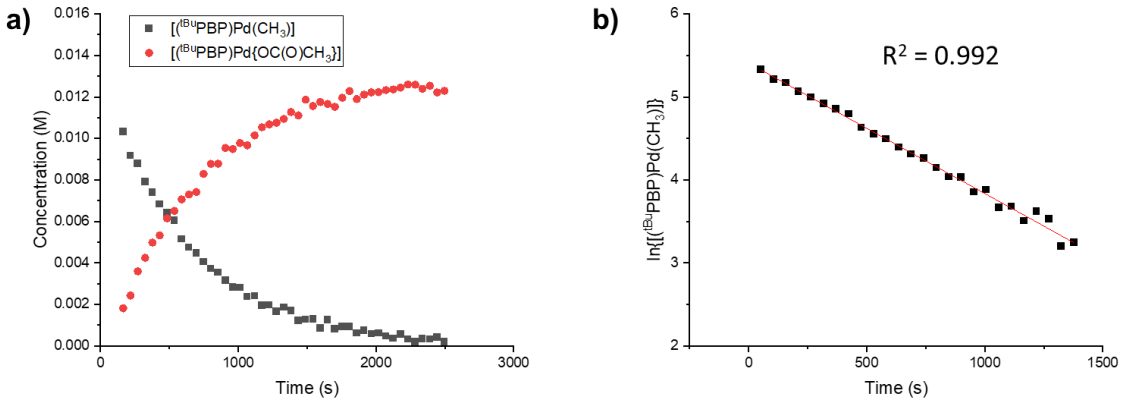

Figure S14. Representative traces for the insertion of CO_2 into (^{tBu}PBP)Pd(CH_3) at 40 °C in C_6D_6 with 1 atm of CO_2 showing a) the concentrations of (^{tBu}PBP)Pd(CH_3) and (^{tBu}PBP)Pd{OC(O)CH_3} as a function of time and b) the ln of the concentration of (^{tBu}PBP)Pd(CH_3) as a function of time.

SIX. Eyring Analysis for the insertion of CO_2 into (^{tBu}PBP)Pd(CH_3) in C_6D_6

The rate of insertion of CO_2 into (^{tBu}PBP)Pd(CH_3) was obtained at temperatures varying from 40-60 °C (Figure S15). Eyring plots were constructed from this data in order to obtain values for $\Delta S^{\ddagger}$ and $\Delta H^{\ddagger}$. $\Delta G^{\ddagger}$ was calculated using $\Delta G^{\ddagger} = \Delta H^{\ddagger} - T\Delta S^{\ddagger}$.

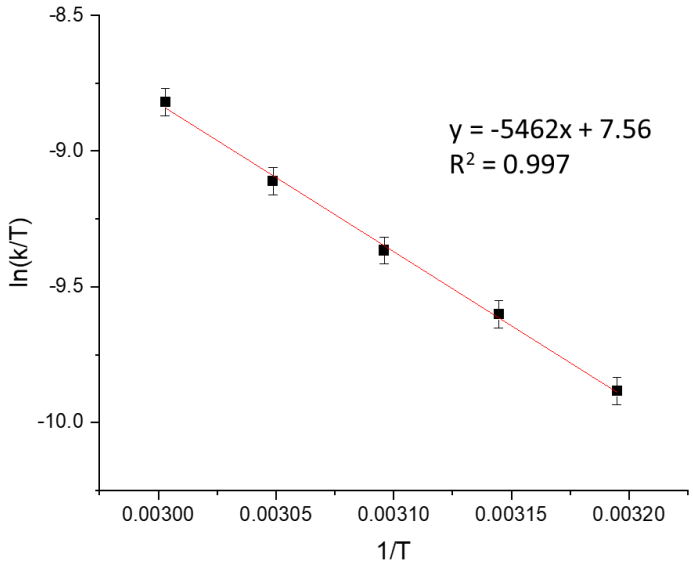

Figure S15. Eyring plot for the reaction of (^{tBu}PBP)Pd(CH_3) with 1 atm CO_2 in C_6D_6. Activation parameters: $\Delta H^{\ddagger}$ = 10.9 ± 1.1 kcal/mol, $\Delta S^{\ddagger}$ = -32.2 ± 3.2 cal/molK, and $\Delta G^{\ddagger}$ = 20.5 ± 2.1 kcal/mol.

SX. Solvent Effects: Dielectric Constant and Gutmann Acceptor Number

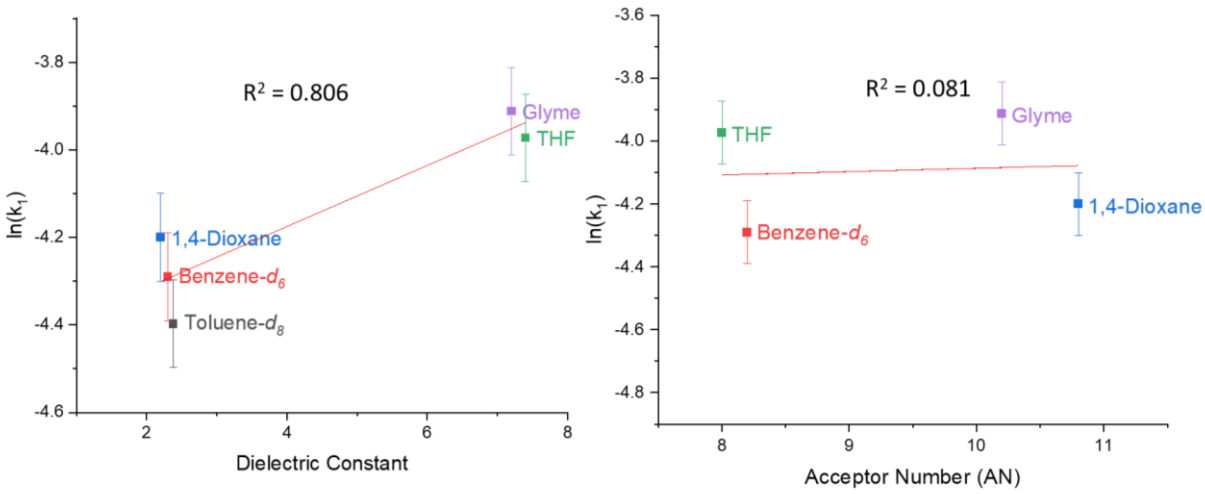

Figure S16. Plot of $\ln(k_1)$ for the insertion of CO_2 into (^{tBu}PBP)Pd(CH_3) versus the dielectric constant (left) and Gutmann Acceptor Number[11] (right) solvent parameters for various solvents at 40 °C and 1 atm of CO_2.

SXI. NMR and IR Spectra of New Compounds

(^{tBu}PBP)Pd(CH_3)

NMR spectra for (^{tBu}PBP)Pd(CH_3) at 25 °C in C_6D_6 are shown in Figures S17-S19.

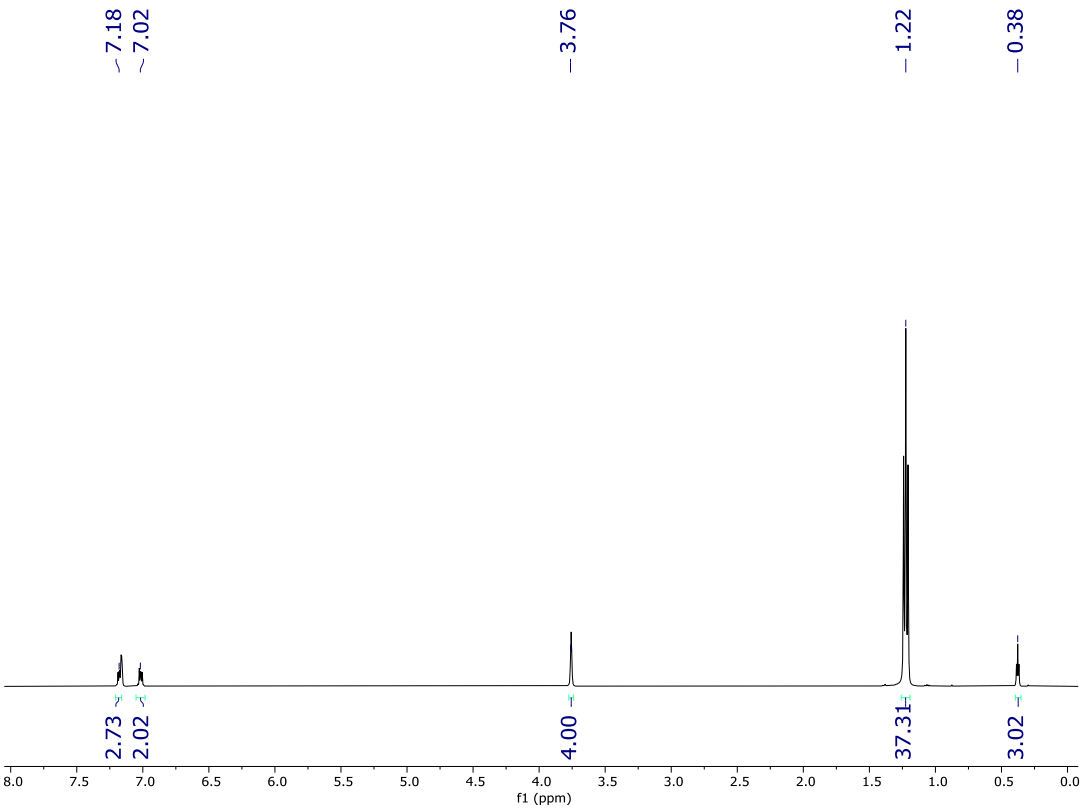

Figure S17. ^{1}H NMR spectrum of (^{tBu}PBP)Pd(CH_3) in C_6D_6 at room temperature.

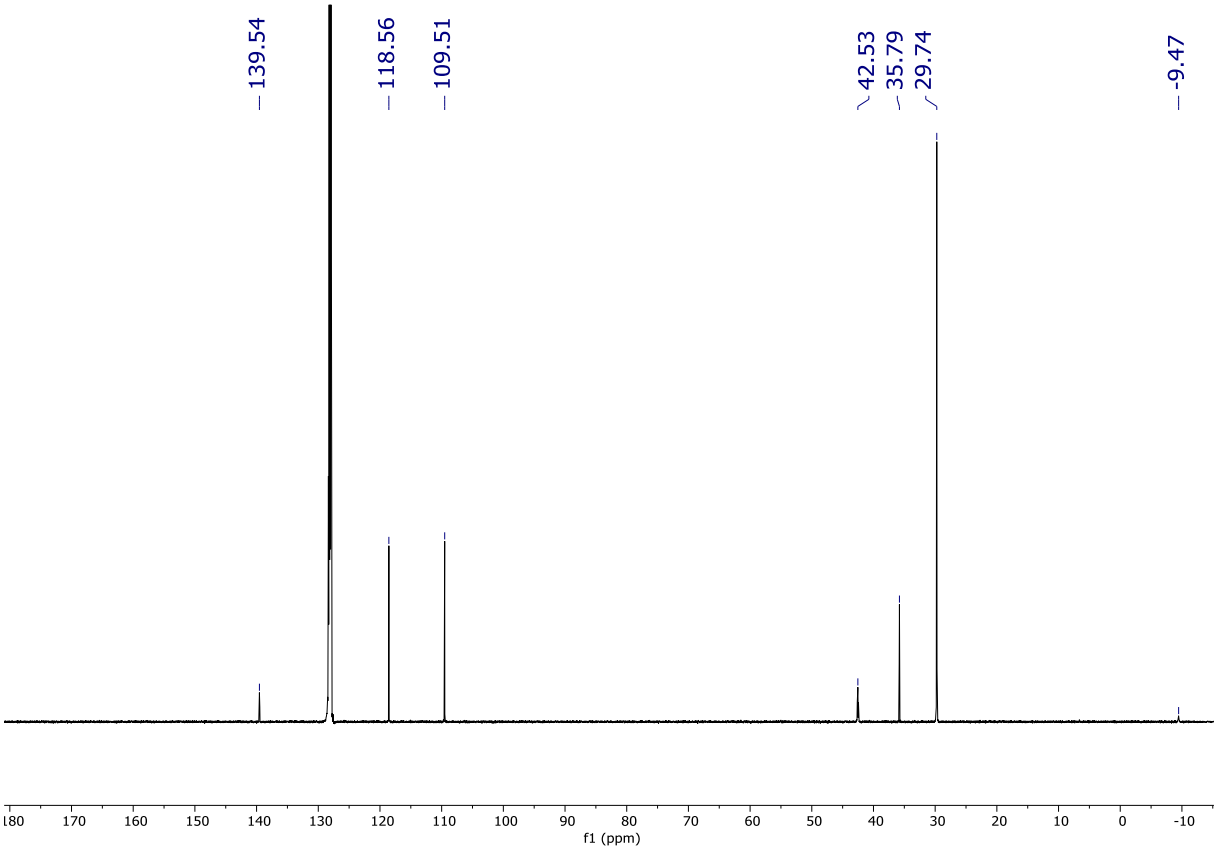

Figure S18. $^{13}C\{^{1}H\}$ NMR spectrum of (^{tBu}PBP)Pd(CH_3) in C_6D_6 at room temperature.

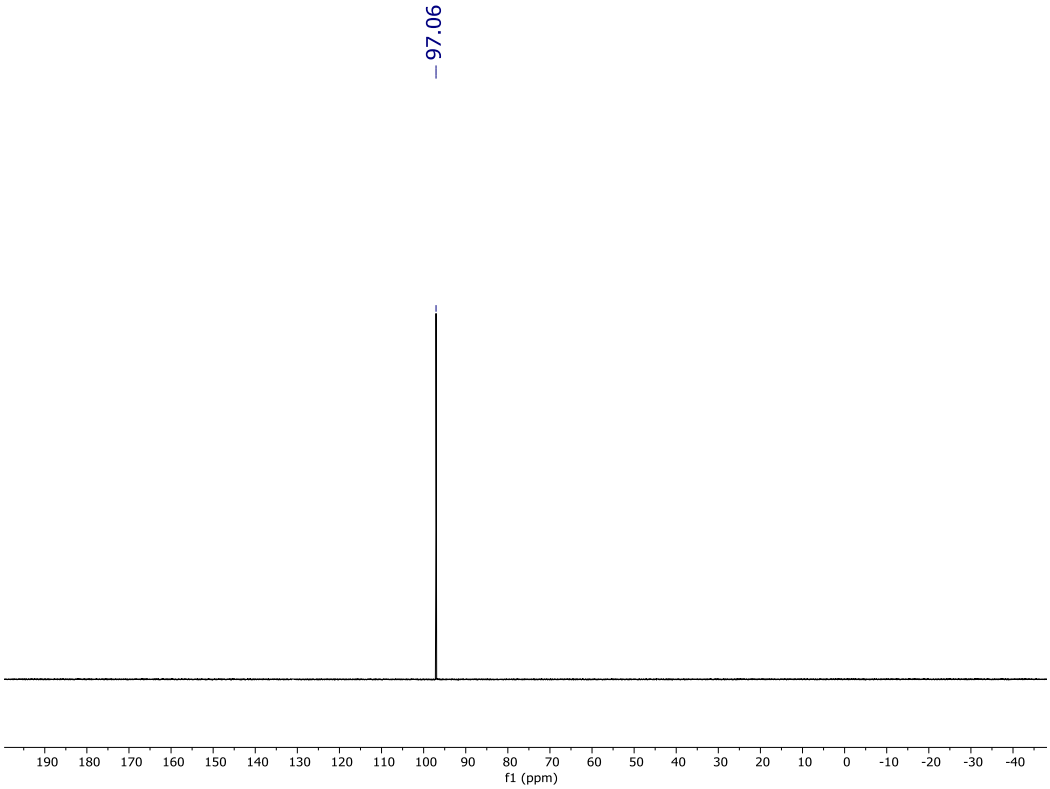

Figure S19. $^{31}P\{^{1}H\}$ NMR spectrum of (^{tBu}PBP)Pd(CH_3) in C_6D_6 at room temperature.

(^{tBu}PBP)Pd{OC(O)CH_3}

NMR and IR spectra for (^{tBu}PBP)Pd{OC(O)CH_3} at 25 °C in C_6D_6 are shown in Figures S20-S23.

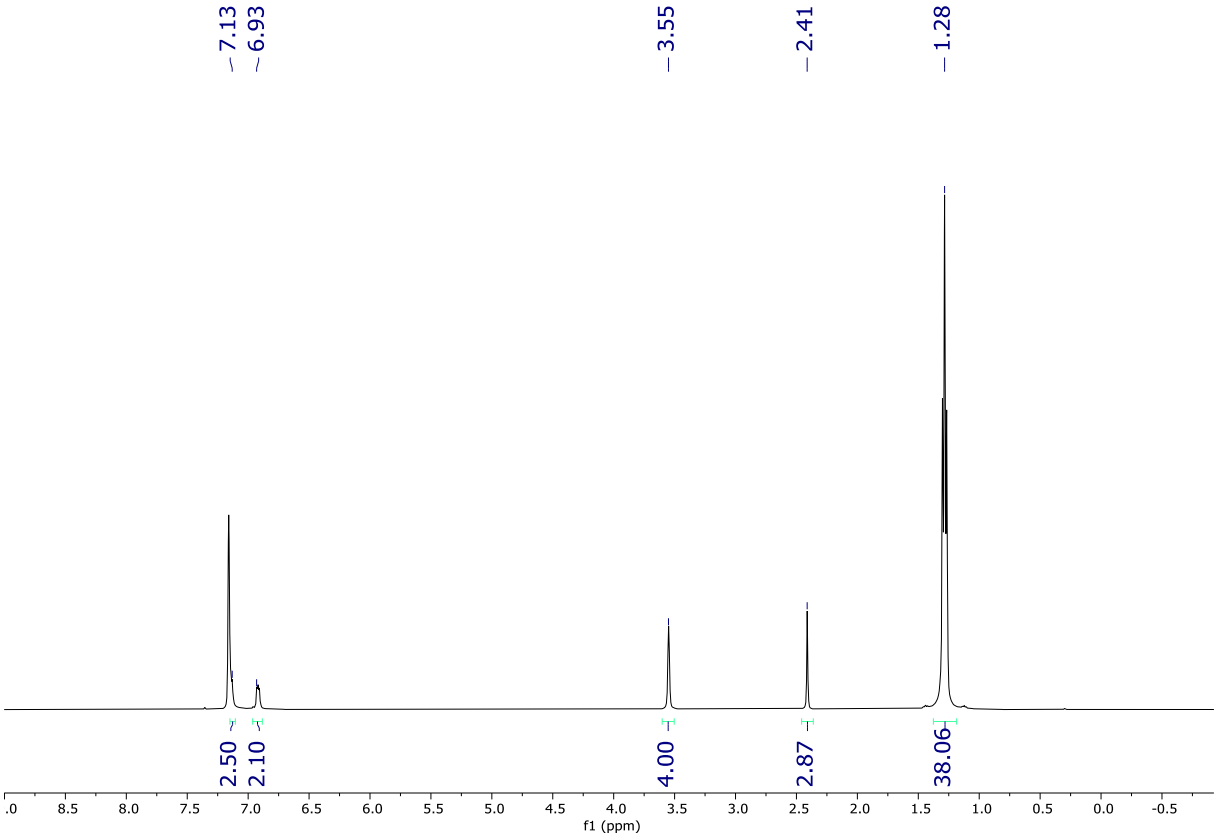

Figure S20. ^{1}H NMR spectrum of (^{tBu}PBP)Pd{OC(O)CH_3} in C_6D_6 at room temperature.

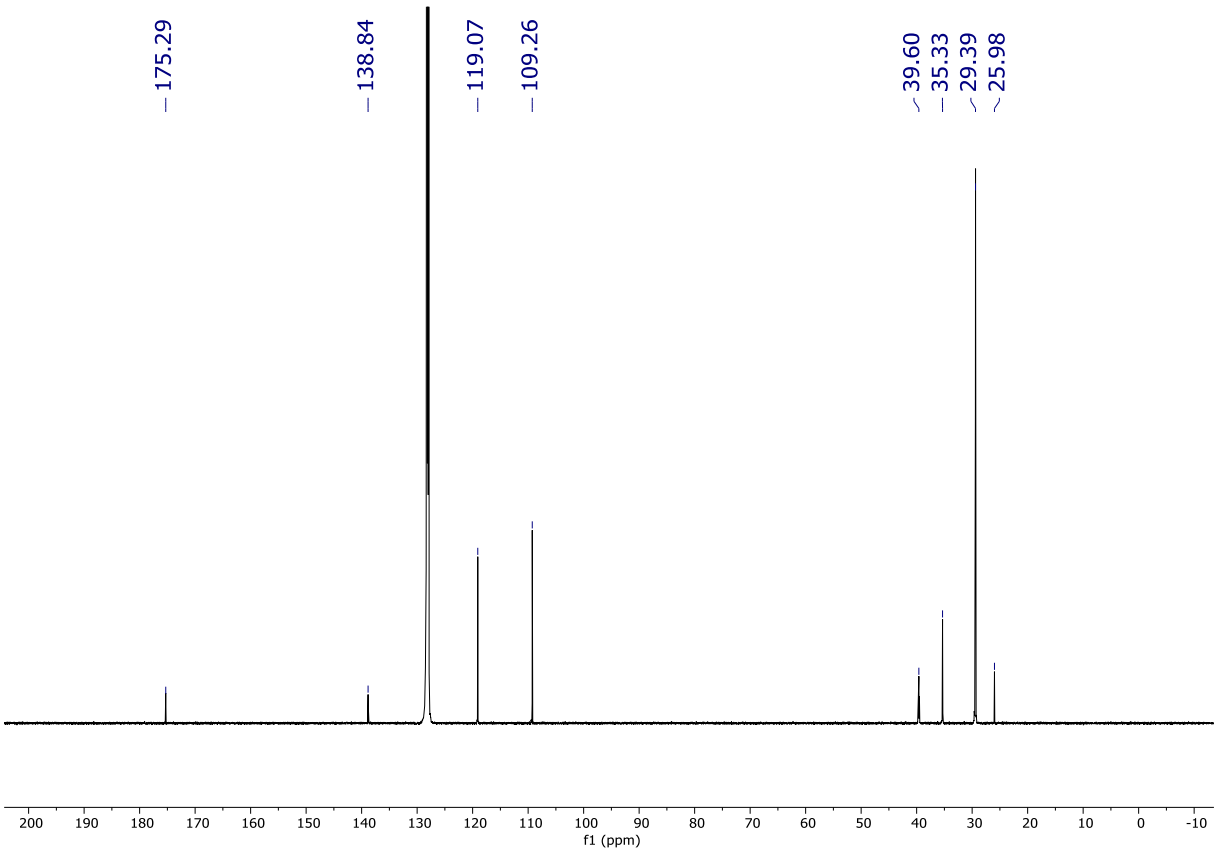

Figure S21. $^{13}C\{^{1}H\}$ NMR spectrum of (^{tBu}PBP)Pd{OC(O)CH_3} in C_6D_6 at room temperature.

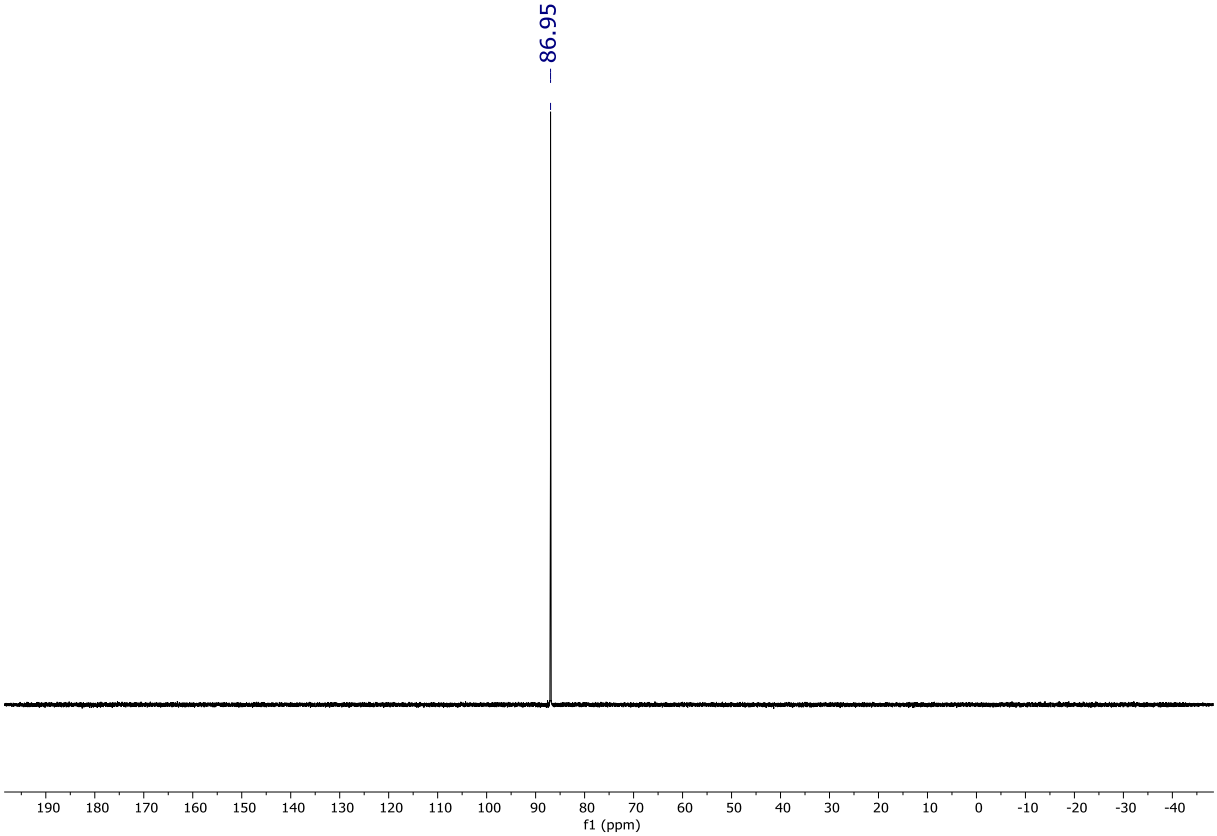

Figure S22. $^{31}P\{^{1}H\}$ NMR spectrum of (^{tBu}PBP)Pd{OC(O)CH_3} in C_6D_6 at room temperature.

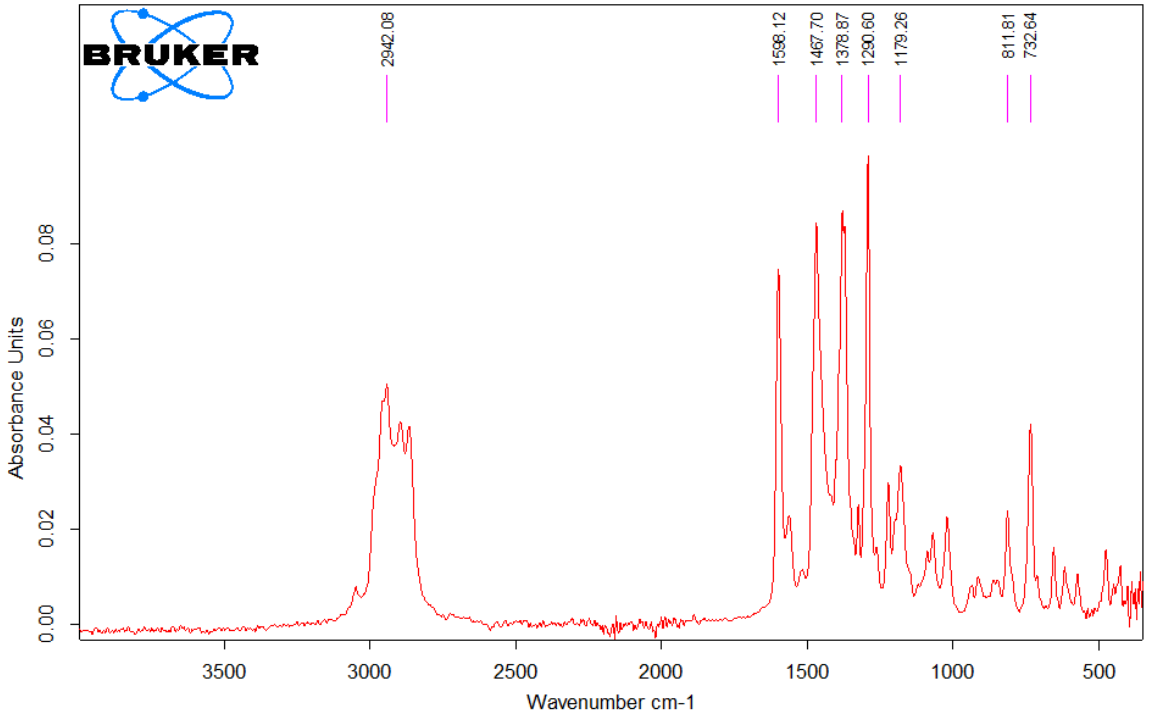

Figure S23. IR spectrum of (^{tBu}PBP)Pd{OC(O)CH$_3$}.

(^{Cy}PBP)PdCl

NMR spectra for (^{Cy}PBP)PdCl at 25 °C in C_6D_6 are shown in Figures S24-S26.

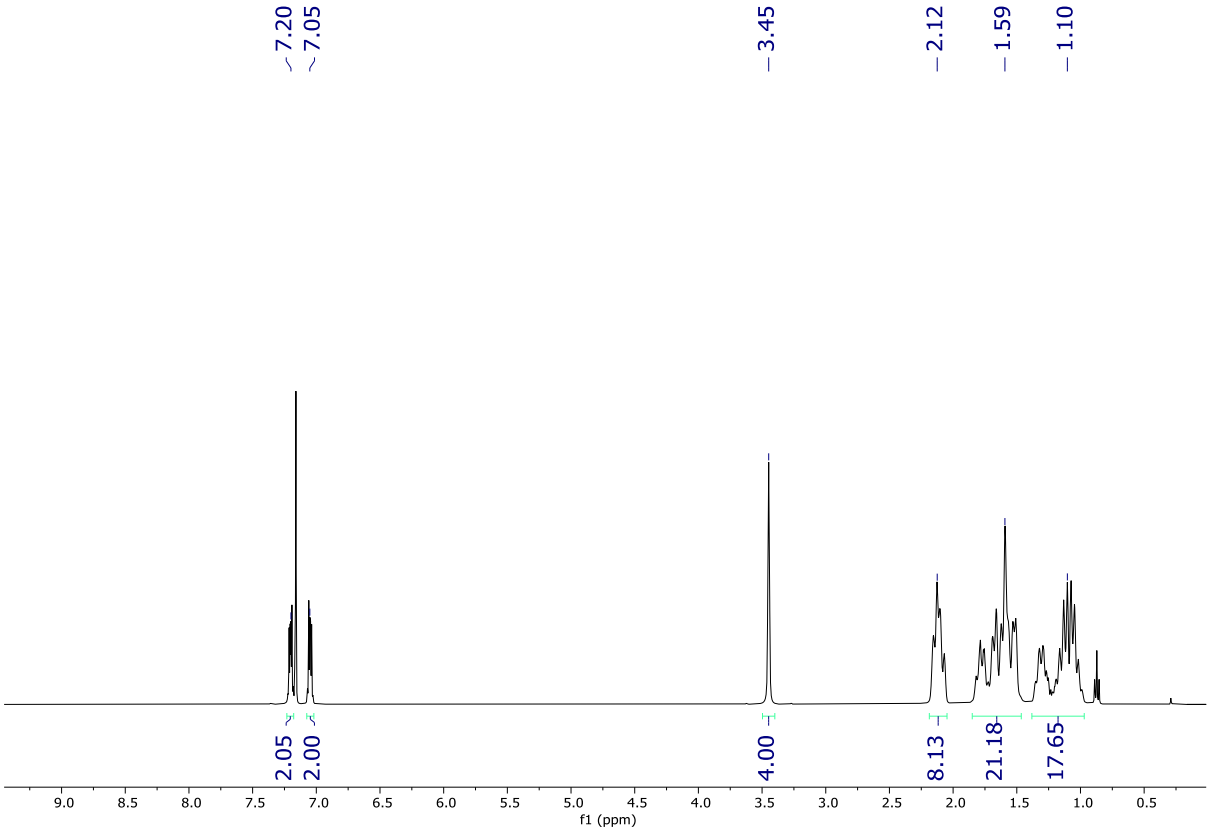

Figure S24. ^{1}H NMR spectrum of (^{Cy}PBP)PdCl in C_6D_6 at room temperature. *n*-Pentane (0.87, 1.23 ppm) is present in the spectrum.

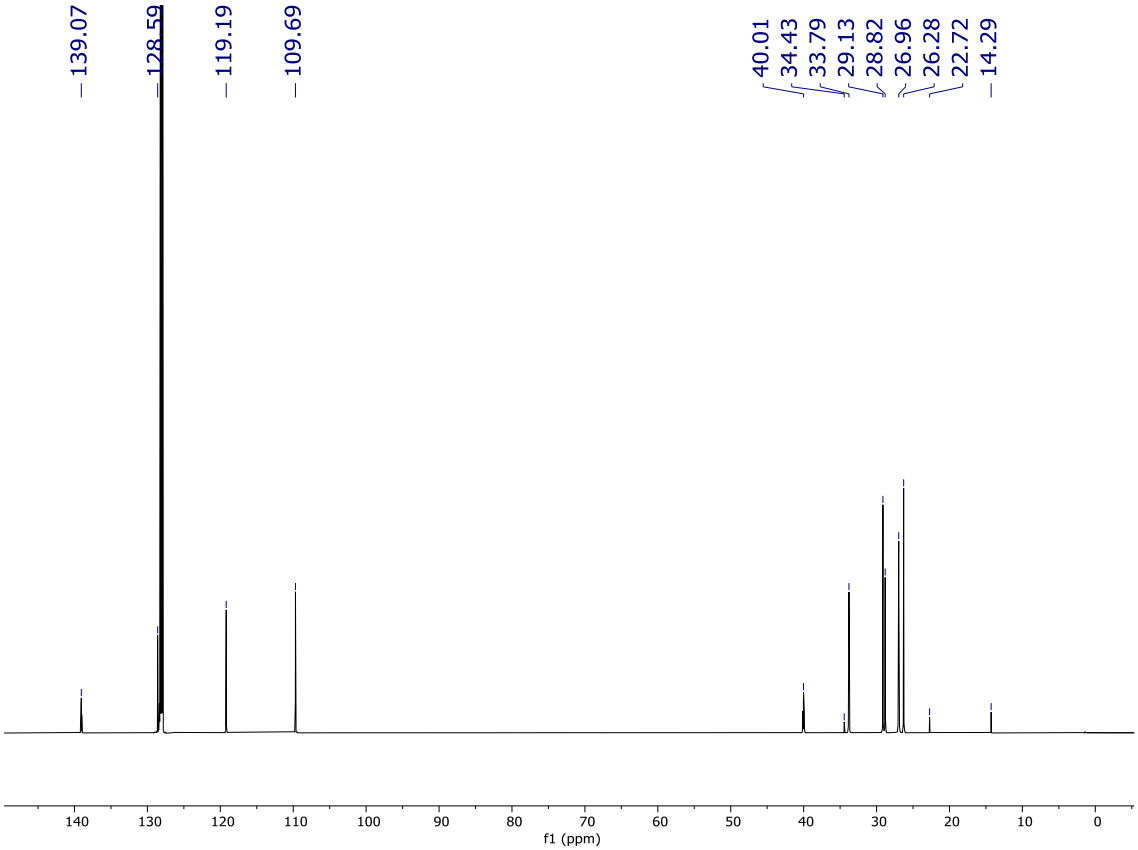

Figure S25. $^{13}C\{^{1}H\}$ NMR spectrum of (^{Cy}PBP)PdCl in C_6D_6 at room temperature. *n*-Pentane (34.33, 22.72, 14.29 ppm) is present in the spectrum.

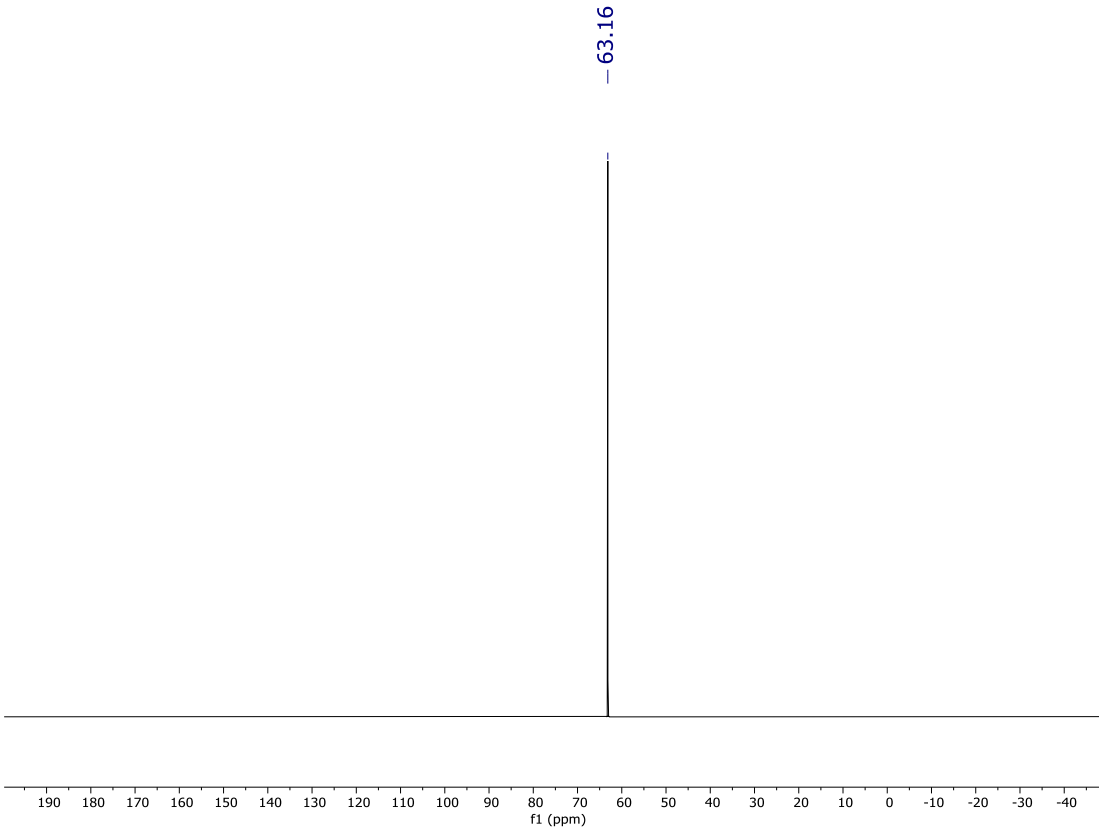

Figure S26. $^{31}P\{^{1}H\}$ NMR spectrum of (^{Cy}PBP)PdCl in C_6D_6 at room temperature.

(^{Cy}PBP)Pd(CH_3)

NMR spectra for (^{Cy}PBP)Pd(CH_3) at 25 °C in C_6D_6 are shown in Figures S27-S29.

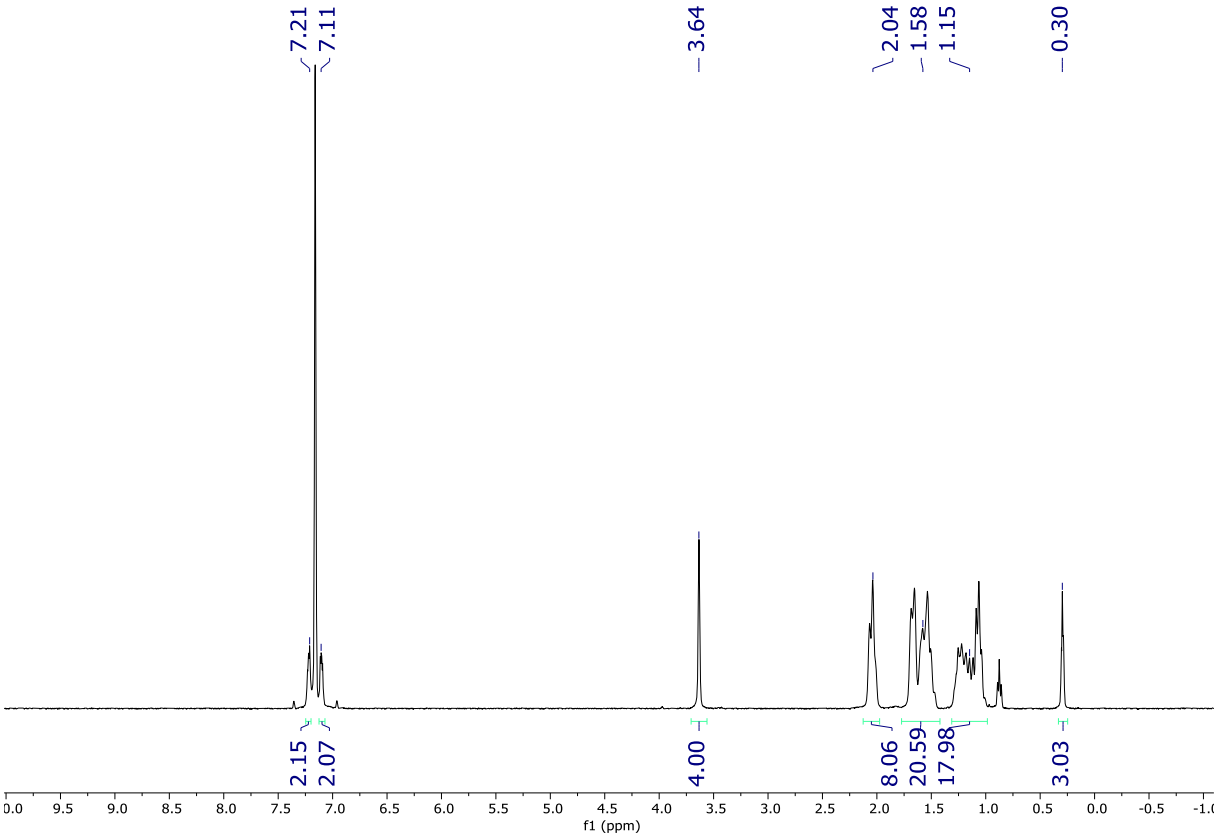

Figure S27. ^{1}H NMR spectrum of (^{Cy}PBP)Pd(CH_3) in C_6D_6 at room temperature. *n*-Pentane (0.87, 1.23 ppm) is present in the spectrum.

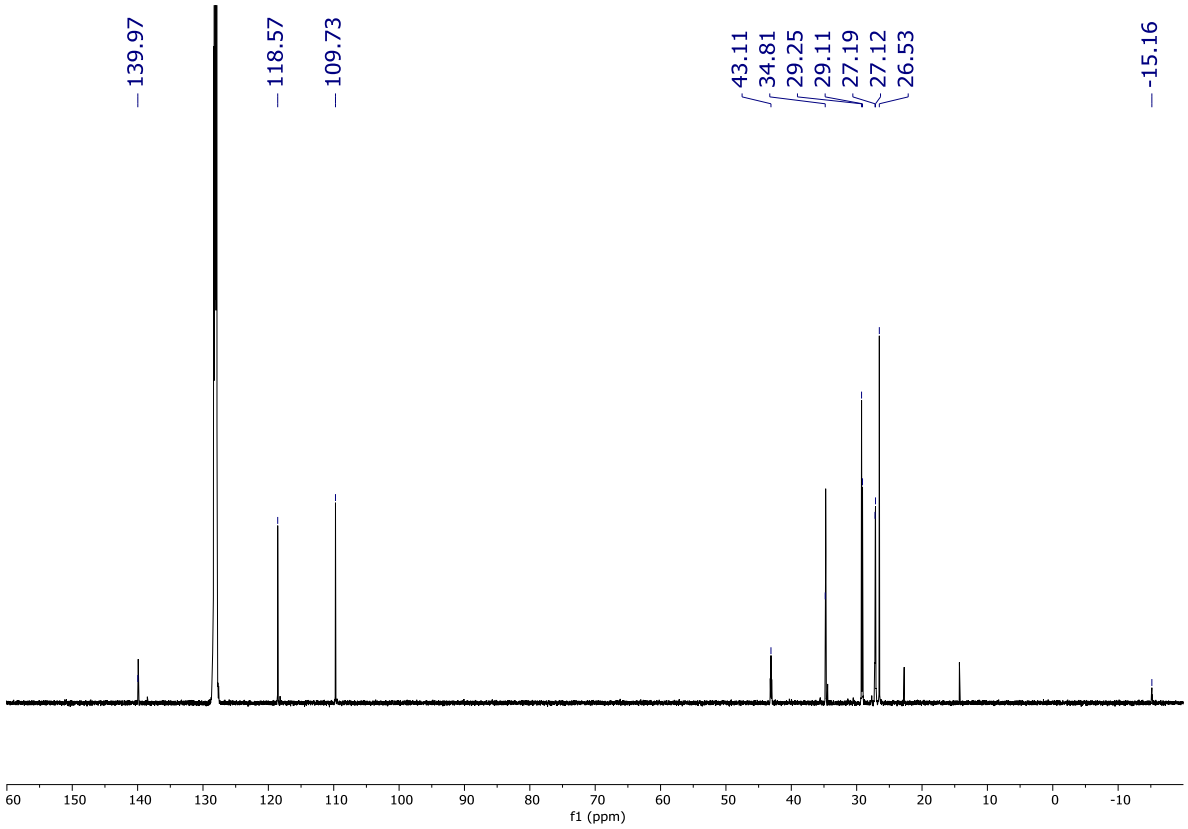

Figure S28. $^{13}C\{^{1}H\}$ NMR spectrum of (^{Cy}PBP)Pd(CH_3) in C_6D_6 at room temperature. *n*-Pentane (34.44, 22.73, 14.28 ppm) is present in the spectrum.

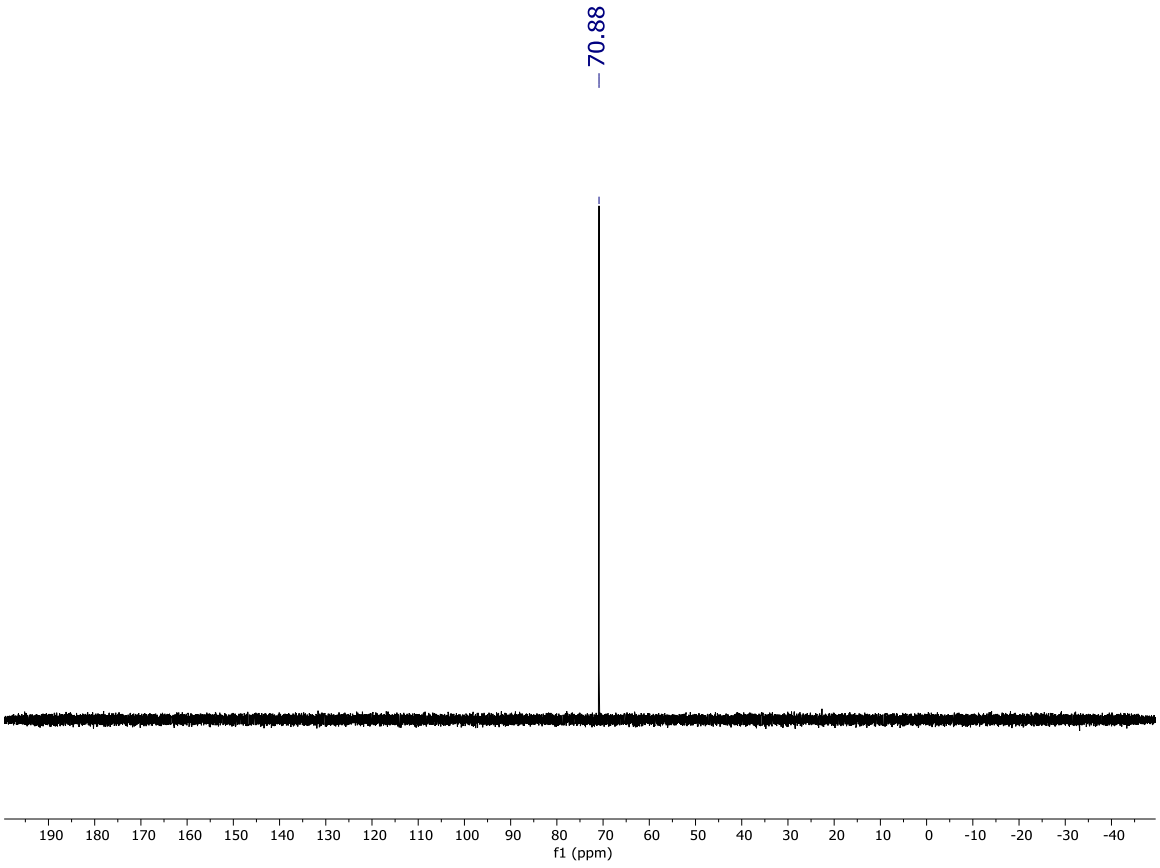

Figure S29. $^{31}P\{^{1}H\}$ NMR spectrum of (^{Cy}PBP)Pd(CH_3) in C_6D_6 at room temperature.

(^{Cy}PBP)Pd{OC(O)CH$_3$}

NMR and IR spectra for (^{Cy}PBP)Pd{OC(O)CH$_3$} at 25 °C in C_6D_6 are shown in Figures S30-S33.

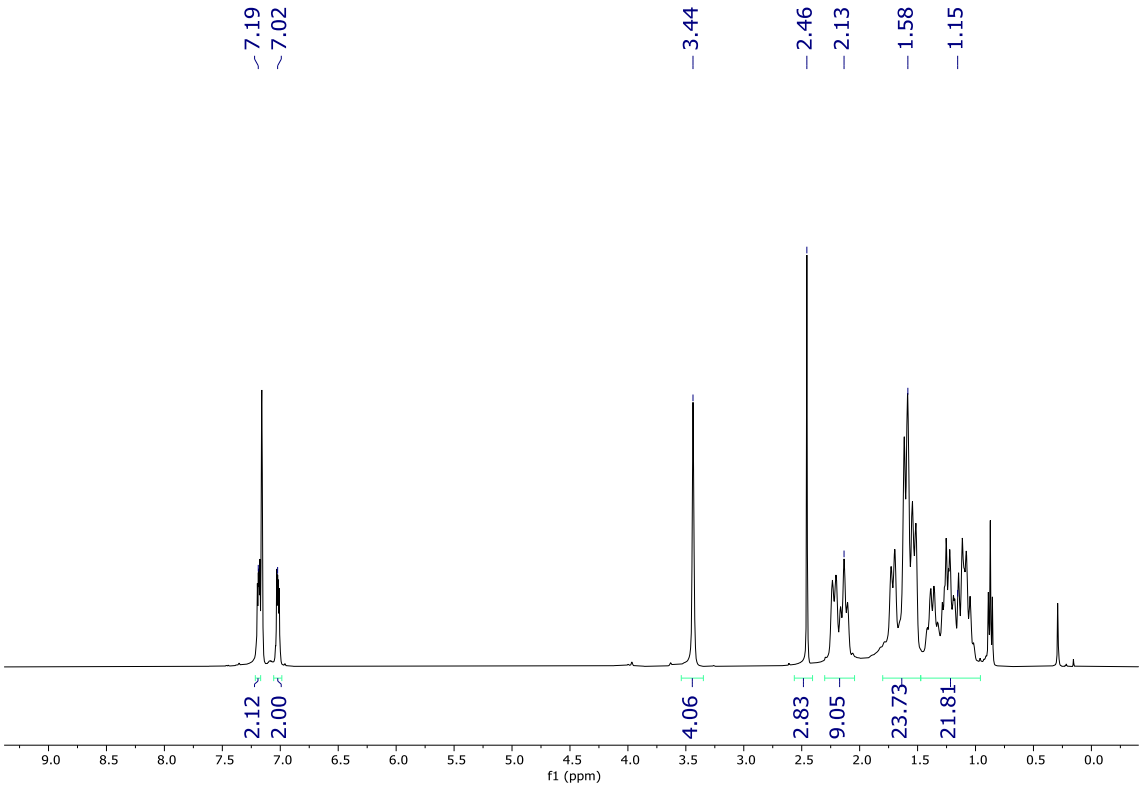

Figure S30. ^{1}H NMR spectrum of (^{Cy}PBP)Pd{OC(O)CH$_3$} in C_6D_6 at room temperature. Silicon grease (0.33 ppm) and *n*-pentane (0.87, 1.23 ppm) are present in the spectrum. The presence of *n*-pentane leads to higher integration of the cyclohexyl peaks than expected.

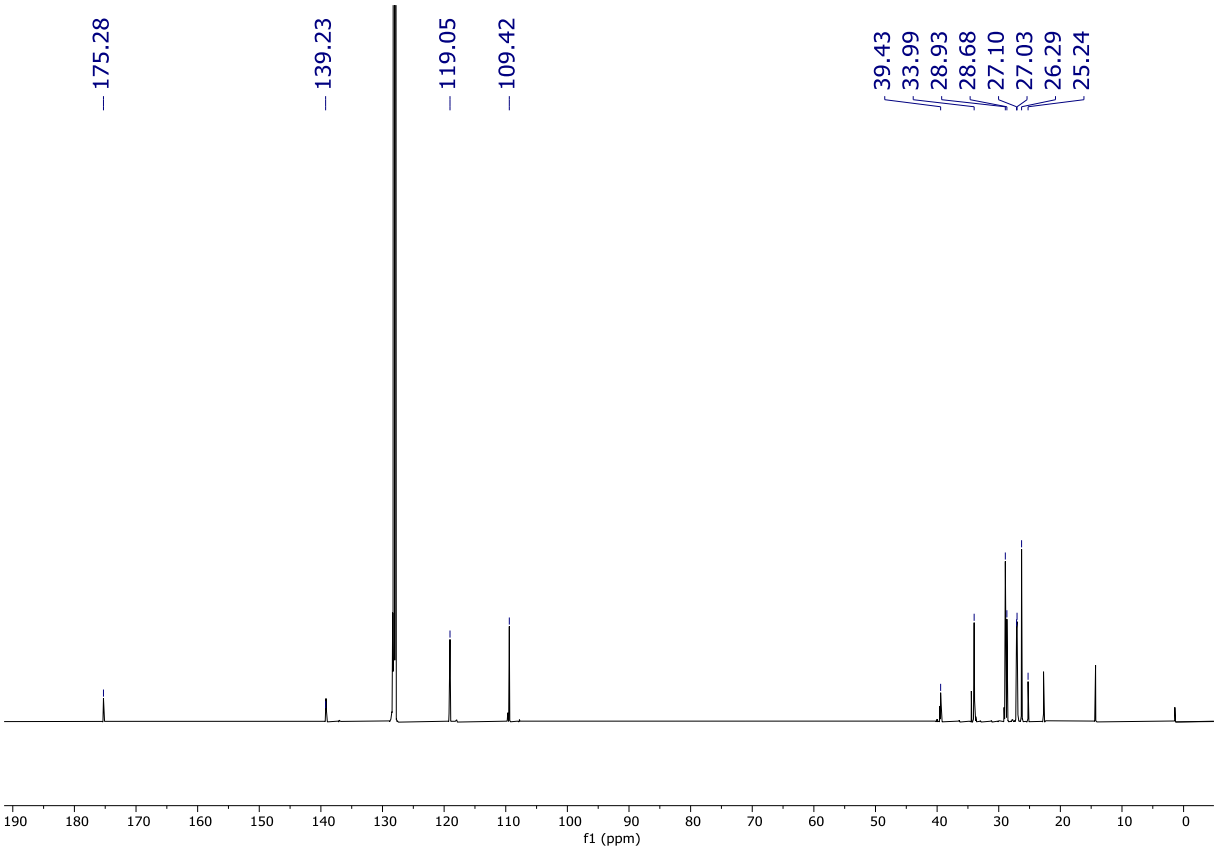

Figure S31. $^{13}C\{^{1}H\}$ NMR spectrum of (^{Cy}PBP)Pd{OC(O)CH_3} in C_6D_6 at room temperature. Silicon grease (1.42 ppm) and *n*-pentane (34.44, 22.73, 14.2 ppm) are present in the spectrum.

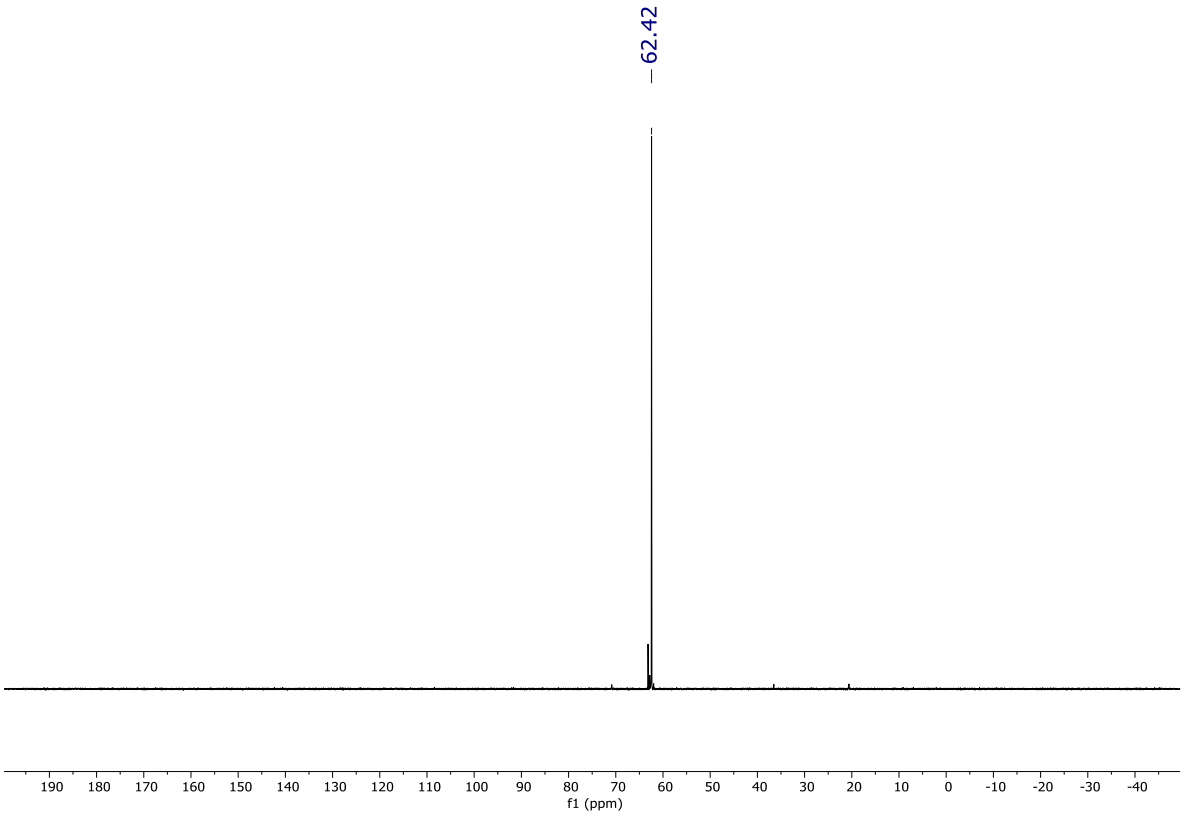

Figure S32. $^{31}P\{^{1}H\}$ NMR spectrum of (^{Cy}PBP)Pd{OC(O)CH_3} in C_6D_6 at room temperature.

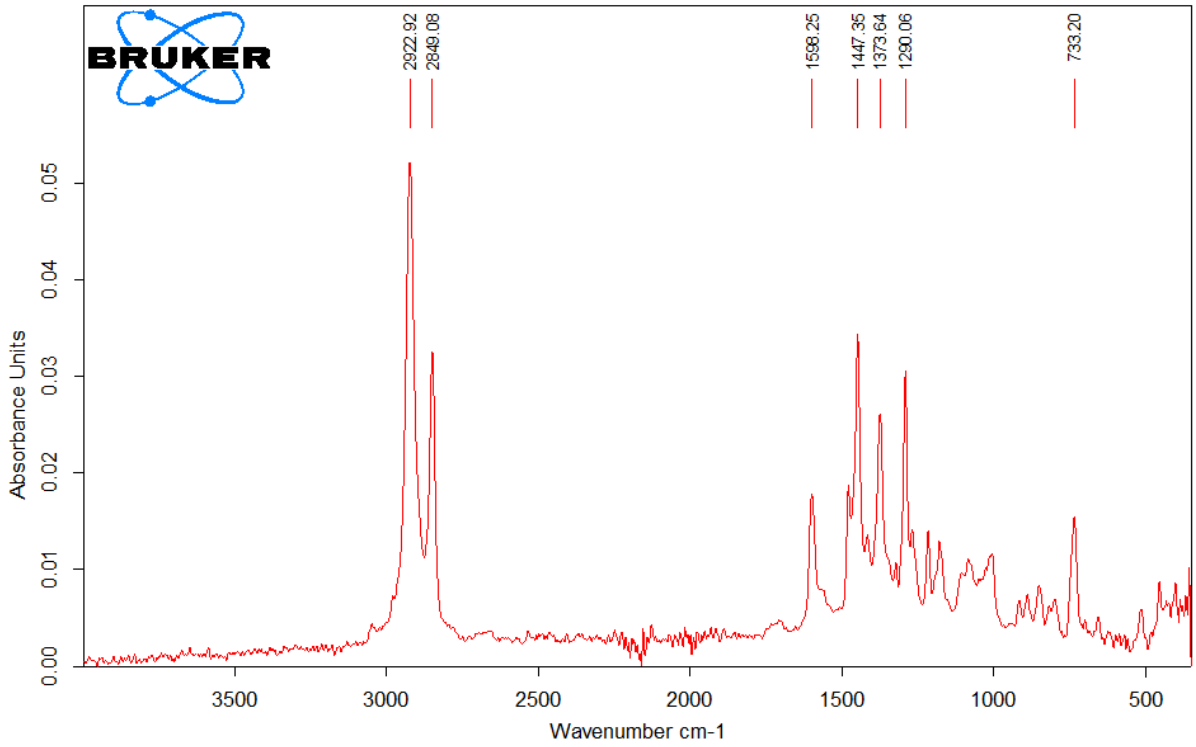

Figure S33. IR spectrum of (^{Cy}PBP)Pd{OC(O)CH$_3$}.

(^{Cy}PBP)NiCl

NMR spectra for (^{Cy}PBP)NiCl at 25 °C in C_6D_6 are shown in Figures S34-S36.

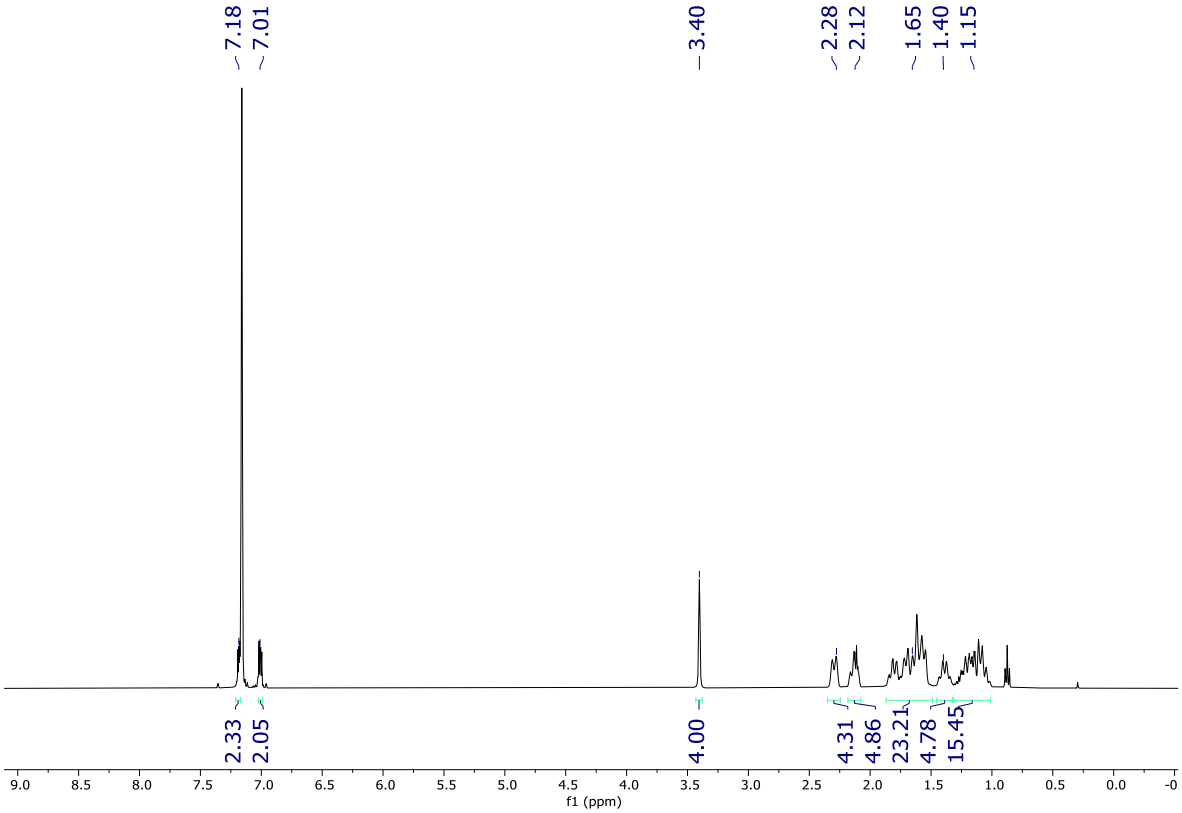

Figure S34. ^{1}H NMR spectrum of (^{Cy}PBP)NiCl in C_6D_6 at room temperature. *n*-Pentane (0.87, 1.23 ppm) is present in the spectrum

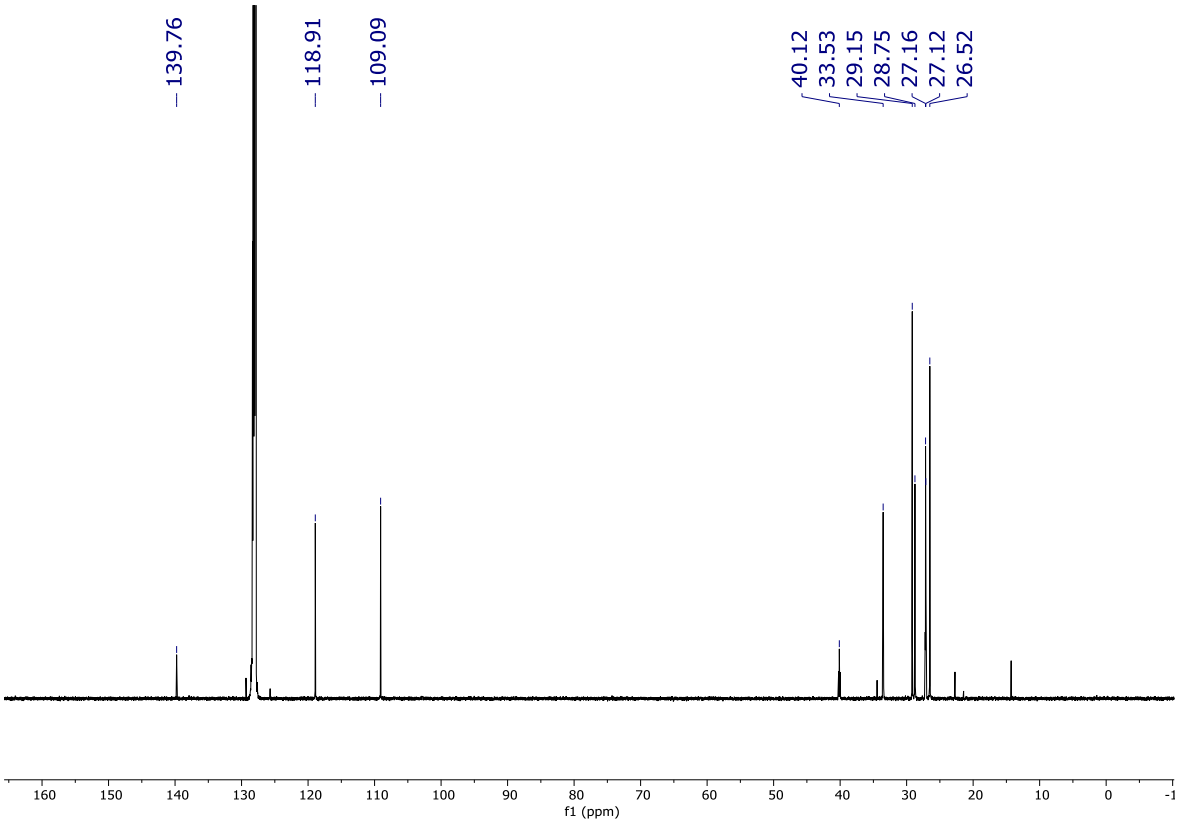

Figure S35. $^{13}C\{^{1}H\}$ NMR spectrum of (^{Cy}PBP)NiCl in C_6D_6 at room temperature. *n*-Pentane (34.44, 22.73, 14.2 ppm) is present in the spectrum.

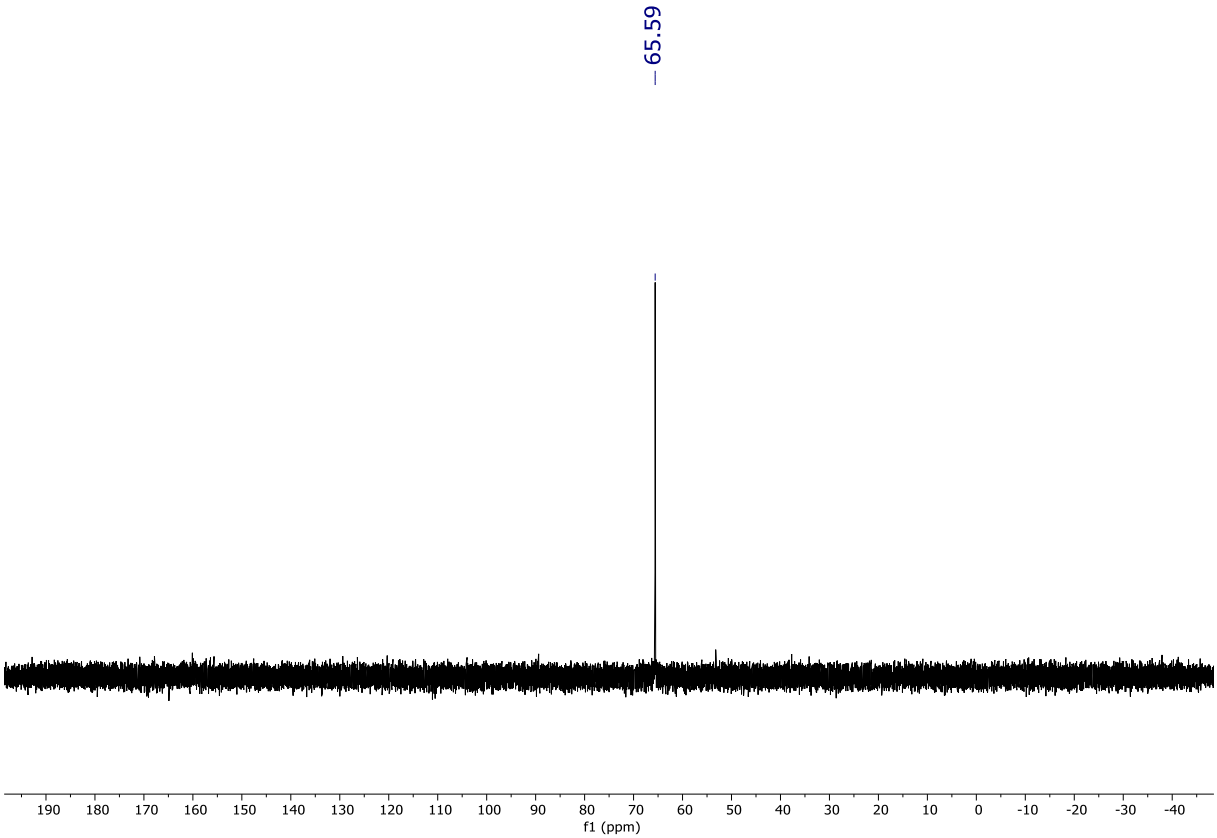

Figure S36. $^{31}P\{^{1}H\}$ NMR spectrum of (^{Cy}PBP)NiCl in C_6D_6 at room temperature.

(^{Cy}PBP)Ni(CH_3)

NMR spectra for (^{Cy}PBP)Ni(CH_3) at 25 °C in C_6D_6 are shown in Figures S37-S39.

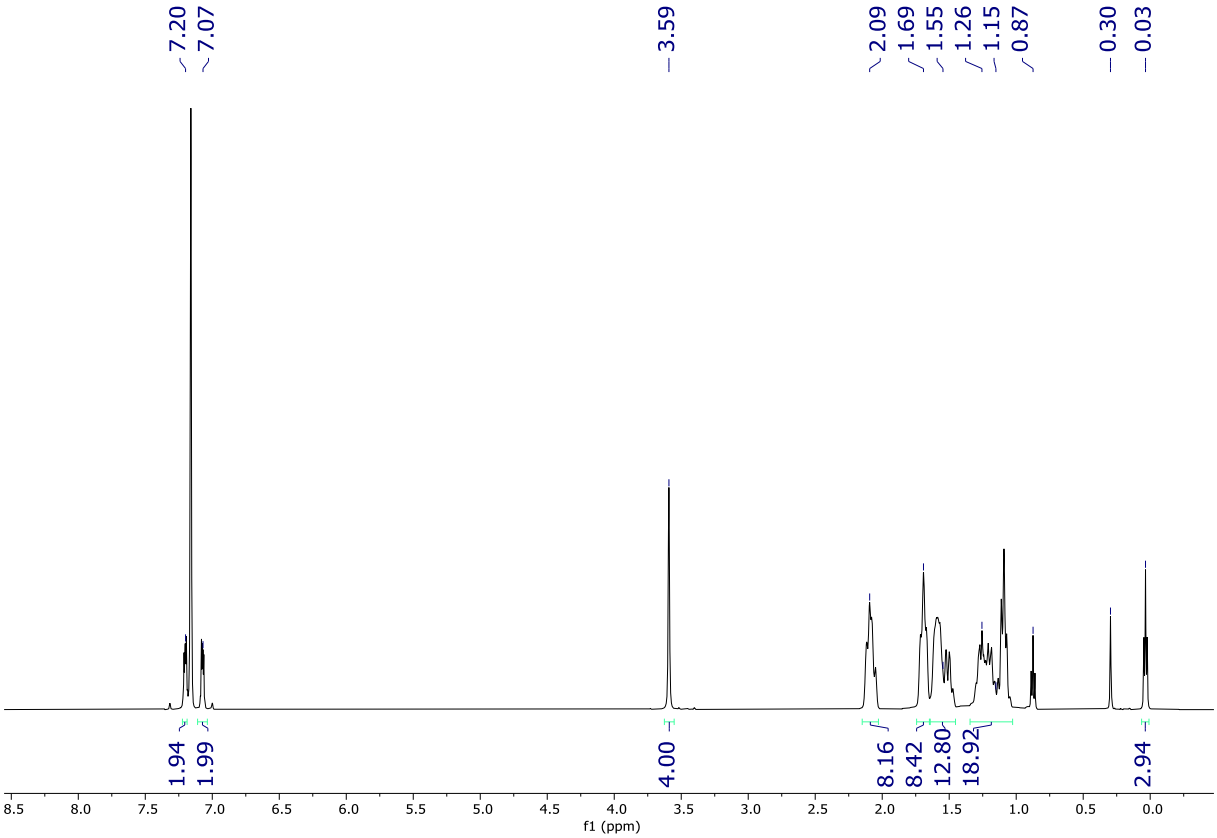

Figure S37. ^{1}H NMR spectrum of (^{Cy}PBP)Ni(CH_3) in C_6D_6 at room temperature. Silicon grease (0.30 ppm) and *n*-pentane (0.87, 1.25 ppm) are present in the spectrum.

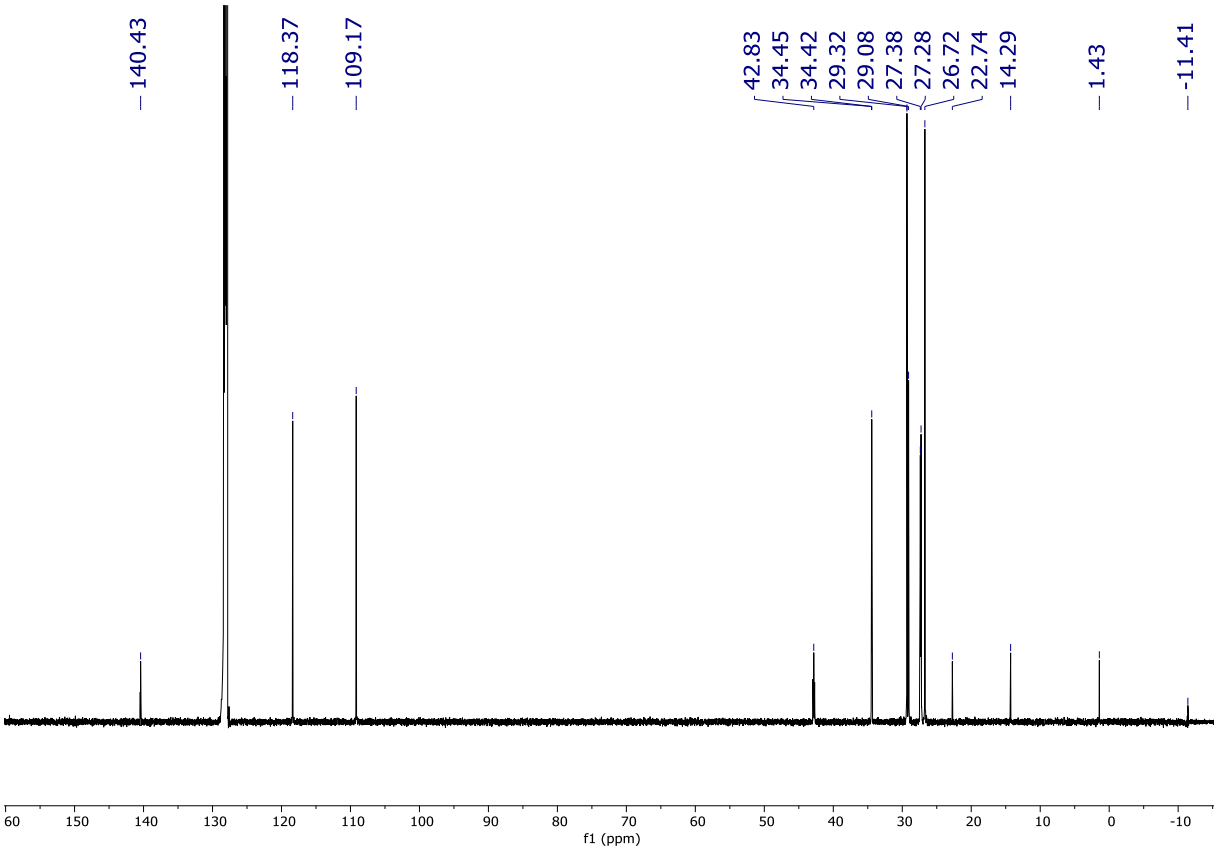

Figure S38. $^{13}C\{^{1}H\}$ NMR spectrum of (^{Cy}PBP)Ni(CH_3) in C_6D_6 at room temperature. Silicon grease (1.43 ppm) and *n*-pentane (34.45, 22.74, 14.29 ppm) are present in the spectrum.

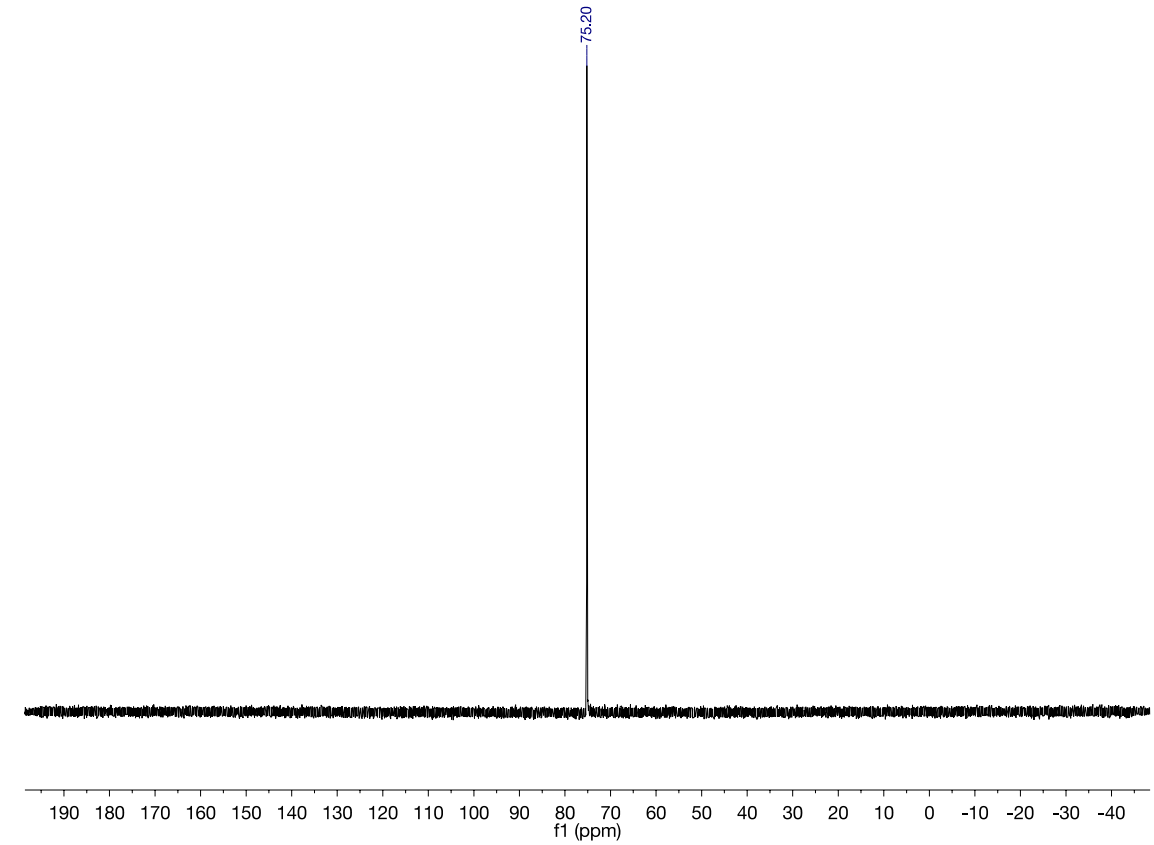

Figure S39. $^{31}P\{^{1}H\}$ NMR spectrum of (^{Cy}PBP)Ni(CH_3) in C_6D_6 at room temperature.

(^{tBu}PSiP)PdCl

NMR spectra for (^{tBu}PSiP)PdCl at 25 °C in C_6D_6 are shown in Figures S40-S42.

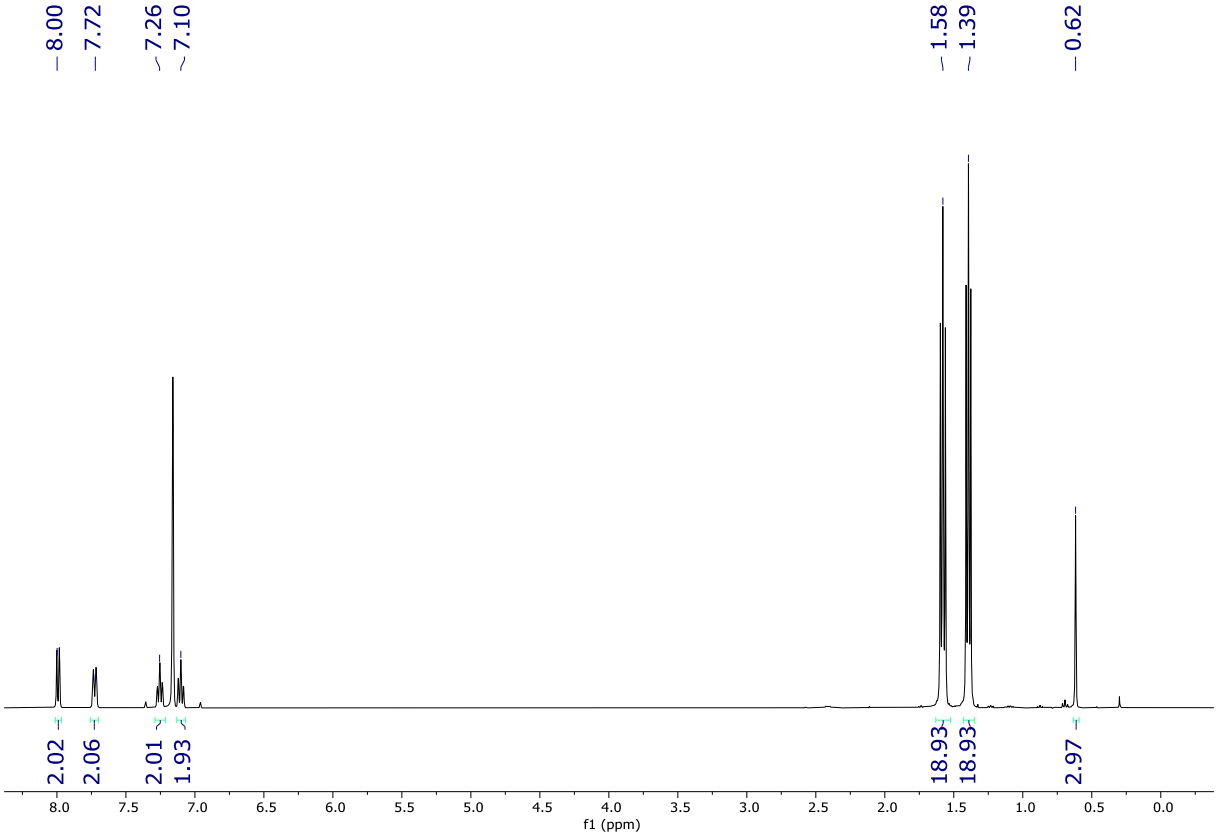

Figure S40. ^{1}H NMR spectrum of (^{tBu}PSiP)PdCl in C_6D_6 at room temperature.

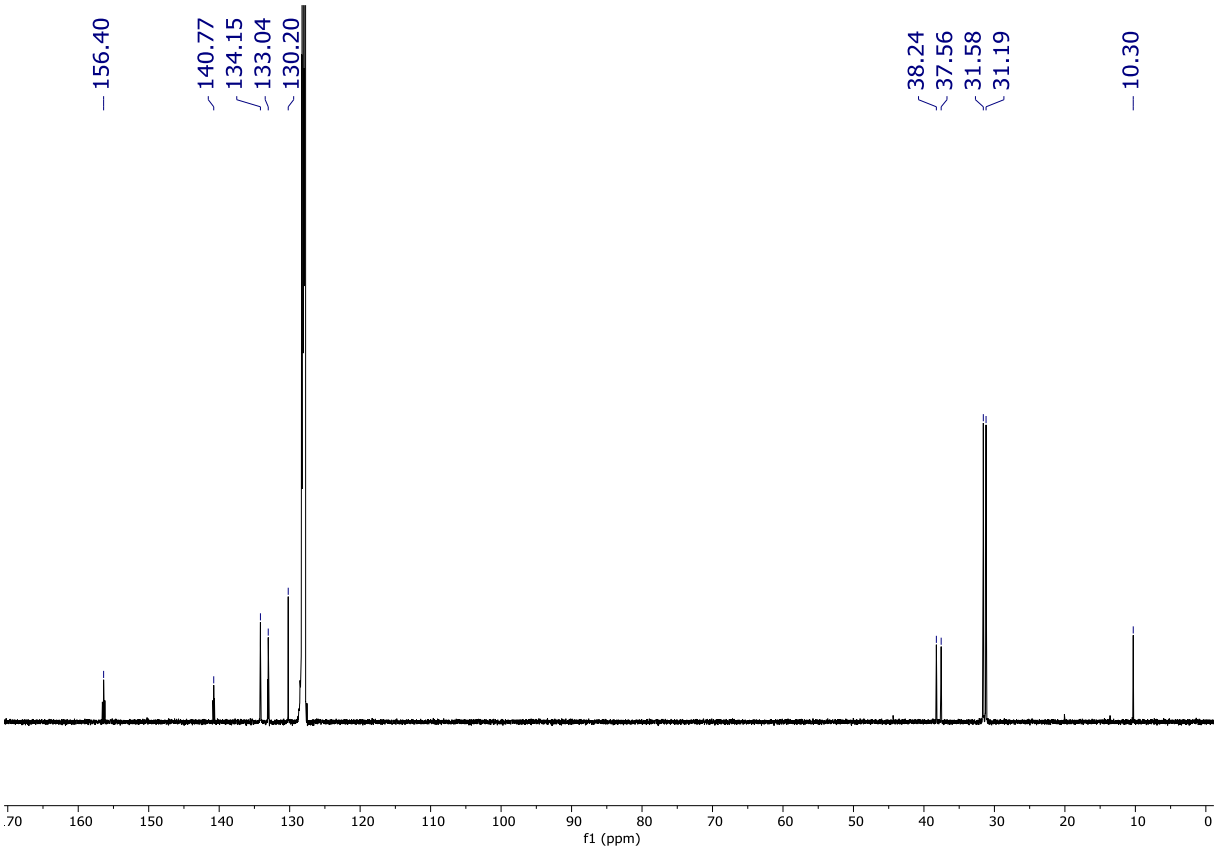

Figure S41. $^{13}C\{^{1}H\}$ NMR spectrum of (^{tBu}PSiP)PdCl in C_6D_6 at room temperature. One aryl carbon could not be assigned as it overlaps with the residual solvent signal at 128.06 ppm.

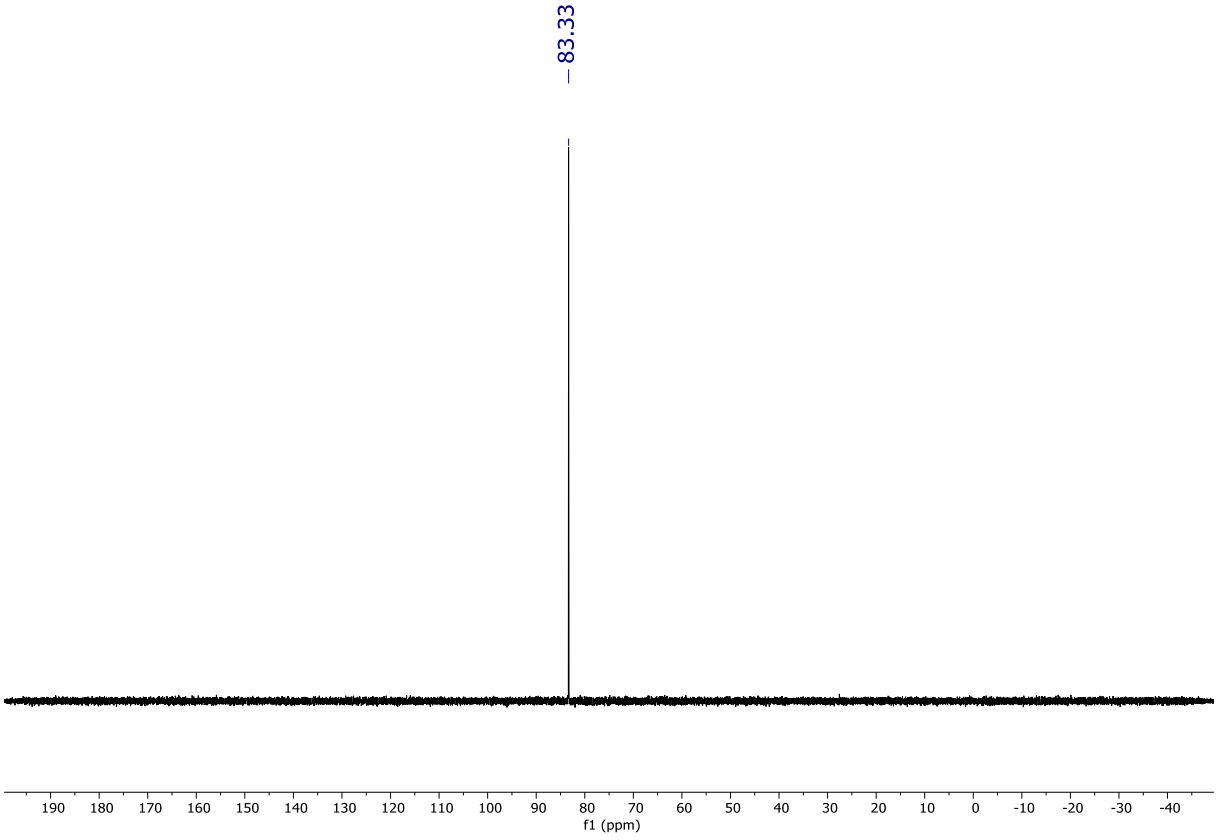

Figure S42. $^{31}P\{^{1}H\}$ NMR spectrum of (^{tBu}PSiP)PdCl in C_6D_6 at room temperature.

SXII. Computational Details

General Computational Details

All calculations were performed with the Gaussian 16 software package Rev. *C.01*. The DFT functional B3LYP including the Grimme empirical dispersion correction (D3) and the conductor-like polarizable continuum model, CPCM (solvent: Benzene). Two additional DFT functionals were tested, PBE0-D3BJ and ωB97XD, to evaluate the robustness of the computed results.

The basis set BS1, which includes the split-valence double-zeta Ahlrichs basis set def2-SVP on B, C, N, P, O, H, Ni was used for geometry optimizations. A SDD basis set and pseudopotential was used on palladium. In order to correct the energies, we performed single point calculations by employing a BS2 basis set, which comprises the augmented split-valence triple-zeta basis set def2-TVPPD on B, C, N, P, O, H, Ni, and a SDD (f) pseudopotential and basis set on palladium.

For the CO_2 insertion step, we computed counterpoise corrections at the BS2 level of theory. For all studied complexes, the computed CP corrections are given in Table S2.

A standard state (SS) correction was included to translate the computed free energies (ΔG°1atm, BS1) in the gas phase to the 1M standard state energies. Only the CO_2 insertion step is affected as the number of moles change from 2 to 1 mole. At 298 K, the SS correction is -1.89 kcal/mol.

The standard state Gibbs free energies ($\Delta G°_{1M,298K}$) reported in the main text correspond to:

$$\Delta G°_{1M,298K} = \Delta G_{1atm,\ 298K,BS1} - \Delta E_{1atm,BS1} + \Delta E_{1atm,BS2} + CP_{BS2} + SS_{298K}$$

Complex	B3LYP-D3		PBE0-D3BJ		ωB97XD	
	TS1_Out	TS_Inn	TS1_Out	TS_Inn	TS1_Out	TS_Inn
(^{tBu}PBP)Pd(CH_3)	0.23	0.33	0.21	0.30	0.26	0.37
(^{Me}PBP)Pd(CH_3)	0.25	0.36	0.23	0.33	0.27	0.38
(^{tBu}PCP)Pd(CH_3)	0.25	0.34	0.22	0.31	0.22	0.38
(^{Me}PCP)Pd(CH_3)	0.30	0.34	0.27	0.40	0.31	0.45
(^{tBu}PBP)Ni(CH_3)	0.26	0.44	0.24	0.38	0.30	0.48

Table S2. The computed CP corrections (kcal/mol) for the CO_2 insertion step for Pd- and Ni-pincer complexes. For studied complexes, corrections were computed using three different DFT protocols for the outer sphere TS_Out (S_E2 path) and inner sphere TS_Inn (1,2-insertion).

The optimized geometries of TS1_Out, TS2 and TS1_Inn with the (^{tBu}PBP)Pd(CH_3) complex are shown in Figures S43-S45.

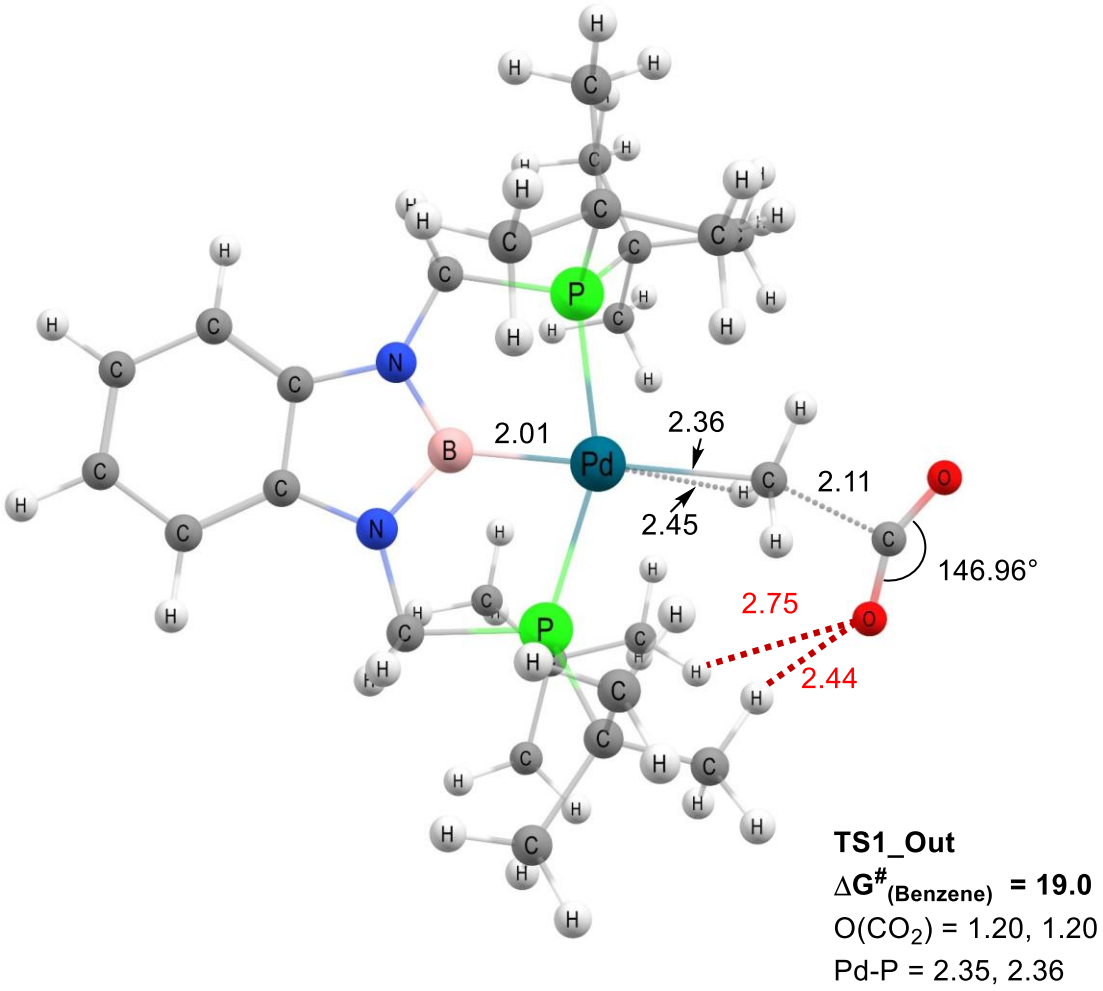

Figure S43. The optimized geometry of the outer sphere TS1 (B3LYP-D3/def2-SVP[CPCM:Benzene]) where CO_2 performs a S_E2 attack on (^{tBu}PBP)Pd(CH_3). The TS displays a sigma interaction (2.45 Å) between Pd and the methyl group. Non-covalent interactions include two CH···O interactions between the ^{t}Bu group of the ligand and the oxygen of the CO_2 (2.44 Å, 2.75 Å). Energies are in kcal/mol, distances in Å.

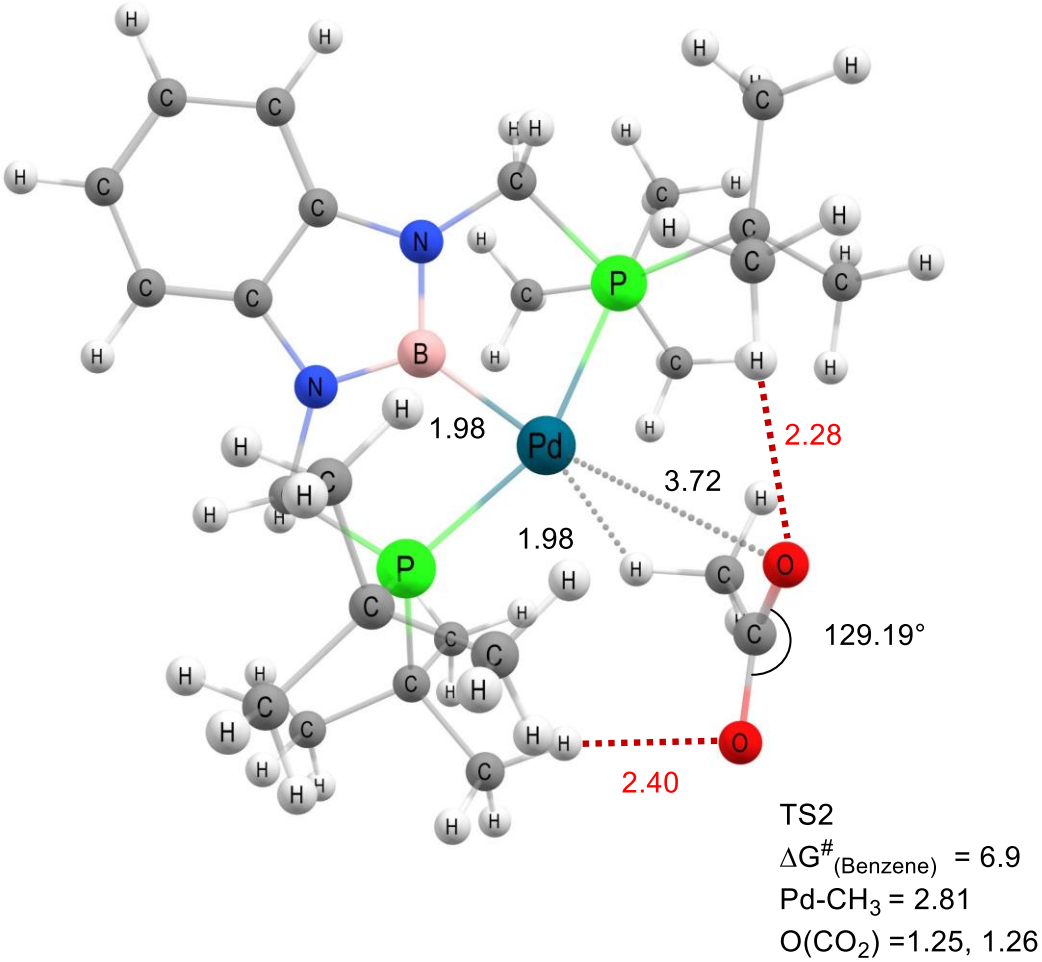

Figure S44. The optimized geometry of TS2 for (^{tBu}PBP)Pd(CH_3) (B3LYP-D3/def2-SVP[CPCM:Benzene]). Non-covalent interactions include two CH···O interactions between the ^{t}Bu group of the ligand and the oxygen of the CO_2 (2.28 Å, 2.40 Å). Energies are in kcal/mol, distances in Å.

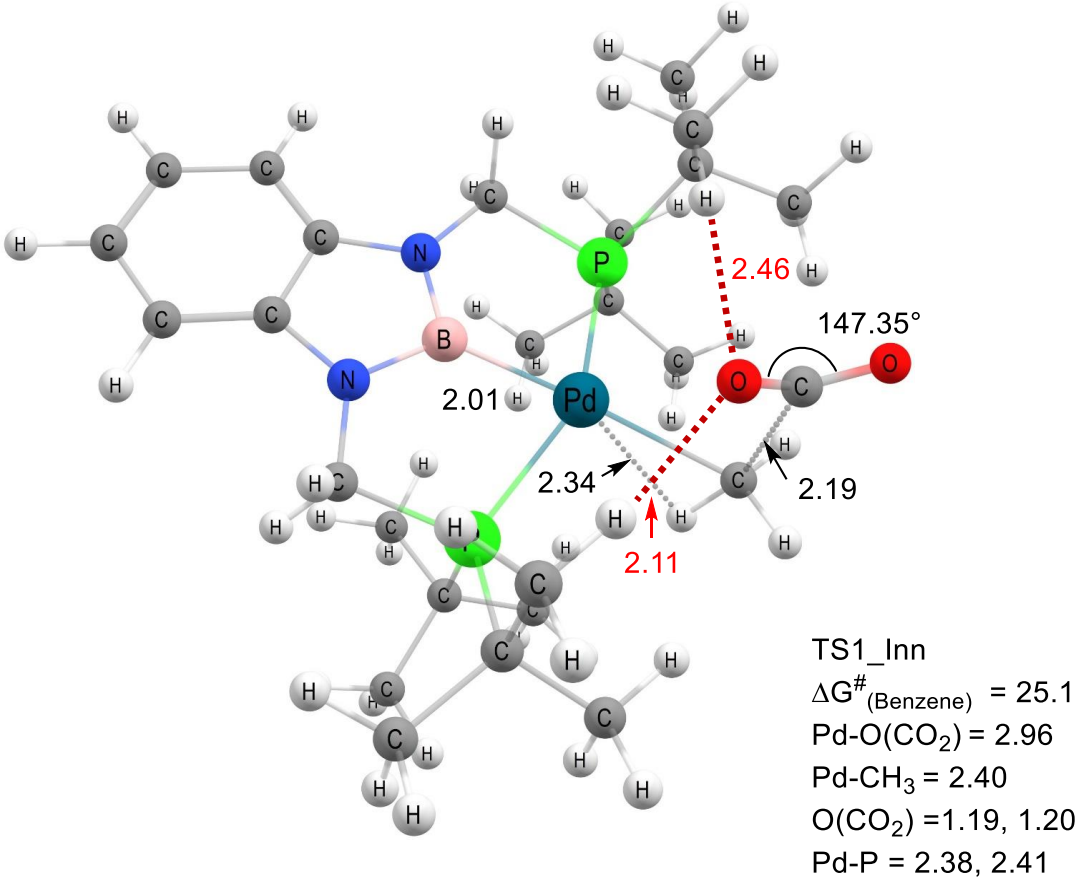

Figure S45. The optimized geometry of the inner sphere TS (B3LYP-D3/def2-SVP[CPCM:Benzene]) where CO_2 undergoes a *1,2*-insertion into (^{tBu}PBP)Pd(CH_3). The TS displays a sigma interaction (2.34 Å) between Pd and the methyl group. Non-covalent interactions include two CH···O interactions between the ^{t}Bu group of the ligand and the oxygen of CO_2 (2.11 Å, 2.46 Å). Energies are in kcal/mol, distances in Å.

The optimized geometries of TS1_Out and TS1_Inn with the (^{Me}PBP)Pd(CH_3) complex are shown in Figures S46-S47.

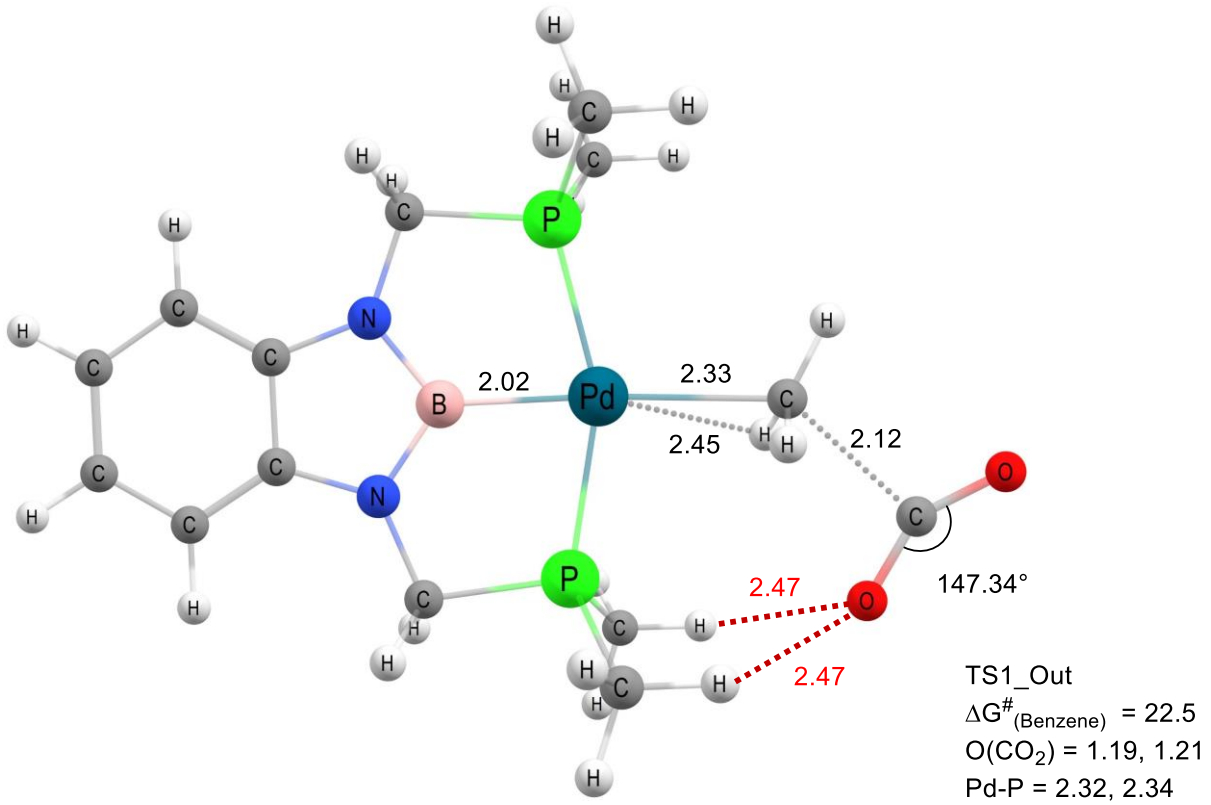

Figure S46. The optimized geometry of the outer sphere TS (B3LYP-D3/def2-SVP[CPCM:Benzene]) where CO_2 performs a S_E2 attack on (^{Me}PBP)Pd(CH_3). The TS displays a sigma interaction (2.45 Å) between Pd and the methyl group. Non-covalent interactions include two CH···O interactions between the Me group of the ligand and the oxygen of the CO_2 (2.47 Å, 2.47 Å). Energies are in kcal/mol, distances in Å.

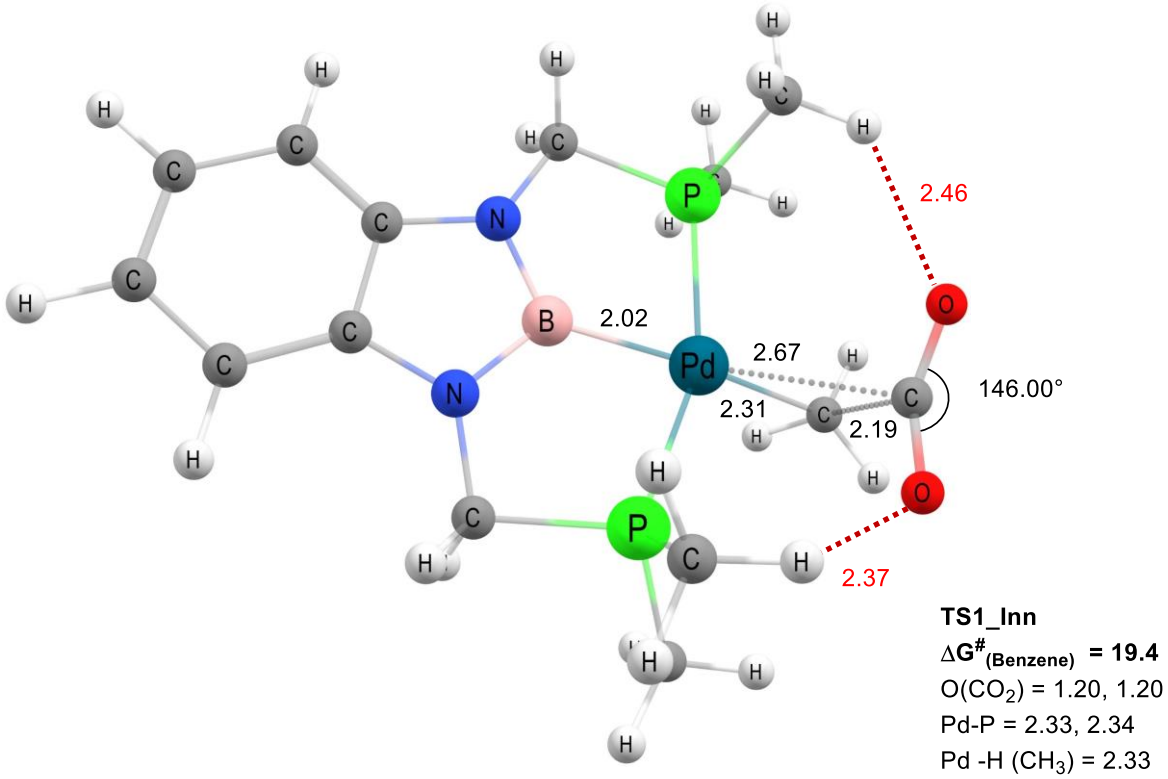

Figure S47. The optimized geometry of the inner sphere TS (B3LYP-D3/def2-SVP[CPCM:Benzene]) where CO_2 performs a *1,2*-insertion into (^{Me}PBP)Pd(CH_3). The TS displays a sigma interaction (2.33 Å) between Pd and the methyl group. Non-covalent interactions include two CH···O interactions between the Me group of the ligand and the oxygen of CO_2 (2.37 Å, 2.46 Å). Energies are in kcal/mol, distances in Å.

The optimized geometries of TS1_Out, TS2 and TS1_Inn with the (^{tBu}PCP)Pd(CH_3) complex are shown in Figures S48-S50.

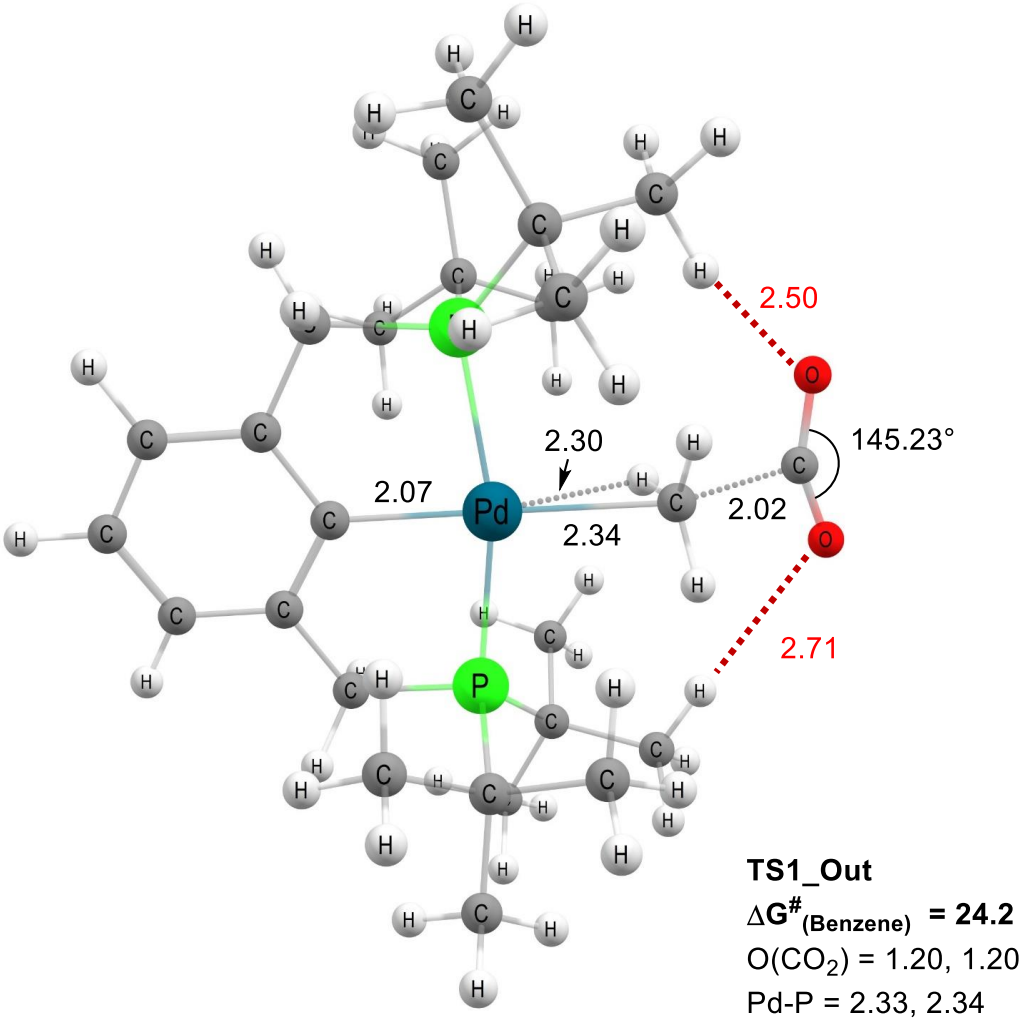

Figure S48. The optimized geometry of the outer sphere TS1 (B3LYP-D3/def2-SVP[CPCM:Benzene]) where CO_2 performs a S_E2 insertion on (^{tBu}PCP)Pd(CH_3). The TS displays a sigma interaction (2.30 Å) between Pd and the methyl group which is shorter for (^{tBu}PCP)Pd(CH_3) than for the (^{tBu}PBP)Pd(CH_3) complex. Both oxygens of CO_2 are involved in non-covalent interactions with ^{t}Bu groups. Non-covalent interactions include two CH···O interactions between the ^{t}Bu groups of the ligand and the oxygen of CO_2 (2.50 Å, 2.71 Å). Energies are in kcal/mol, distances in Å.

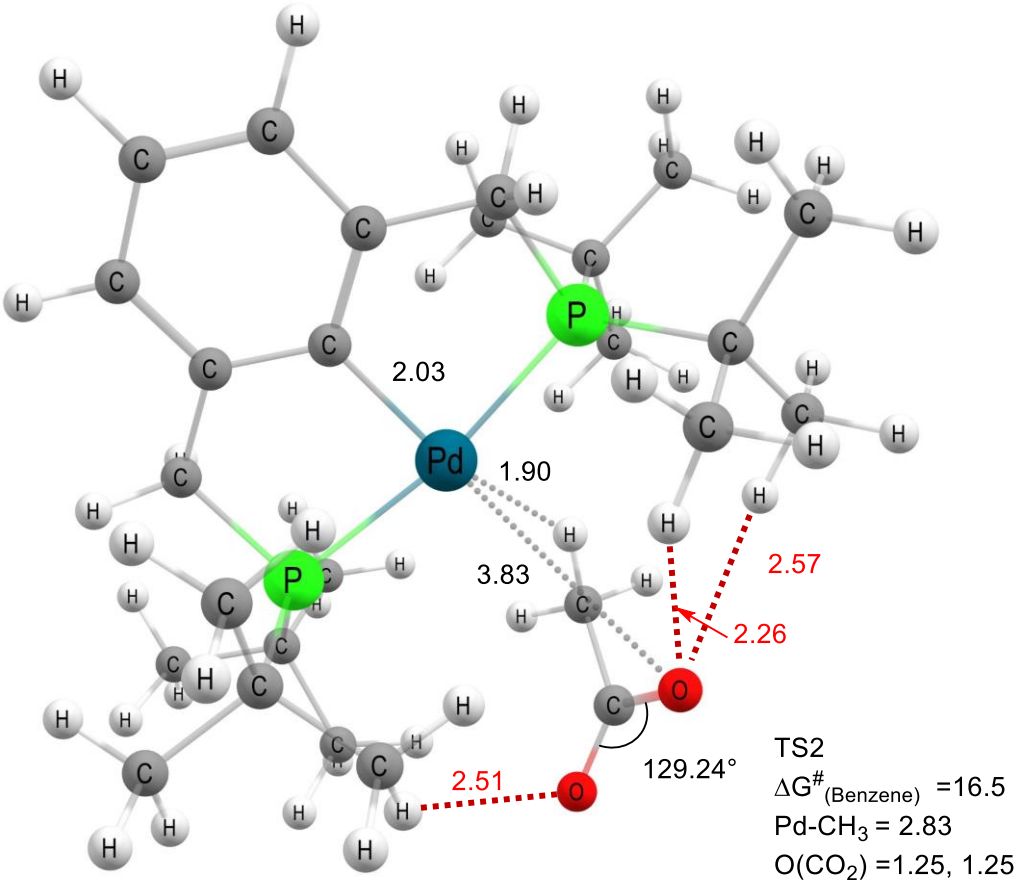

Figure S49. The optimized geometry of the TS2 for (^{tBu}PCP)Pd(CH_3) (B3LYP-D3/def2-SVP[CPCM:Benzene]). Non-covalent interactions include three CH···O interactions between the ^{t}Bu group of the ligand and the oxygen of the CO_2 (2.26 Å, 2.51 Å, 2.57 Å). Energies are in kcal/mol, distances in Å.

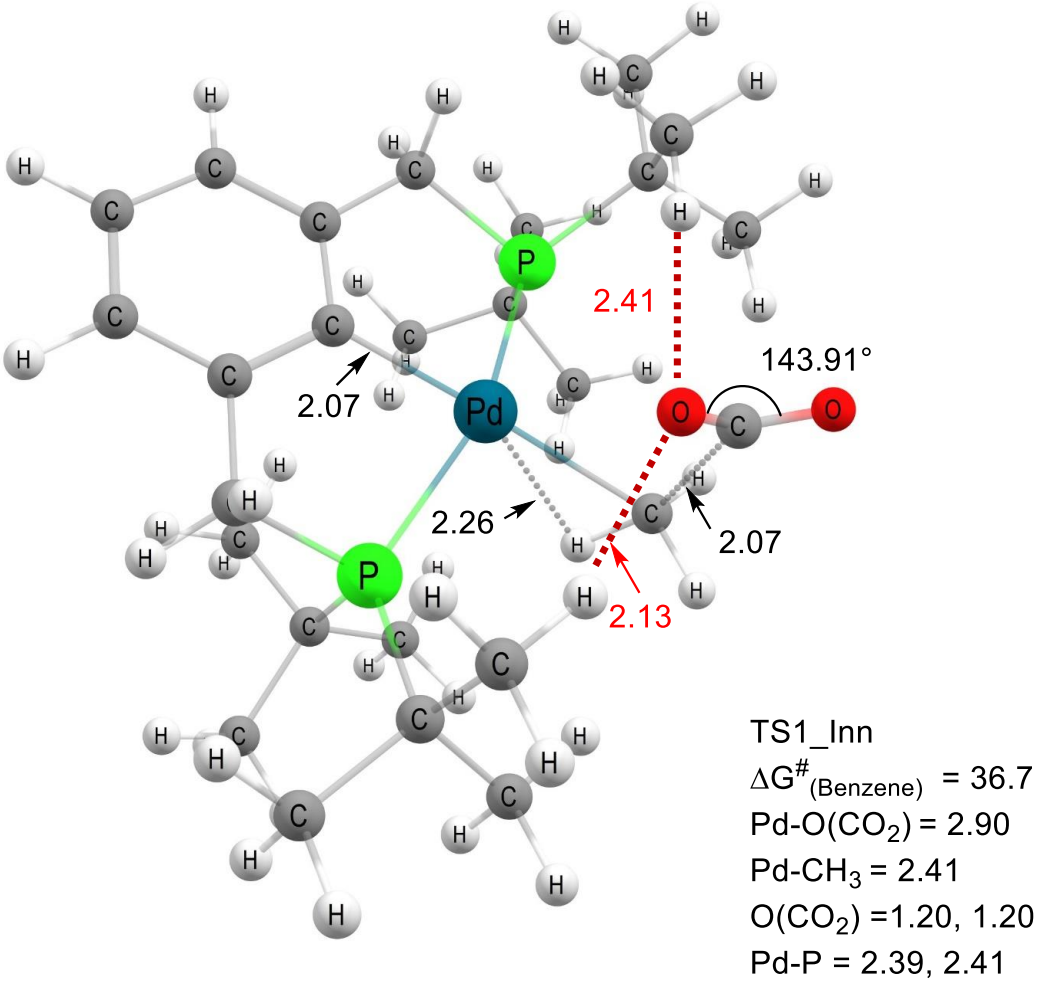

Figure S50. The optimized geometry of the inner sphere TS (B3LYP-D3/def2-SVP[CPCM:Benzene]) where CO_2 undergoes a 1,2-insertion into (^{tBu}PCP)Pd(CH_3). The TS displays a sigma interaction (2.26 Å) between Pd and the methyl group which is stronger for (^{tBu}PCP)Pd(CH_3) than for (^{tBu}PBP)Pd(CH_3). Non-covalent interactions include two CH···O interactions between the ^{t}Bu groups of the ligand and the oxygen of CO_2 (2.13 Å, 2.41 Å). Energies are in kcal/mol, distances in Å.

The optimized geometries of TS1_Out and TS1_Inn with the (^{tBu}PBP)Ni(CH_3) complex are shown in Figures S51-S52.

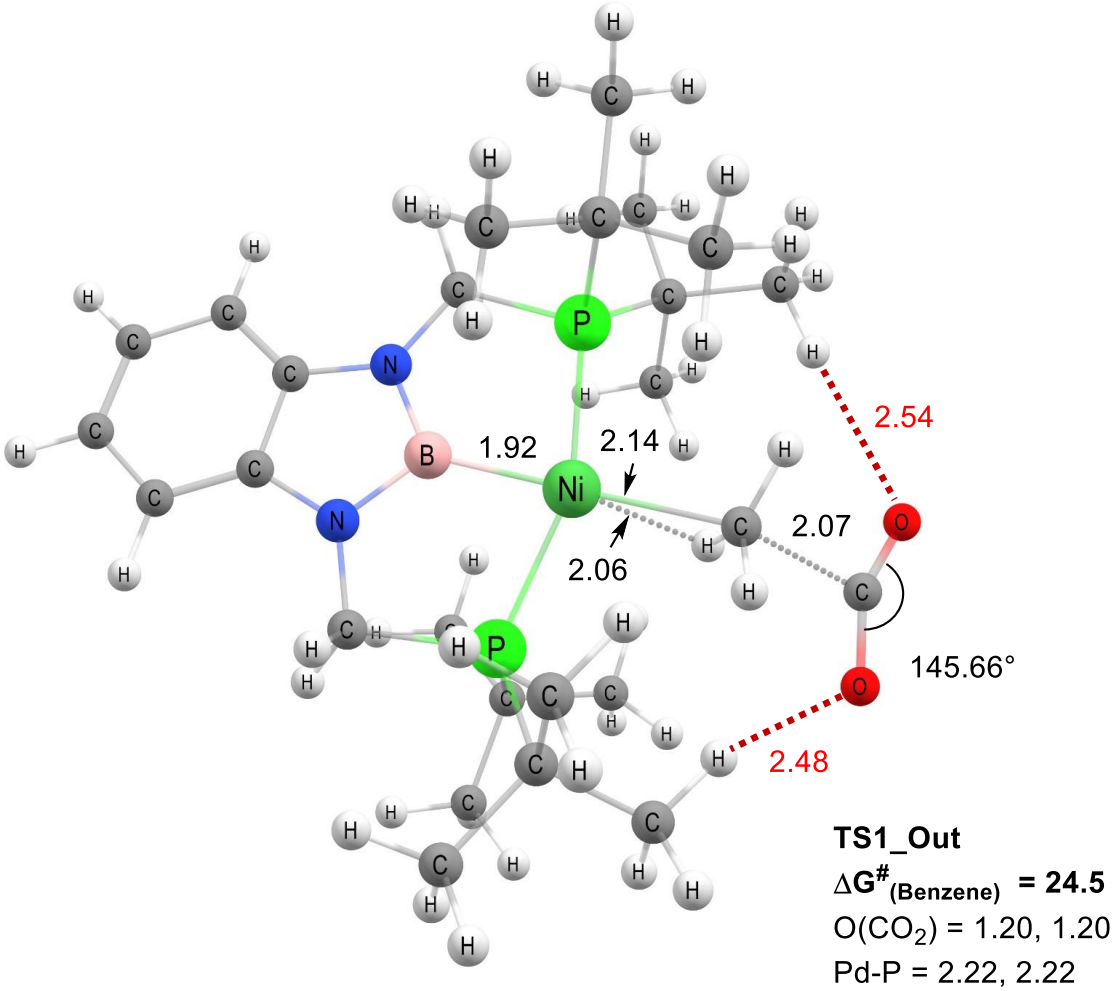

Figure S51. The optimized geometry of the outer sphere TS (B3LYP-D3/def2-SVP[CPCM:Benzene]) where CO_2 performs a S_E2 attack onto (^{tBu}PBP)Ni(CH_3). The TS displays a sigma interaction (2.06 Å) between Ni and the methyl group, which is shorter, compare to the studied Pd-pincer complexes. Both oxygens of CO_2 are involved in non-covalent interactions with the ^{t}Bu groups. Non-covalent interactions include two CH···O interactions between the ^{t}Bu groups of the ligand and the oxygen of CO_2 (2.48 Å, 2.54 Å). Ni-P bonds are shorter by 0.15 Å relative to the Pd-pincer complexes as Ni has smaller atomic radius. Energies are in kcal/mol, distances in Å.

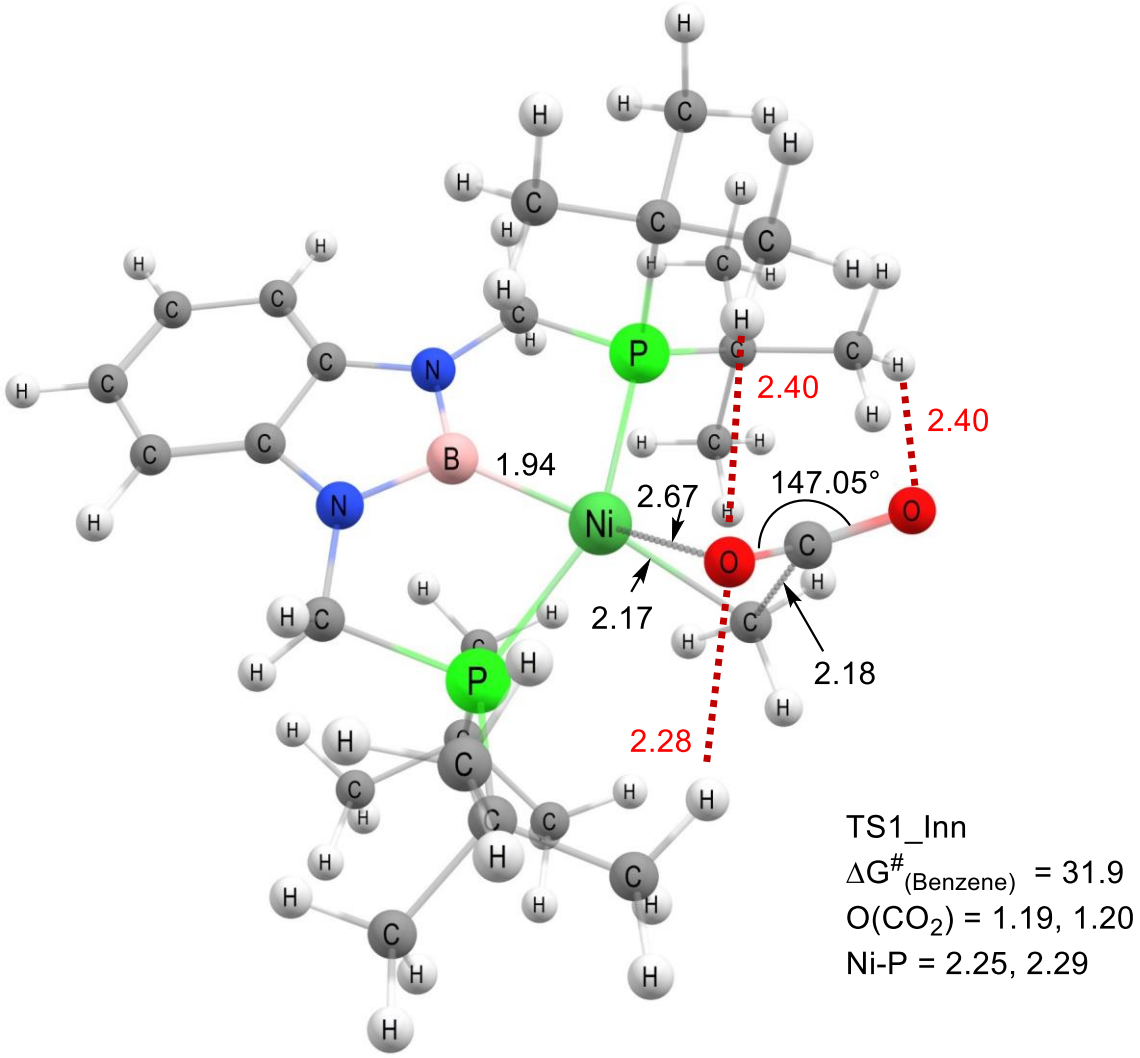

Figure S52. The optimized geometry of the inner sphere TS1 (B3LYP-D3/def2-SVP[CPCM:Benzene]) where CO_2 performs a 1,2-insertion into (^{tBu}PBP)Ni(CH_3). The oxygen of CO_2 interacts with Ni at 2.67 Å. Non-covalent interactions include three CH···O interactions between the ^{t}Bu groups of the ligand and the oxygen of CO_2 (2.28 Å, 2.40 Å, 2.40 Å). Energies are in kcal/mol, distances in Å.

The optimized geometries of TS1_Out and TS1_Inn with (^{Me}PCP)Pd(CH_3) complex are shown in Figures S53-S54.

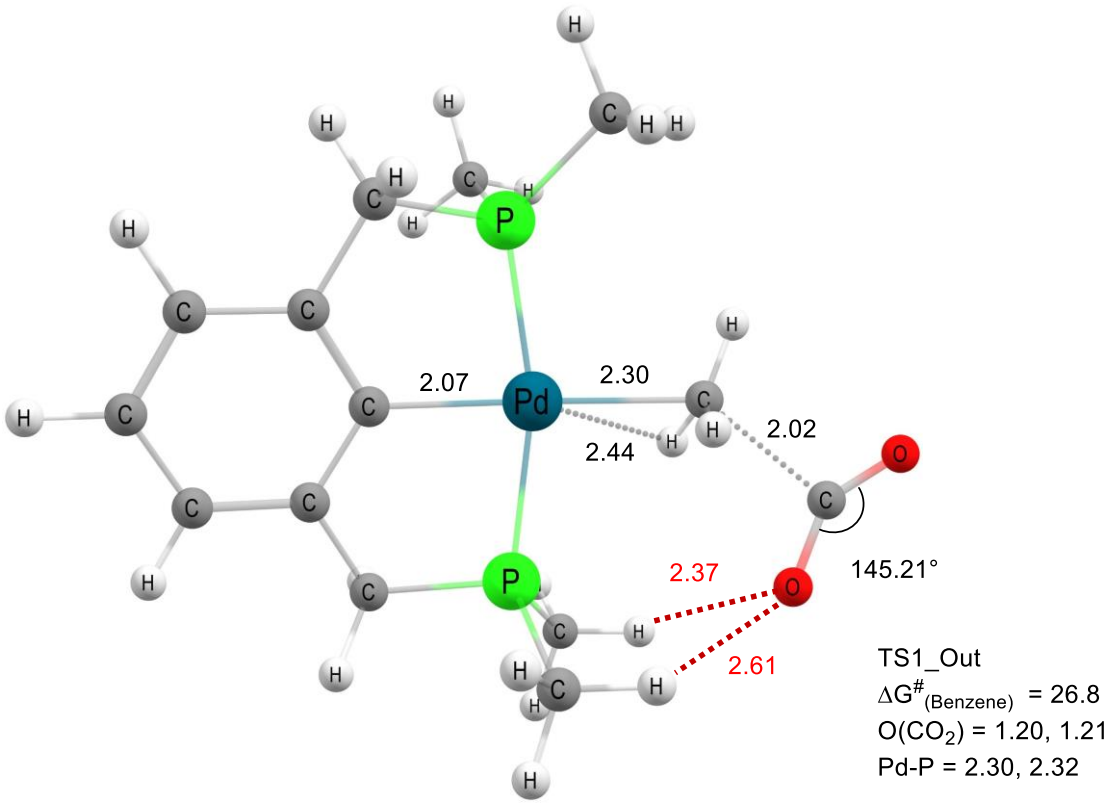

Figure S53. The optimized geometry of the outer sphere TS1 (B3LYP-D3/def2-SVP[CPCM:Benzene]) where CO_2 performs a S_E2 attack onto (^{Me}PCP)Pd(CH_3). The TS displays a sigma interaction (2.44 Å) between Pd and the methyl group. Non-covalent interactions include two CH···O interactions between the Me group of the ligand and the oxygen of the CO_2 (2.37 Å, 2.61 Å). Energies are in kcal/mol, distances in Å.

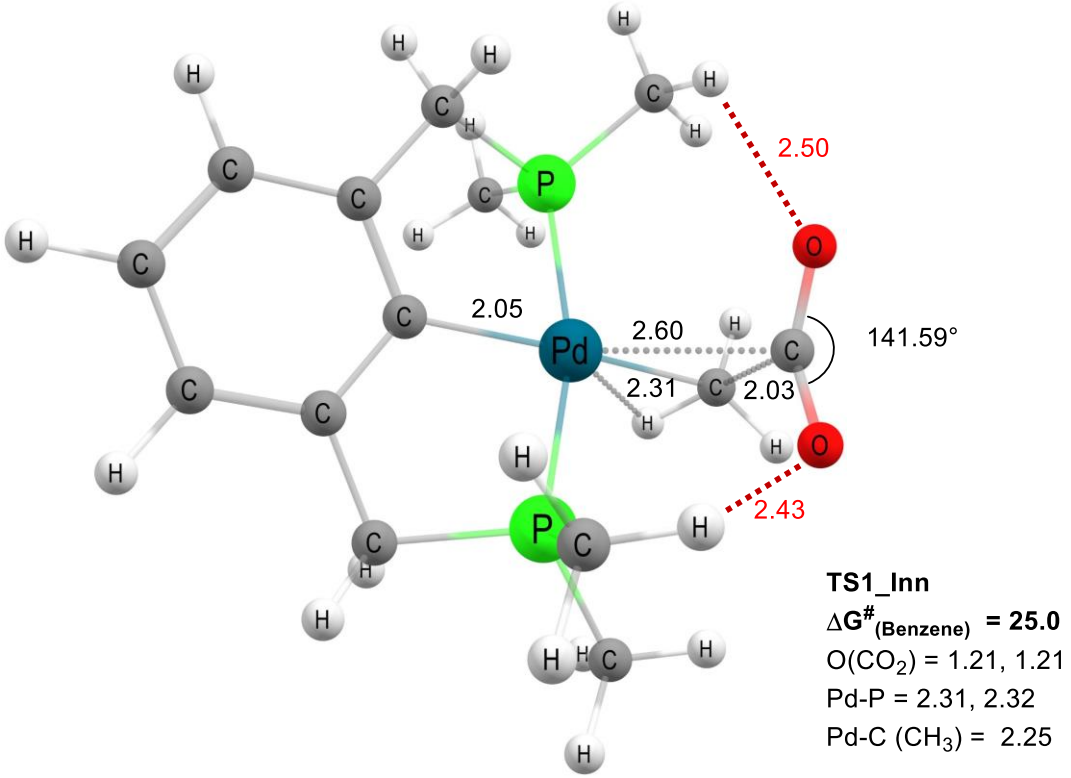

Figure S54. The optimized geometry of the inner sphere TS1 (B3LYP-D3/def2-SVP[CPCM:Benzene]) where CO_2 undergoes a *1,2*-insertion into (^{Me}PCP)Pd(CH_3). The TS displays a sigma-interaction (2.25 Å) between Pd and the methyl group. Non-covalent interactions include two CH···O interactions between the Me group of the ligand and the oxygen of CO_2 (2.43 Å, 2.50 Å). Energies are in kcal/mol, distances in Å.

	B3LYP-D3			ωB97XD			PBE0-D3BJ		
	TS1_Inn	TS1_Out	Difference (kcal/mol)	TS1_Inn	TS1_Out	Difference (kcal/mol)	TS1_Inn	TS1_Out	Difference (kcal/mol)
(^{Me}PCP)Pd	**25.0**	26.8	1.8	**27.8**	30.0	2.2	**23.5**	25.2	1.7
(^{Me}PBP)Pd	**19.4**	22.5	3.1	**21.0**	23.4	2.4	**16.7**	18.9	2.2
(^{tBu}PCP)Pd	36.7	**24.2**	12.5	41.1	**29.2**	11.9	37.1	**24.6**	12.5
(^{tBu}PBP)Pd	25.1	**19.0**	6.1	30.6	**23.9**	6.7	26.6	**18.9**	7.7
(^{tBu}PBP)Ni	31.9	**24.5**	7.4	33.7	**27.8**	5.9	30.6	**22.8**	7.8

Table S3. Computed barriers for inner and outer sphere C-CO_2 bond formation with different complexes.

SXIII. X-ray Diffraction Data

General X-ray Experimental

Low-temperature diffraction data (ω-scans) were collected on either a Rigaku MicroMax-007HF diffractometer coupled to a Dectris Pilatus3R detector with Mo Kα (λ = 0.71073 Å) or a MicroMax-007HF diffractometer coupled to a Saturn994+ CCD detector with Cu Kα (λ = 1.54178 Å). The diffraction images were processed and scaled using Rigaku Oxford Diffraction software (CrysAlisPro; Rigaku OD: The Woodlands, TX, 2015). The structure was solved with SHELXT and was refined against F^2 on all data by full-matrix least squares with SHELXL.[12] All non-hydrogen atoms were refined anisotropically. Unless stated otherwise, hydrogen atoms were included in the model at geometrically calculated positions and refined using a riding model. The isotropic displacement parameters of all hydrogen atoms were fixed to 1.2 times the U value of the atoms to which they are linked (1.5 times for methyl groups). The full numbering scheme of all submitted compounds can be found in the full details of the X-ray structure determination (CIF), which is included as Supporting Information.

X-ray details for (^{Cy}PBP)NiCl

The program SQUEEZE[13] was used to compensate for the contribution of disordered solvents contained in voids within the crystal lattice from the diffraction intensities. This procedure was applied to the data file and the submitted model is based on the solvent removed data. The total electron density found in the voids was 244 e/A^3. See "_platon_squeeze_details" in the .cif for more information.

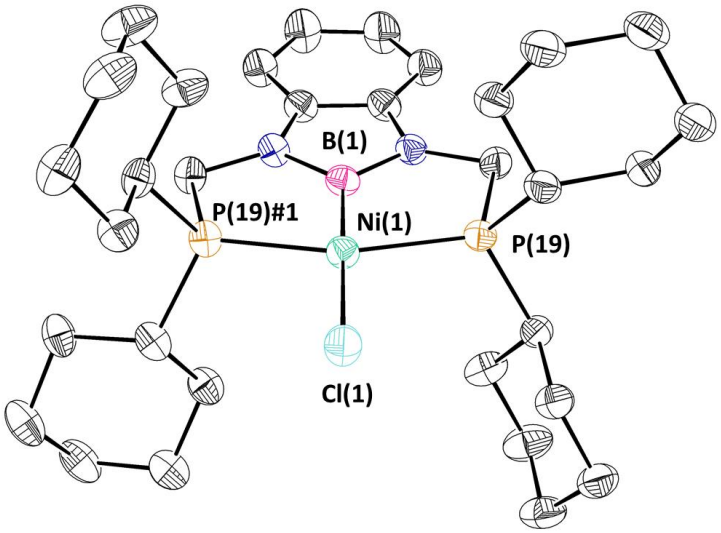

Figure S55. The complete numbering scheme of (^{Cy}PBP)NiCl with 30% thermal ellipsoid probability levels. The hydrogen atoms are shown as circles for clarity.

X-ray details for (^{Cy}PBP)Ni(CH_3)

This data was refined as a 2-component twin. The fractional volume contribution of the minor twin component was freely refined to a converged value of 0.3485(18).

X-ray details for ($^{tBu}PB^{Me}P)_2Ni_2(\mu\text{-}N_2)$

The supporting ligand is disordered over two, nearly equally occupied sites. All disordered C-C and C-P distances were restrained to be similar. The thermal parameters in the disordered model were restrained to behave as rigid bodies. The program SQUEEZE[13] was used to compensate for the contribution of disordered solvents contained in voids within the crystal lattice from the diffraction intensities. This procedure was applied to the data file and the submitted model is based on the solvent removed data. The total electron density found in the voids was 54 e/Å^3. See "_platon_squeeze_details" in the .cif for more information.

Compound	(^{Cy}PBP)NiCl	(^{Cy}PBP)Ni(CH_3)	(^{tBu}PBP)Pd(CH_3)
CCDC	2108774	2107492	2107493
Empirical Formula	$C_{33}H_{52}ClNiN_2P_2$	$C_{34.67}H_{59}BN_2NiP_2$	$C_{25}H_{47}BN_2P_2Pd$
Wavelength (Å)	1.54184	0.71073	1.54184
Temperature (K)	93(2)	93(2)	93(2)
FW	630.00	635.30	554.79
Crystal System	Trigonal	Monoclinic	Orthorhombic
Space Group	$R\bar{3}c$	$P2_1/c$	*Pbca*
***a* (Å)**	26.0265(8)	23.1838(12)	11.91390(10)
***b* (Å)**	26.0265(8)	26.0619(11)	14.4308(2)
***c* (Å)**	26.0801(8)	17.5360(7)	32.1655(5)
α (°)	90	90	90
β (°)	90	101.639(5)	90
γ (°)	120	90	90
***V* (Å^3)**	15299.3(11)	10377.6(8)	5530.12(12)
Z	18	12	8
ρ (g/cm^3)	1.234	1.220	1.333
μ (mm^{-1})	2.595	0.679	6.600
Data / restraints / parameters	3048 / 0 / 178	36095 / 0 / 1105	4890 / 0 / 293
***R*1, w*R*2 (I > 2σ(I))**	0.0658, 0.1396	0.0945, 0.2577	0.0364, 0.0917
***R*1, *wR*2 (all data)**	0.0893, 0.1546	0.1464, 0.3333	0.0408, 0.0946
GOF	1.143	1.026	1.043
Largest Diff. Peak, Hole (e A^{-3})	0.423, -0.276	1.476, -1.236	0.771, -1.389

Table S4. Details of X-ray crystal structures.

Compound	(^{tBu}PBP)Pd{OC(O)CH$_3$}	(^{tBu}PB^{Me}P)$_2$Ni$_2$(μ-N$_2$)	[(κ^2–^{t}Bu$_2$PC$_6$H$_4$SiMe$_2$)Pd(κ^2–^{t}Bu$_2$PC$_6$H$_4$)]
CCDC	2107494	2107495	2107496
Empirical Formula	$C_{26}H_{47}BN_2O_2P_2Pd$	$C_{50}H_{94}B_2N_6Ni_2P_4$	$C_{30}H_{50}P_2PdSi$
Wavelength (Å)	0.71073	1.54184	1.54184
Temperature (K)	93(2)	93(2)	293(2)
FW	598.80	1042.23	607.13
Crystal System	Monoclinic	Triclinic	Triclinic
Space Group	$P2_1/c$	$P\bar{1}$	$P\bar{1}$
***a* (Å)**	12.5308(4)	10.5516(6)	9.5911(5)
***b* (Å)**	15.0351(4)	11.9228(9)	9.8051(6)
***c* (Å)**	15.9890(5)	13.7755(12)	19.1276(7)
α (°)	90	103.985(7)	90.444(4)
β (°)	103.614(3)	111.062(7)	94.813(4)
γ (°)	90	90.654(5)	117.164(5)
***V* (Å^3)**	2927.72(16)	1560.0(2)	1592.59(15)
Z	4	1	2
ρ (g/cm^3)	1.359	1.109	1.266
μ (mm^{-1})	0.768	1.969	6.111
Data / restraints / parameters	7258 / 0 / 320	5403 / 565 / 477	5722 / 0 / 321
***R*1, w*R*2 (I > 2σ(I))**	0.0290, 0.0605	0.0794, 0.2006	0.0314, 0.0696
***R*1, *wR*2 (all data)**	0.0402, 0.0643	0.1188, 0.2239	0.0405, 0.0740
GOF	1.067	1.041	1.030
Largest Diff. Peak, Hole (e A^{-3})	0.696, -0.584	1.025, -0.476	0.397, -0.572

Table S5. Details of X-ray crystal structures.

SXIV. References

1. Harris, R. K.; Becker, E. D.; De Menezes, S. M.; Grager, P.; Hoffman, R. E.; Zilm, K. W. Further Conventions for NMR Shielding and Chemical Shifts (IUPAC Recommendations 2008). *Magn. Reson. Chem.* **2008**, *46*, 582-598.
2. Steinhoff, P.; Paul, M.; Schroers, J. P.; Tauchert, M. E. Highly Efficient Palladium-Catalysed Carbon Dioxide Hydrosilylation Employing PMP Ligands. *Dalton Trans.* **2019**, *48*, 1017-1022.
3. Segawa, Y. Yamashita, M.; Nozaki, K. Diphenylphosphino- or Dicyclohexylphosphino-Tethered Boryl Pincer Ligands: Syntheses of PBP Iridium(III) Complexes and Their Conversion to Iridium-Ethylene Complexes. *Organometallics* **2009**, *28* 6234-6242.
4. Segawa, Y. Yamashita, M.; Nozaki, K. Syntheses of PBP Pincer Iridium Complexes: A Supporting Boryl Ligand. *J. Am. Chem. Soc.* **2009**, *131*, 9201-9203.
5. Curado, N.; Maya, C.; López-Serrano, J.; Rodríguez, A. Boryl-Assisted Hydrogenolysis of a Nickel-Methyl Bond. *Chem. Commun.* **2014**, *50*, 15718-15721.
6. Li, Y.; Zhang, Y.; Ding, X. Synthesis, Structure, and Catalytic Behavior of a PSiP Pincer-Type Iridium(III) Complex. *Inorg. Chem. Commun.* **2011**, *14*, 1306-1310.
7. Ding, Y.; Ma, Q.; Kang, J.; Zhang, J.; Li, S.; Chen, X. Palladium(II) Complexes Supported by PBP and POCOP Pincer Ligands: A Comparison of Their Structure, Properties, and Catalytic Activity. *Dalton Trans.* **2019**, *48*, 17633-17643.
8. Falivene, L.; Cao, Z.; Petta, A.; Serra, L.; Poater, A.; Oliva, R.; Scarano, V.; Cavallo, L. Towards the Online Computer-Aided Design of Catalytic Pockets. *Nat. Chem.* **2019**, *11*, 872-879.
9. Ríos, P; Curado, N; López-Serrano, J.; Rodríguez, R. Selective Reduction of Carbon Dioxide to Bis(silyl)acetal Catalyzed by a PBP-Supported Nickel Complex. *Chem. Commun*. **2016**, *52*, 2114-2117.
10. Johnson, M. T.; Johansson, R.; Kondrashov, M.; Steyl, G.; Ahlquist, M. S. G.; Roodt, A.; Wendt, O. F. Mechanisms of the CO_2 Insertion into (PCP) Palladium Allyl and Methyl σ-Bonds. A Kinetic and Computational Study. *Organometallics* **2010**, *29*, 3521-3529.
11. Mayer, U.; Gutmann, V.; Gerger, W. The Acceptor Number – A Quantitative Empirical Parameter for the Electrophilic Properties of Solvents. *Monatsh. Chem.* **1975**, *106*, 1235-1257.
12. Sheldrick, G. M. A Short History of SHELX. *Acta Cryst.* **2008**, *A64*, 112-122.
13. Spek, A. L. PLATON SQUEEZE: A Tool for the Calculation of the Disordered Solvent Contribution to the Calculated Structure Factors *J. Appl. Cryst.* **2015**, *C71*, 9-18.